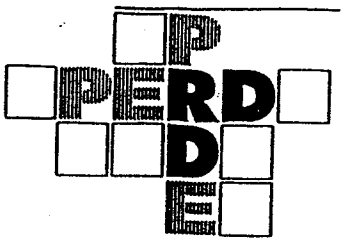

DEVELOPMENT OF A COMPUTER BASED CALORIMETER INTERFEROMETER FACILITY TO EVALUATE HIGH PERFORMANCE WINDOWS

PREPARED FOR:

The CANMET Energy Technology Centre (CETC)
Energy Technology Branch, Energy Sector
Department of Natural Resources Canada
Ottawa, Ontario, Canada, K1A 0E4
DSS Contract No. 23440-09418/01-SQ
June, 1995

PREPARED BY:

Dr. E.S. Nowak, P.Eng
Energy Conservation Laboratory
Faculty of Engineering
University of Western Ontario
London, Ontario, N6A 5B8
Tel: 519-661-2137; Fax: 519-661-3020

SCIENTIFIC AUTHORITY:

Dr. Roger Henry, P. Eng.
The CANMET Energy Technology Centre (CETC)
Energy Technology Branch, Energy Sector
Department of Natural Resources Canada
580 Booth Street, 13th Floor
Ottawa, Ontario, Canada K1A 0E4

Reprint: March 21, 2001

CITATION

Nowak, E. S., *Development of a Computer Based Calorimeter Interferometer Facility to Evaluate High Performance Windows*, Prepared by the Energy Conservation Laboratory, Faculty of Engineering Science, University of Western Ontario, under DSS Contract No. 23440-09418 /01-SQ. Efficiency and Alternative Energy Technology Branch, CANMET, Department of Natural Resources Canada, Ottawa, Ontario, 1992, (127 pages).

Copies of this report may be obtained through the following:

Efficiency and Alternative Energy Technology Branch (CANMET)
Department of Natural Resources Canada
580 Booth Street, 9th Floor
Ottawa, Ontario
K1A 0E4
or

Document Delivery Service
Library and Documentation Services Division (CANMET)
Department of Natural Resources Canada
562 Booth Street
Ottawa, Ontario
K1A 0G1

DISCLAIMER

NOTE

Funding for this project was provided by the Federal Panel on Energy Research and Development of Natural Resources Canada.

Catalogue No. M91-7/261-1993E
ISBN. 0-662-12210-X

ACKNOWLEDGEMENT

The execution of this project includes the conduction of research and the preparation of the preliminary and final reports has been carried out with the help of my research associate Dr. Raschid A. Showole and my graduate student Mr. Mohamed Ibrahim. Some of the materials (the selective coated glass and window glazing super spacer) used in this research was provided courtesy of Edgetech Ltd., Ottawa. The author received valuable inputs on some aspects of this work from the general audience at the workshop - Window Heat Transfer Diagnostics organized by EMR CANMET in Ottawa on November 24-25, 1992.

The author would like to thank all the individuals and organizations mentioned above. Their dedication, comments and constructive criticism contribute in different ways to the successful completion of this report.

ABSTRACT

This report presents the results of an intensive research conducted using a state-of-the-art laser interferometer technique to evaluate the thermally induced convection heat losses in double glazed windows with or without convection suppressor in the air gaps. The local and average heat transfer distributions on the hot and cold glass vertical surfaces of the windows are investigated. Heat loss or gain through the horizontal top and bottom end wall surfaces of the air gap is investigated to provide accurate information on the temperature and heat transfer profiles along these surfaces. Here-to-fore there has been confusion over what is the realistic or the true real-world temperature boundary conditions and the heat transfer characteristics at the horizontal bottom and top end wall surfaces of the window slot. Previous researchers have assumed simplified boundary conditions of adiabatic or linear temperature profiles on the top and bottom end wall surfaces of the slot. The present study resolves this controversy and demonstrates the invalidity of the adiabatic or linear temperature boundary conditions which are different from the observed and recorded real world temperature profiles at these surfaces. The temperature profiles along the vertical centerline of the air gaps is also investigated for different air gap spacings.

The effect of the convection cooling occurring at the top and bottom sections of the window slot on the formation of surface condensation is investigated. The elimination of the surface condensation using convection suppressor of different heights is also investigated. Equations relating the overall convection heat transfer coefficients (Nu) to heat transmission (U) coefficients are presented. Correlation equations of the overall average heat transfer coefficients

as a function of Grashof number are developed for the vertical surfaces and the two horizontal top and bottom end wall surfaces. Similar correlation equation for the average Nusselt number as a function of the ratio of the suppressor height to the height of the slot was also developed. The general discussion includes the observed relationship between the thermally coupled convection heat transfer in air gaps and the formation of window condensation. It is concluded that the present knowledge on the phenomenon of the coupled film coefficients and air gap convection coefficients is insufficient for detailed and accurate evaluation of thermal performance of insulated windows. Further studies are required to evaluate the coupled external and internal film coefficients in double glazing. This will require that the full-scale hot box apparatus developed in this project be equipped in future with large optical windows to facilitate simultaneous measurements of the internal and external surface film coefficients along the height of the window slot. This modification will widen the scope of this study currently limited to internal convection study to include in the future the coupling effect of the internal and external convection leading to the development of a correlation equation for the external film coefficients in double window glazing. Recommendation for future research works required to resolve the outstanding questions on window convection heat losses and condensation is offered.

Key words: Convection, condensation, heat-transfer-coefficient, film-coefficient, heat-resistance-coefficient, heat-transmission-coefficient, edge seal, interferometer, hot-box, calorimeter, temperature-profiles.

ABSTRAIT

Ce rapport présente les résultats de recherches intensives menées par une technique d'interféromètre de laser pour évaluer la chaleur de convection théramatiquement conçue de pertes de chaleur dans les fenêtres doubles vitrées avec ou sans suppressor de convection dans les poches d'air. Le transfer de chaleur moyen et sur place de distributions sur les surfaces verticales de chaleur et de froid des fenêtres est examinée. La perte ou le gain de chaleur par moyen des surfaces de mur sur les bouts horizontaux de haut et de bas de la poche d'air est étudiée afin de donner des renseignements sur la température et le transfer de chaleur sur ces surfaces. Avant cette présente étude il existait une confusion sur ce qui est la température réelle ou réalistique des conditions de frontière et les caractéristiques de transfer de chaleur à l'extrémité supérieure des surfaces de la fente. Cette étude résoud cette controverse et démontre l'invalidité des conditions de frontière de la température adiabatique ou linéaire qui sont differentes du monde réel observé et enregistré sur les profils actuels de conditions sur ces surfaces. Les profils de température le long de la ligne de centre verticale des poches d'air est également étudiée pour l'espacement des différentes poches d'air.

L'effet de refriodissement de convection qui a lieu aux sections inférieures et supérieures de la fente de fenêtre sur la formation de la condensation de surface est égalements étudiée. L'élimination de la condensation de surface employant des suppressors de convection des hauteurs différentes est aussi examinée. Les équations se rapportant aux coéfficients (Nu) de transfer de chaleur par convection globale aux coéfficients de transmissions de chaleur (U) sont également données. La correlation d'équations du transfer de chaleur en moyenne comme une

fonction du nombre Grashof est développée pour les surfaces verticales et les deux surfaces - haut et bas. Une correlation similaire du chiffre moyen Nusselt comme équation vue en fonction de la ratio de la hauteur de suppressor à la hauteur de la fente fut également étudiée. La discussion générale comporte le rapport observé entre la chaleur de convection théramatiquement couplée de transfer de chaleur par convection dans les poches d'air et dans la formation de condensation des fenêtre. On conclut que ce que nous savons actuellement sur le phénomène des coéfficients couplés de films et des coéfficients de convection pour les poches d'air est insuffisant pour une évaluation détaillée et juste de la performance thémale des fenêtres isolantes. D'autres études sont nécessaires afin d'évaluer les coéfficients de surface de film intérieur et extérieur le long de la hauter de la fente de fenêtre. Cette modification étendra la portée de cette étude limitée actuellement à l'étude de convection intérieure et extérieure menant au developpement d'une équation de correlation pour les coéfficients de film dans les dou les fenêtres vitrées. Il est offert une recommendation à la recherche éventuelle nécessaire à résoudre les questions qui restent sur les pertes de chaleur de convection de fenêtres et la condensation.

MOTS CLEFS Convection, condensation, coéfficient de transfer de chaleur, coéfficient de film, coéfficient de résistanfe à la chaleur, coéefficient de transmission de chaleur, scellement de bord, interféromètre, boite chaude calorimètre, profil de température.

RECOMMENDATIONS

The versatility and the uniqueness of the laser interferometer is demonstrated in this report. It is a design and research tool that was employed in this study to remotely investigate convection phenomena in a confined window slot environment. To the best of the author's knowledge no other methods will provide a more detailed and accurate information on confined heat convection in sealed double glazed windows than the laser interferometric technique. It is therefore recommended that the laser interferometric technique be modified accordingly and used in future studies on the coupled internal and external convection heat transfer in a double or multi-glazed advanced windows (see Figure ia). To accomplish this goal the small scale apparatus will be replaced with a larger apparatus which could hold a large size window glazing. The present optical window (see Figure 2.6a to c) will also be replaced with a large optical window shown in Figure i.a. The large optical window will serve a dual purpose of providing a permanent or semi-permanent vertical seal for the double glazing while permitting, without any obstruction, the transmission of the laser beam through the air gap enclosure along the entire height of the glazing with no need to adjust or traverse the optical window (see Figures i.a and b). In the present arrangement the small optical window has to be traversed or shifted at 8 cm. interval along the height of the vertical slot for the laser beam to transmit through every section of the air layer. With the proposed large optical window for the future study only the laser beam need be shifted using a traversing mechanism while the test section and the optical window remain stationary. This arrangement will prevent disturbing the vertical seals and hence improve the accuracy of the experiment.

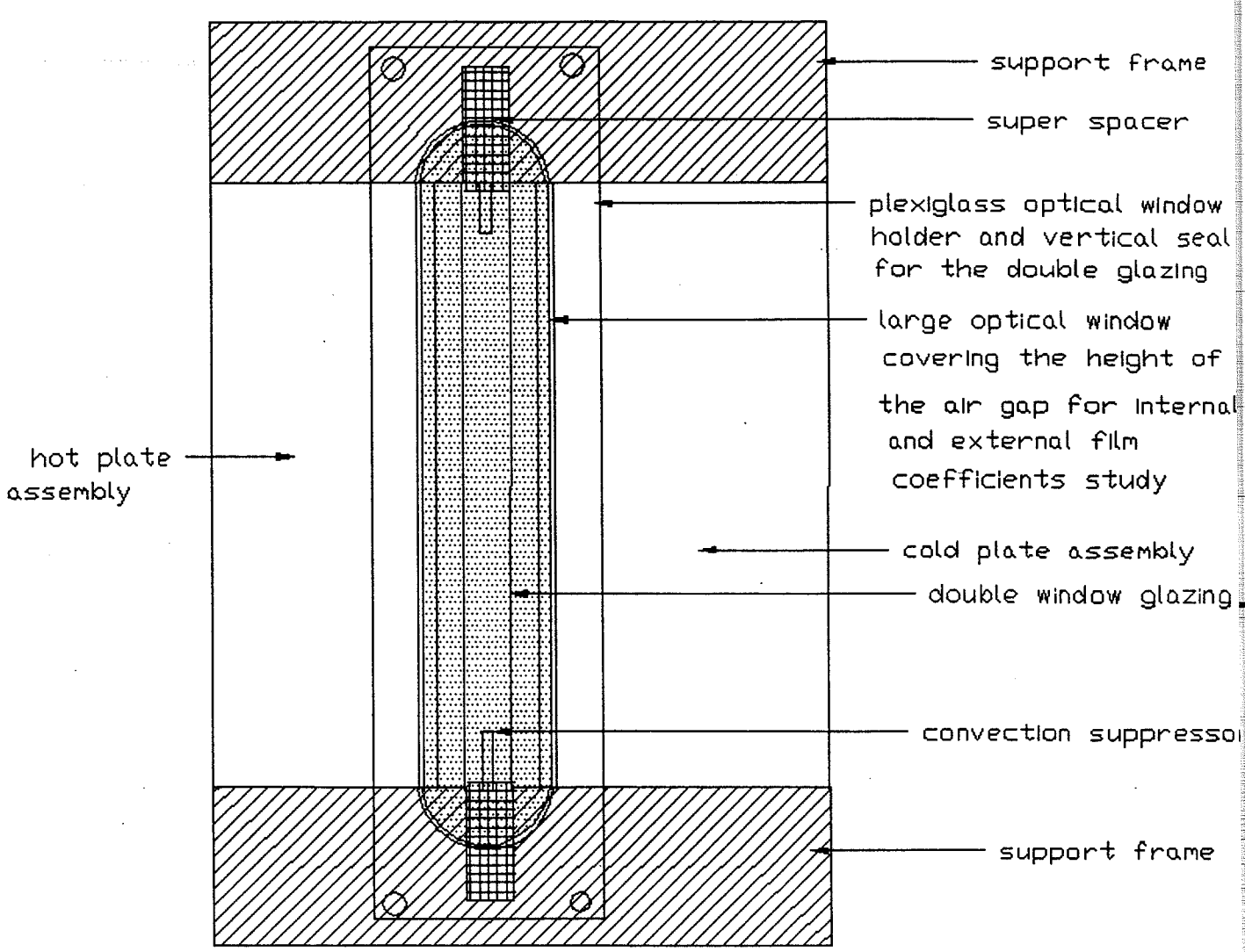

Fig. ia **Front View of the Hot-Cold Plate Apparatus Showing the Proposed Large-Size Optical Window for Future Studies on the Coupled Internal and External Film Coefficients in Double Window Glazing**

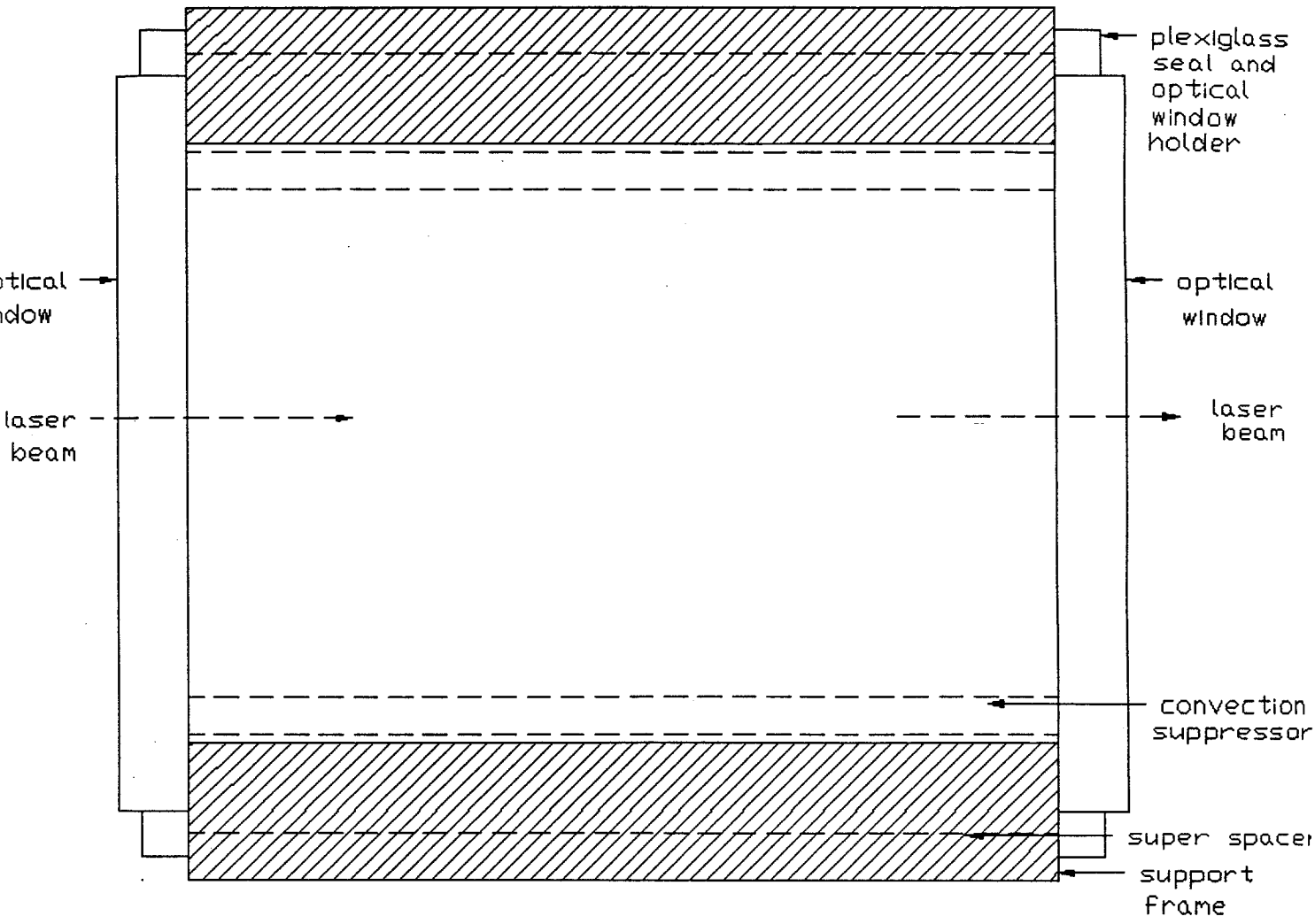

Fig. ib **The Side View of the Hot-Cold Plate Apparatus Showing the Proposed Large-Size Optical Window**

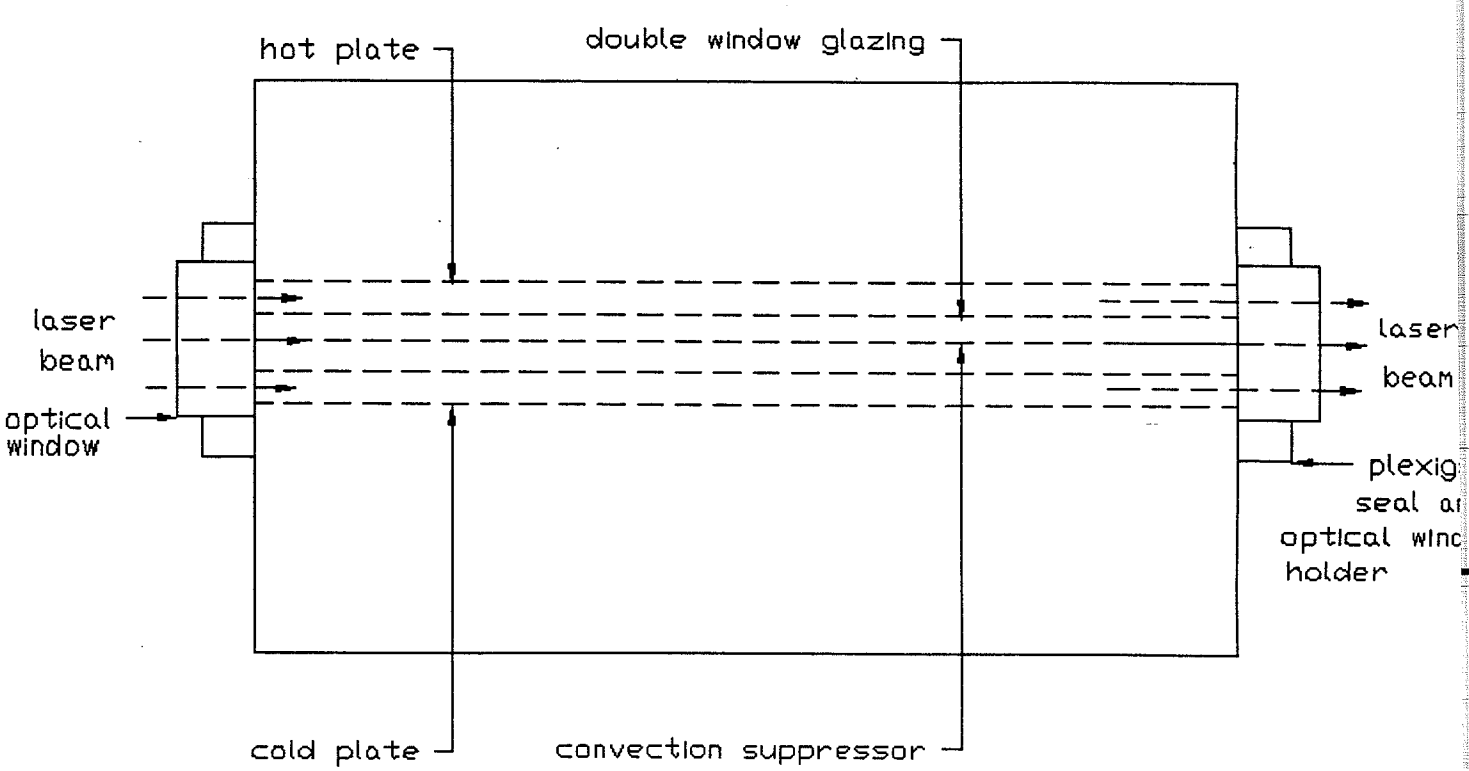

Fig. ic **The Top of the Hot-Cold Plate Apparatus Showing the Proposed Large-Size Optical Window**

The present study examined and provided correlation equations for the convection heat transfer coefficients in window air gap enclosure. Further studies are recommended, with modification to the present experimental apparatus as discussed above, to develop similar correlation equations for the coupled external and internal film coefficients. No such correlation equation, which is absolutely important for window design and evaluation, is available at present.

The external film coefficients on hot and cold glass surfaces of windows and their interaction or coupling relationship with the internal heat transfer coefficients require a detailed study to provide the badly needed external and internal film coefficients data and correlations often required by window designers, manufacturers and computer simulation programmers. The coupled internal and external film coefficient correlation data is required for the calculation of the heat resistance value (R-value) and overall heat transmission value (U-value) of double glazed window. The fact that the internal and external film coefficients are coupled phenomena which co-exist and interact means that they must be studied together to obtain accurate data and develop realistic design correlation equations. A random selection of these data from tables of data developed from experiments which do not take into consideration the couple phenomenon of the internal and external film coefficients, is outdated and inaccurate procedure. We recommend that the interferometric technique be used to carry out this important study in order to develop correlation equations for the coupled external and internal film coefficients and hence update window design procedure with the changing technology.

To complete the convection heat loss and condensation studies, we recommend that the analysis of the external film coefficients and its coupling relationship with the internal heat

transfer coefficients be made the second phase of the proposed study. We also recommend that the study be carried out using the modified UWO facility which comprises a well controlled hot box apparatus to be equipped with large size optical windows and modified laser interferometer. The modified apparatus will be unique and suitable for a simultaneous study of the coupled internal and external film coefficients in double or multiple window glazing. Moreover the real world temperature distributions on the non-isothermal window glass surfaces and non-adiabatic top and bottom surfaces of the enclosure can be accurately measured using the modified UWO apparatus. The new apparatus with the laser interferometer - a special optical arrangement, can provide temperature map of the window glass surfaces enclosed in the hot box while the experiment is in progress. No other technique including thermography can be used to accomplish this task. No need of thermocouple installation or weighted average temperature calculation. Because the hot box cannot be accessed while the experiment is in progress, therefore, the **infrared thermography** cannot be used to map the glass surface temperature of the double window glazing undergoing thermal testing and evaluation. With the large optical window and the modified laser interferometer apparatus, the mapping of the surface temperature of the window glazing being tested in the hot box can be carried out while the experiment is in progress (see Figures ia to c and 2.1) using the laser interferometer. So no other apparatus or experimental technique other than the laser interferometer can be used to study the coupled internal and external film coefficients in the confined environment of the double window glazing. In carrying out the future study the laser interferometer will be used to evaluate

* the temperature map in the air gap enclosure needed for the calculation of **internal heat transfer coefficients**

* the temperature map on **the external hot and cold glasss surfaces** needed for the calculation of the **external film coefficients on hot and cold glass surfaces** as well as for the **surface condensation analysis**
* the correlation equations for **internal heat transfer and external film coefficients**

It is recommended that a comprehensive energy balance study be carried out in the laboratory to simultaneously measure conductive, radiative and convective heat transfer coefficients in order to obtain for new advanced windows, the standard R-value and U-value which accurately account for the coupled external and internal film coefficients. Presently the values for these coupled parameters are randomly selected from tables of data developed from empirical or analytical equations. The modified UWO apparatus can measure the convective heat transfer coefficient accurately as mentioned above, and can be used through calorimetry capability of the equipment to determine the conductive and the radiative heat transfer coefficients.

The infrared thermography is an apparatus which has been demonstrated to be suitable for field measurements of the temperature of opaque surfaces when properly calibrated. The laser interferometer can be used to map the temperature of both the opaque surfaces and transparent media as well. Because of its versatility and accuracy we recommend that the laser interferometer apparatus be used in future to calibrate and validate infrared thermography.

TABLE OF CONTENTS

LIST OF FIGURES

LIST OF TABLES

NOMENCLATURE

A	Cavity aspect ratio
C_p	Specific heat
C	Constant
DP	Dew point temperature
F	True fringe number
g	Acceleration due to gravity
Gr	Grashof number
Gr_c	The critical Grashof number
Gr_{cc}	Grashof number at the centre cell
Gr_w	Grashof number based on width of air layer
Gr_H	Grashof number based on height of air layer
h	Heat transfer coefficient
h_c	Heat transfer coefficient in the central part of the air layer
h	Average heat transfer coefficient
H	Enclosure height along the y-axis
H_s	Baffle or suppressor height
K	Thermal conductivity
K_e	Effective or apparent thermal conductivity
K_m	Thermal conductivity at the mean enclosure temperature, $(T_h+T_c)/2$

K_w	Thermal conductivity of air at the wall temperature
L	Span length of the model in the direction of light
Nu_y	Local Nusselt number
Nu_{ave}	Average Nusselt number
Nu_{cc}	The average Nusselt number at the centre cell
Nu_H	Average Nusselt number based on the height of the air layer
Nu_w	Nusselt number based on the width of the air layer
P	Pressure
Pr	Prandtl number
q"	Local heat flux
q	Average heat flux
R	Gas constant; thermal resistance
Ra	Rayleigh number
Ra_c	Critical Rayleigh number
T	Temperature
T^*	Non-dimensional temperature
T_{amb}	Ambient temperature
T_h	Average temperature of the hot wall
T_c	Average temperature of the cold wall
T_m	Absolute mean temperature of the model

T_{ref}	Reference temperature
TEG	Triethylene glycol
U_{conv}	Thermal transmittance due to convection
w	Width of the air layer along the x-axis
x	Coordinate along the cavity width
x^*	Non-dimensional x-coordinate
y	Coordinate along the cavity height
y^*	Non-dimensional y-coordinate

Greek Symbols

α	Thermal diffusivity
δ	Thermal boundary layer thickness
ΔPL	Optical path length difference
ΔT	Temperature difference
ϵ	Fringe shift
$\epsilon_{x,y}$	Total fringe shift
λ	Wavelength of the traversing light
λ_o	Light wavelength in vacuum
λ_t	Light wavelength in test medium
η	Refractive index
η_{ref}	Refractive index of the reference medium
η_t	Refractive index of the test medium

μ	Dynamic viscosity
ν	Kinematic viscosity
ρ	Density of air
∞	Infinite; free stream

Subscripts

amb	Ambient
ave	Average
A	Aspect ratio
c	Critical; cold
conv	Convective
e	Effective
h	Hot
H	Height
m	Mean
o	Vacuum
p	Peak
ref	Reference
s	Suppressor
t	Test medium
T	Total
w	wall or width

1.0 INTRODUCTION

One of the most important factors affecting the thermal and condensation performance of double glazed windows is the thermally coupled convection heat transfer occurring on the external surfaces as well as in the air gap of double glazed windows, Figure 1.1. Therefore, a better understanding of the coupled relationship between the hot and cold window glazings external film coefficients and the thermally induced convection flow in the air gap is essential in order to facilitate accurate analysis of window thermal performance and surface condensation. The knowledge of the thermally induced convection flow characteristics is essential to resolve the present discrepancies in window thermal testing and evaluation procedures resulting from the use of several so called ASTM standard test methods (C 236, C 177, C 518, C 1045), the thermography and the computer simulation methods using analytical or empirical equations. These methods produce conflicting results of the overall heat transfer coefficients of double window because none of the methods could be used to determine the external film coefficients which couples with the internal film coefficients. The coupled internal and external film coefficients must first be determined in order to develop a standard heat transmission measurement method which will not only provide an understanding of the thermal transmission problem but also of the problem of window condensation. The influence of air gap convection on window condensation and the use of convection suppressor, Figure 1.2 as a remedy to the formation of condensation requires special attention in order to fully characterize the thermal performance of insulated glazing (IG) units.

Transmission heat losses account for a large portion of heating loads of residential and

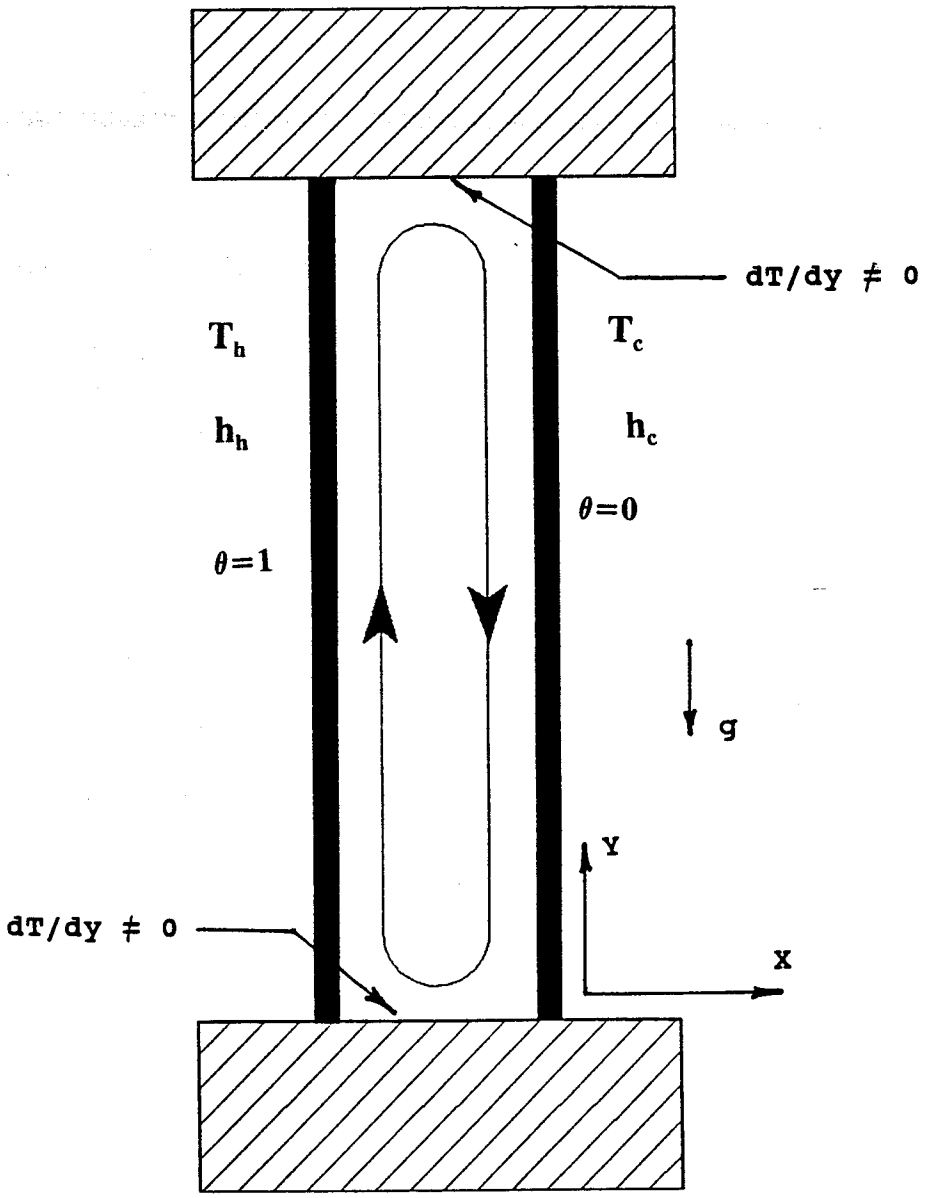

Fig. 1.1 Schematic of Natural Convection in a Window Air Gap Without Suppressor

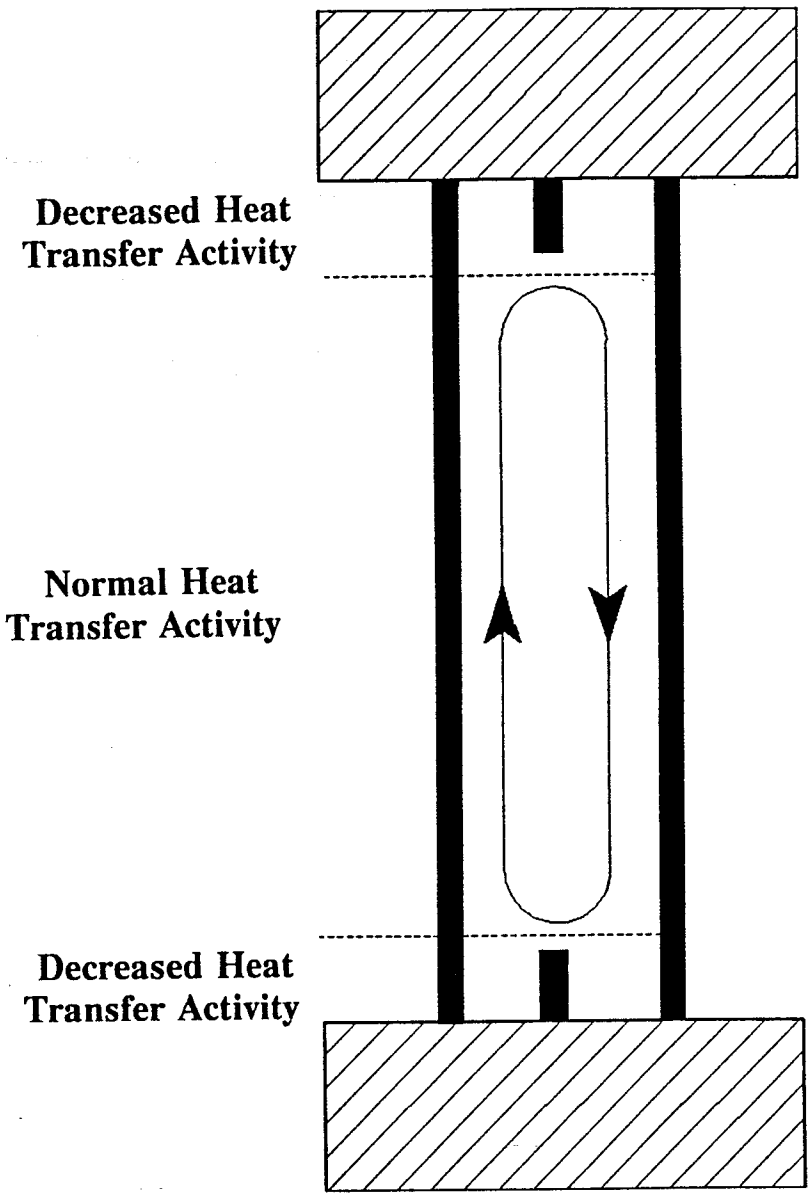

Fig. 1.2 Schematic of Natural Convection in a Window Slot with Suppressors at the Top and Bottom of the Air Gap

small size commercial buildings [Kusuda and Collins, 1978]. These comprise conduction, convection and radiation heat losses through walls, roofs, floors and windows. Recent advances in material science technology has resulted in significant improvements in thermal resistant insulating materials and has led to a considerable reduction in conduction heat losses through walls, roofs and floors. The introduction of "heat mirror" plastic films [Lampert, 1981] and low emittance coatings on glass [Grange and Owens, 1984] has also resulted in considerable reduction in radiation heat losses of sealed glazing units. However, the convection heat losses through air gaps of double or multi-glazed windows and the associated window condensation are problems still posing a major challenge to the building industry in general and to the designers of advanced energy efficient windows in particular. The convection heat losses may account for a large percentage of building heating loads depending on the season and/or the location.

Several efforts have been expended on the development of vacuum-insulated and gas-filled double glazing in order to reduce air gap convection heat losses and eliminate glass surface condensation. These new advances are expected to progress further through the commercialization of electrochromic coatings, gas fills, evacuated glazings, and silica-gel window technologies [Arasteh et al., 1985]. However, the major short-coming of a vacuum insulated or gas filled window has always been the difficulty in maintaining a perfect seal around the edges of the window glazing, thereby losing that advantage. Moreover, extreme and prolong cold winter season in Canada followed by hot weather in summer could deteriorate the seals around the window-mounted glass due to the expansion and contraction of the glass panes. These technical problems associated with the vacuum-insulated and gas-filled window technology in conjunction with high cost of window replacement may discourage the use of these hi-tech

windows in Canada. The technical problems also discouraged U.S. researchers, who produced a prototype of the "hi-tech" window in the '70s to abandon the project and consider other options. The building industry is still searching for a more practical and direct approach to solving the problem of convection heat losses in window. It is important that a new approach takes into consideration a fundamental and physical understanding of the coupled phenomenon of the convection mechanisms occurring within the air gap, and, on the external surfaces of double window glazing. A lot more work is needed to fully understand this complex phenomenon and its relationship to energy loss and window pane surface condensation in order to accomplish the goal of developing high energy efficient and condensation-free advanced window glazings.

Natural convection heat transfer in air layer enclosed between two differentially heated vertical plates (see Figure 1.1) has received a lot of attention since the pioneering theoretical and experimental works of Batchelor [1954] and Eckert and Carlson [1961]. A comprehensive literature review of natural convection in vertical slot has been given by Gray [1985]. These classical fundamental heat transfer studies are related to insulated window technology although simple boundary conditions imposed on the theoretical model and the highly conducting materials (copper) used in the construction of most experimental models resulted in isothermal surface which is hard to achieve in glass pane. In close relation to insulated window technology, Wilson et al. [1959], Brown et al. [1961] and recently Brown and Solvanson [1984] and Bowen [1985] have carried out performance evaluation studies to measure heat transmission through double glazing to determine the U-value of an insulated glazing unit. In the case of Brown and Bowen, the works were carried out to improve the test method (ASTM standard C236) for the evaluation

of heat transmission through window glazing. Because an energy balance technique using a calorimeter is employed in the above performance evaluation studies, the convection mechanisms in the window air gap could not be investigated and only average values were determined. This technique is primarily useful for evaluation purposes and not for the fundamental analysis needed for design of new windows.

Recent works on window technology have also focused on the development of test methods, measurement techniques and computer analyses based on previous empirical or analytical equations. Wright and Sullivan [1987], Lawrence Berkeley Laboratory [1988] and several other computer analysts have developed programs for thermal performance calculation with variable assumptions and idealized boundary conditions. More recently Arasteh et al. [1992], Bailey and Cameron [1992] and several others have described thermography techniques for window surface temperature measurements. All of these works are not fundamental studies of the air gap natural convection heat transfer necessary to provide further understanding of the convection heat losses for conceptual development and design of new advanced window systems.

The objective of the present study goes beyond measurements and evaluation to deal with the problem of fundamental understanding of the air gap heat convection and the associated window surface condensation. The present study provides technical information and correlation equations on heat convection mechanisms occurring in the air gap of a double glazing in order to assist window designers and manufacturers to improve the thermal and condensation performance of advanced energy efficient window systems. At present, serious controversy exists in the window industry over the procedures for thermal testing, evaluation and rating of insulated windows. This controversy has been demonstrated at several window technology

seminars, conferences and workshops where shortcomings of existing testing or evaluation methods have been strongly debated. The confusion is partly due to a lack of understanding of the mechanisms of coupling convection heat loss and the external film coefficients and their effects on surface condensation. The lack of experimental data on the thermal characteristics of glazing and edge seals with real world boundary conditions could also lead to misinterpretation of the heat convection phenomenon and inaccurate thermal analysis and evaluation. This report resolves some of the confusion and provides information and correlation equations that will assist industry in developing a consensus-based standard on thermal performance testing, evaluation and rating of insulated windows.

2.0 DESCRIPTION OF RESEARCH APPARATUS

The research apparatus consists of the following major equipment:

A) Guarded hot box apparatus with window calorimeter for full size window research

B) Hot-cold plate apparatus for research using small-scale window models

C) Mach-Zehnder interferometer for small scale window modelling (could be upgraded for full-size window research)

D) Mach Zehnder Interferometer Auxiliary Equipment

i) Comparator (Travelling microscope)

E) Double window glazing model

2.1 FULL-SIZE GUARDED HOT BOX APPARATUS (Apparatus For Large Scale or Full-Size Window Studies)

The full-size guarded hot box apparatus was developed by the staff of the Energy Conservation Research Laboratory. The hot box equipped with a window calorimeter can be used for thermal and condensation performance evaluation of proto-type advanced windows. This apparatus was designed to be used as a building envelope performance test facility to foster technology transfer and encourage research and development (R&D) collaboration between the university laboratory and the industrial sector. The guarded hot box (Figures 2.1 and 2.1b) consists of four main sections; a cold room capable of maintaining a temperature between 0° and -40°C; a warm (or guard) room, capable of maintaining a temperature between 0° and 30°C; a metering (or calorimeter) which performs the function of a heat flux meter and used to measure heat loss through window glazing or any test panel; a support frame to hold a window unit or any test panel. Other auxiliary units are the computer interface and data loggers. Large size optical window (see Figures i.a to c) will be employed in future studies for the interferometric evaluation of the coupled external and internal film coefficients. To the best of the author's knowledge no experimental method is available any where at present to carry out this function.

2.1.1 Cold Chamber

The cold room is a five-sided box with an outside dimension of approximately 2.44 m (8') in length, 3.35 m (11') in width, and 3.35 m (11') in height. The 3.35 m square open end accommodates the window or any compatible test panel. The box consists of 30.48 cm (12")

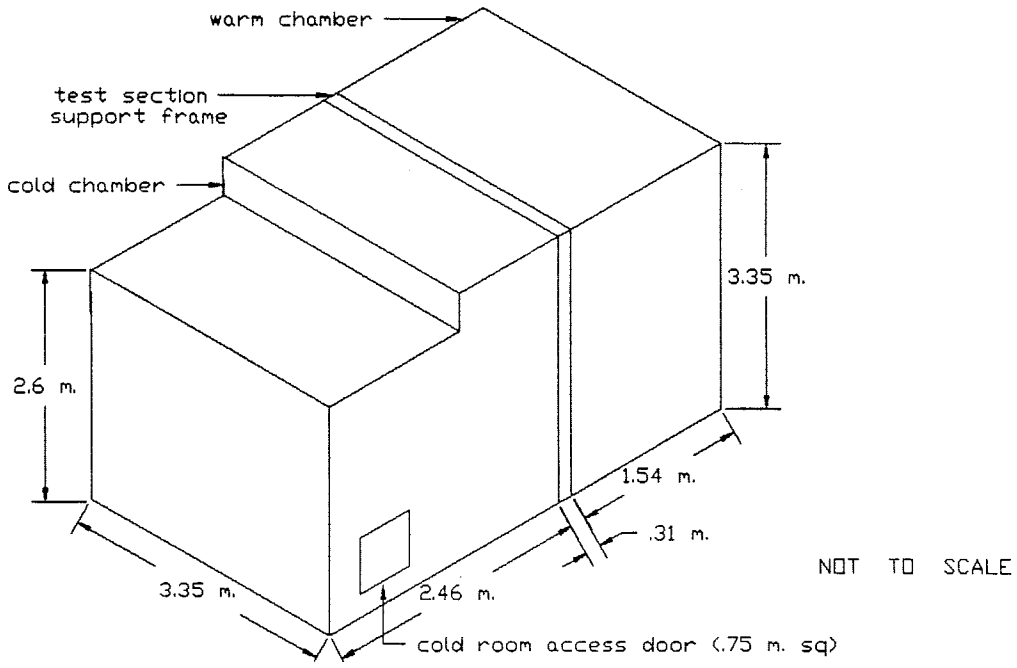

Fig. 2.1 The Schematic of the Guarded Hot Box

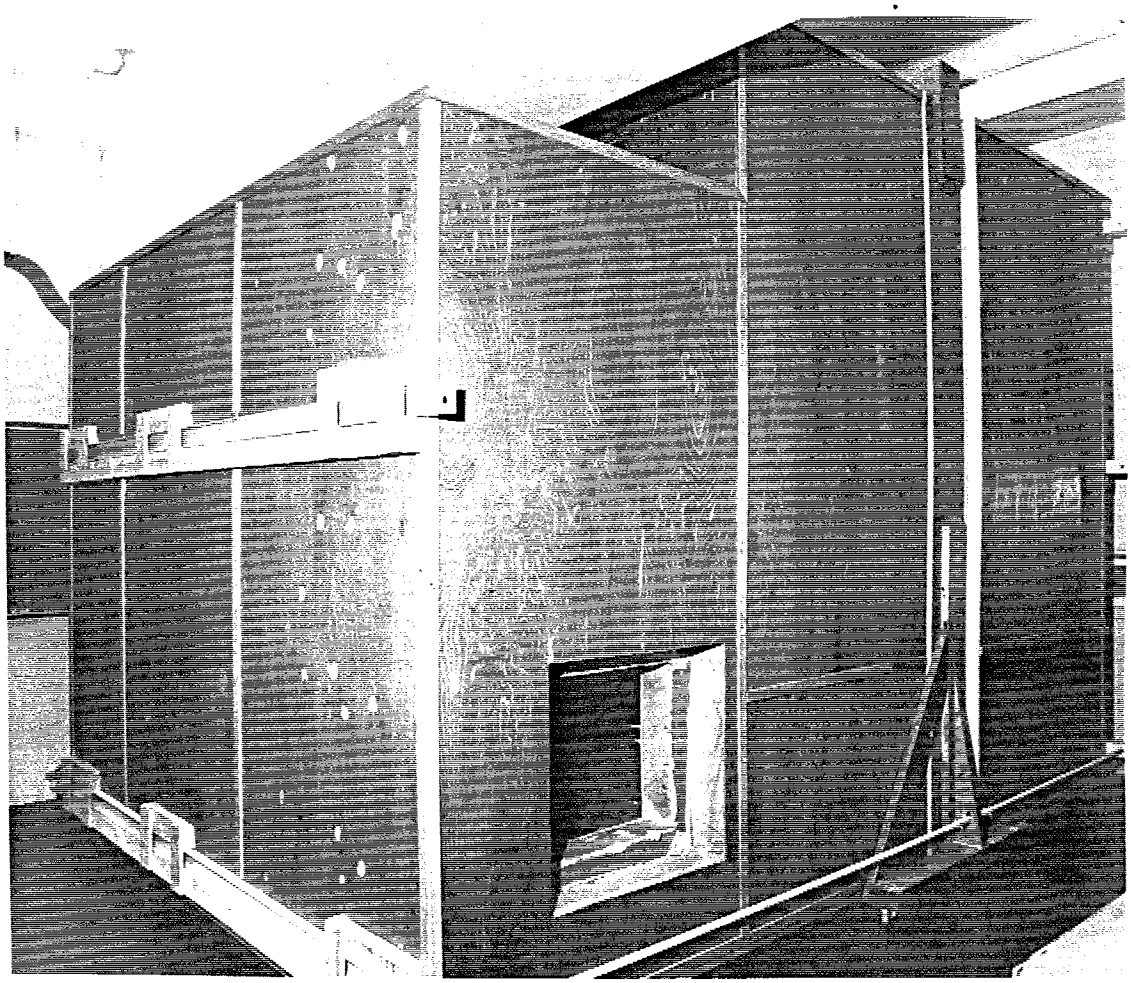

Fig. 2.1b The Guarded Hot Box

polyurethane foam, jacketed with plywood at the outside and steel plate at the inside faces. The cold room rests on six castor wheels. Three steel bars are mounted on the top, middle and lower sections of the back of the cold room and are connected through threaded steel rods to similar steel bars behind the warm (guard) room. This arrangement is used to lock the test frame, guard room and the cold room together. A neoprene gasket is installed between the open end face of the cold room and test frame to prevent air leakage from the cold room.

At the initial stage of operation, the cold room was cooled by a direct expansion refrigeration system using a 2 h.p., single stage, air cooled condensing unit (Copeland, Model C4AE 0200 CAB 001 with Compressor Model 3AB2 0310 CAB). This unit is mounted on air bags outside the cold room to reduce vibration that could be transmitted to the highly sensitive interferometer integrated with the hot box. The refrigeration unit feeds R-502 refrigerant to two expansion evaporators (Keeprite Model KUC410-ED) housed inside the cold room. The evaporator unit is equipped with defrost heaters and a 1/15 h.p. air blower. For a parallel uniform flow across the surface of the test panel (see testing method ASTM 236), air is blown through the evaporator to a deflector which deflects the flow through the space between the baffle and the test panel. In the case of an impinging flow (Bowen,1985), a '24 A-F' tube-axial fan powered by a variable speed 5 h.p. hydraulic motor draws cold air from the evaporators through flow straighteners and distributors to the surface of the test panel mounted on the open end of the cold room. The temperature of the cold room is controlled using a solid state analog temperature controller sensor.

2.1.2 Warm Chamber (or Guard Room)

The design and construction of the warm room is similar to that of the cold room except in length which is approximately 1.52 m (5ft.). Like the cold room, the warm room is mobile and rests on four castor wheels. It is also equipped with neoprene gasket at the open end and steel bar at the back for the locking system.

The temperature and the humidity of the warm room is controlled by an integrated system consisting of an air conditioner, a heater and a humidifier. When the system becomes fully operational, the air conditioning will be provided by a direct expansion refrigeration system using a 2 h.p. (Copeland Model CBAH-0200-TAC-001) air cooled, single stage condensing unit. The cooled air is forced through a duct equipped with a heater and then over a humidifier before being dumped into the warm room. Therefore, temperature of the warm room is controlled by bucking the refrigeration system. The humidity of the room is also maintained by the humidifier in parallel operation with the refrigeration system which retroactively operates as a dehumidifier.

2.1.3 Support Frame

The support frame is also made of plywood and 30.48 cm thick polyurethane foam. The frame rests on four castor wheels and can be wheeled out of the hot box for the installation of the test panel. The frame is equipped with a locking device to fix it tightly to the cold and warm rooms during testing.

2.1.4 Metering (or Calorimeter) Box

The metering box (or window calorimeter) shown in Figure 2.2 was designed primarily to measure heat transmission characteristics of windows but can also be used to measure heat flow through any building assembly. The metering box is about 2.2 m square by 0.91 m deep. The walls of the box were made of moulded fibreglass with 7.62 cm (3") isocyanurate foam core. Prior to the assembly of the metering box, two hundred and four copper-constantan thermocouples were installed beneath each of the inner and outer skins of the box. These thermocouples were later connected to form two hundred and four pairs of differential thermopile (Figure 2.3). The joints between the inner and outer skins of the box were sealed with an epoxy resin and fibreglass cloth to bond the skins (with the foam core) together. The edge of the box in contact with the test panel was narrowed on the outside only and holds a gasket 7 mm wide which meets the requirement specified by ASTM C236. The thermal resistance of the metering box walls also meets the ASTM C236 specifications.

The metering box consists of the following units:

* Uniform temperature baffle
* Uniform temperature convection heater

The uniform temperature baffle is absolutely essential for the thermal performance testing of window glazing unit. The baffle consists of a radiating panel, a copper pipe reservoir containing refrigerant R-12 and a 2000 watts tubular heater for boiling the refrigerant. The radiating panel was constructed of 24 roll-bond single riser panels with 7.62 cm (3") spacing between the risers. The risers were connected to the headers with nipples. The R-12 evaporates

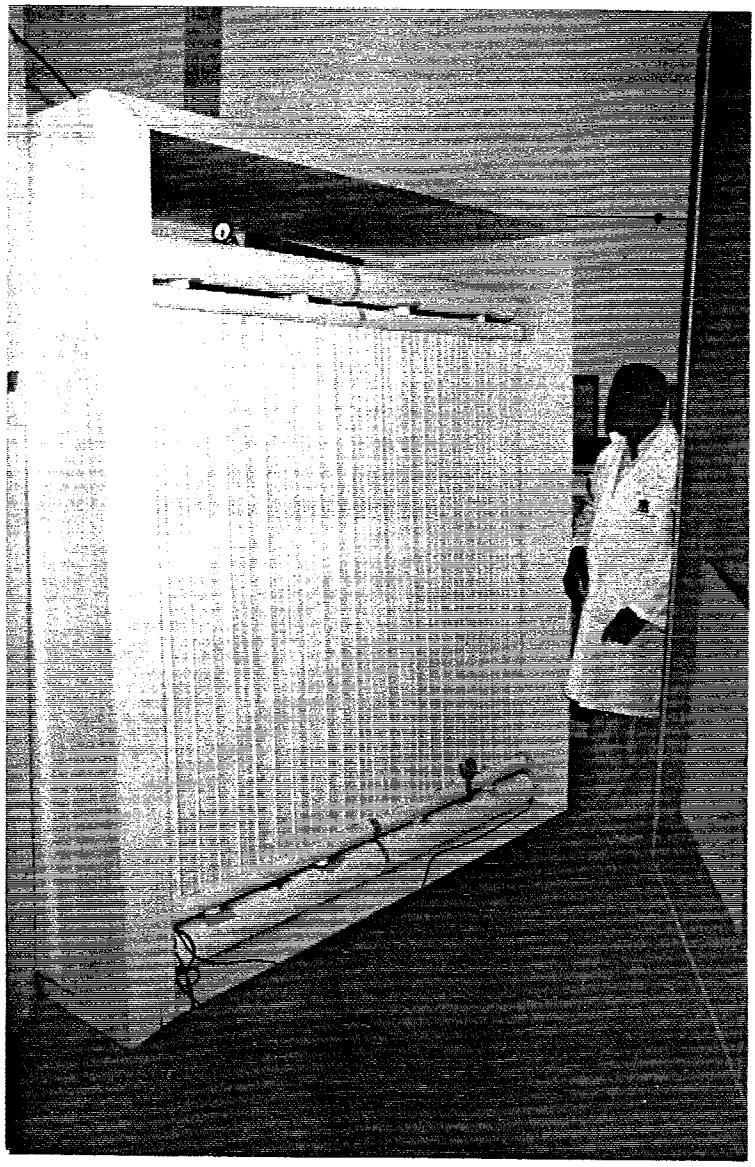

Fig. 2.2 The Full-Size Metering (Calorimeter) Box

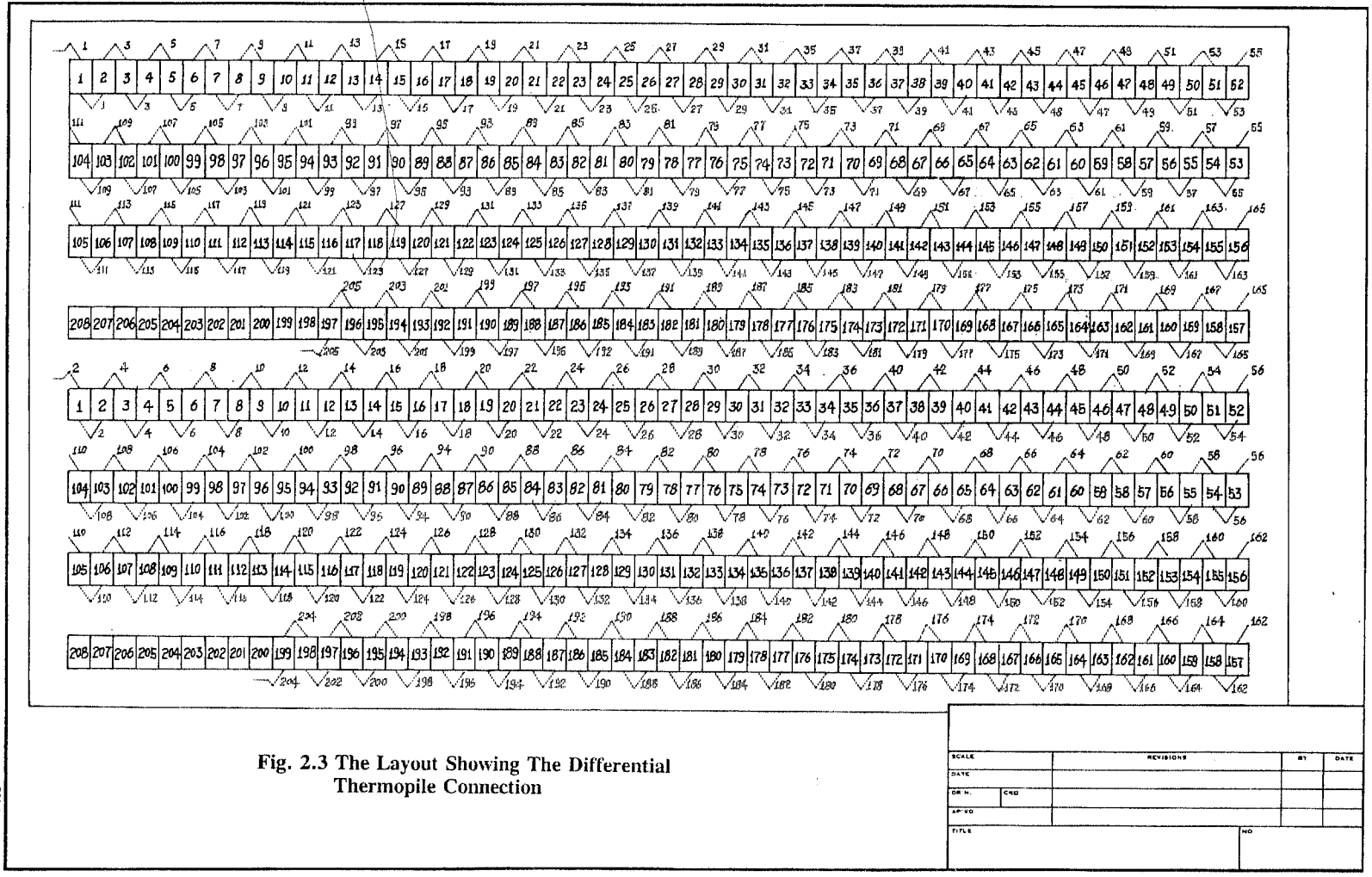

Fig. 2.3 The Layout Showing The Differential Thermopile Connection

in the reservoir and condenses in the radiating panel giving off heat which is radiated onto the hot surface of the window glazing or a test panel.

The convection heater (Figure 2.4) was operated either as a natural or forced convection heating system. It was constructed of two fin tubes connected to a copper pipe reservoir which contains a tubular heater of the same power rating as that installed in the uniform temperature baffle. In the forced convection mode a d.c. 1/2 h.p. centrifugal blower was used. The heater and blower were mounted behind the uniform temperature baffle in the metering box. Air is forced across the hot fin tubes to the top of the metering box and down between the baffle and the test wall.

The temperature of the metering box is controlled by the thermopile system and a solid state digital temperature controller sensor. In an ideal situation, the temperature in the metering box and the warm room (or guard room) must be equal, so there is no net heat flow through the metering box walls. All of the power supplied to the metering box, therefore, must be equal to the heat flow through the window glazing being tested. However, in practice there may be a small temperature difference between the metering box and the air in the warm room indicating a flow of heat into or out of the metering box. This heat flow is detected and accurately measured using the thermopile arrangement.

2.2 HOT-COLD PLATE APPARATUS (for small scale model window studies)

The hot-cold plate apparatus (Figure 2.5) was used in the experimental study presented

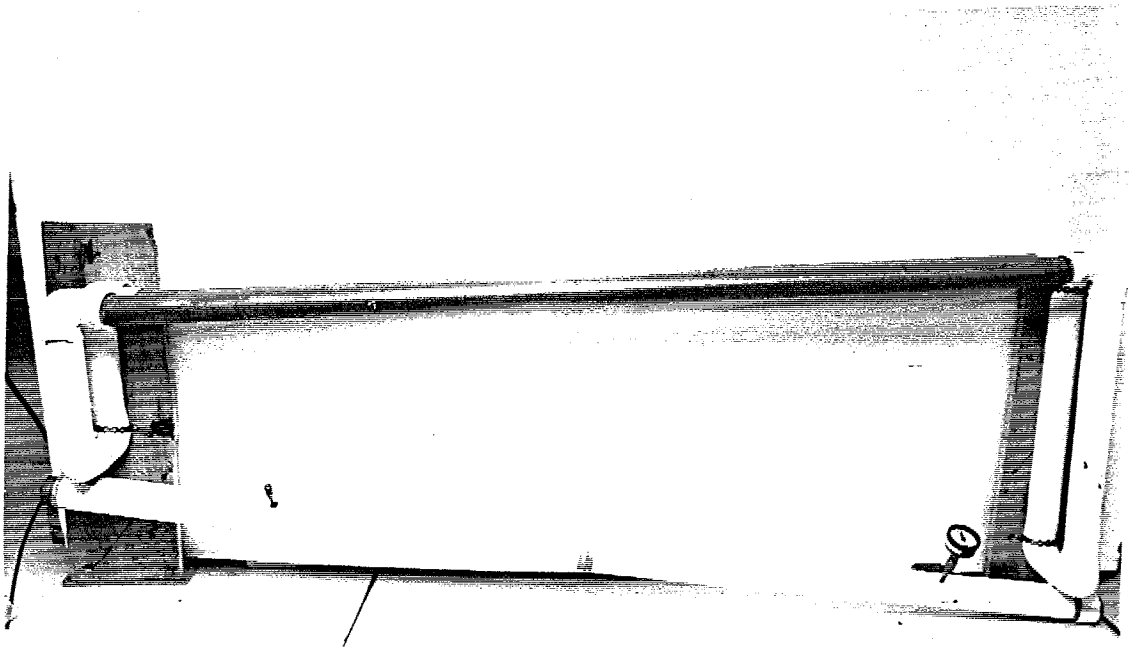

Fig. 2.4 The Convection Heater

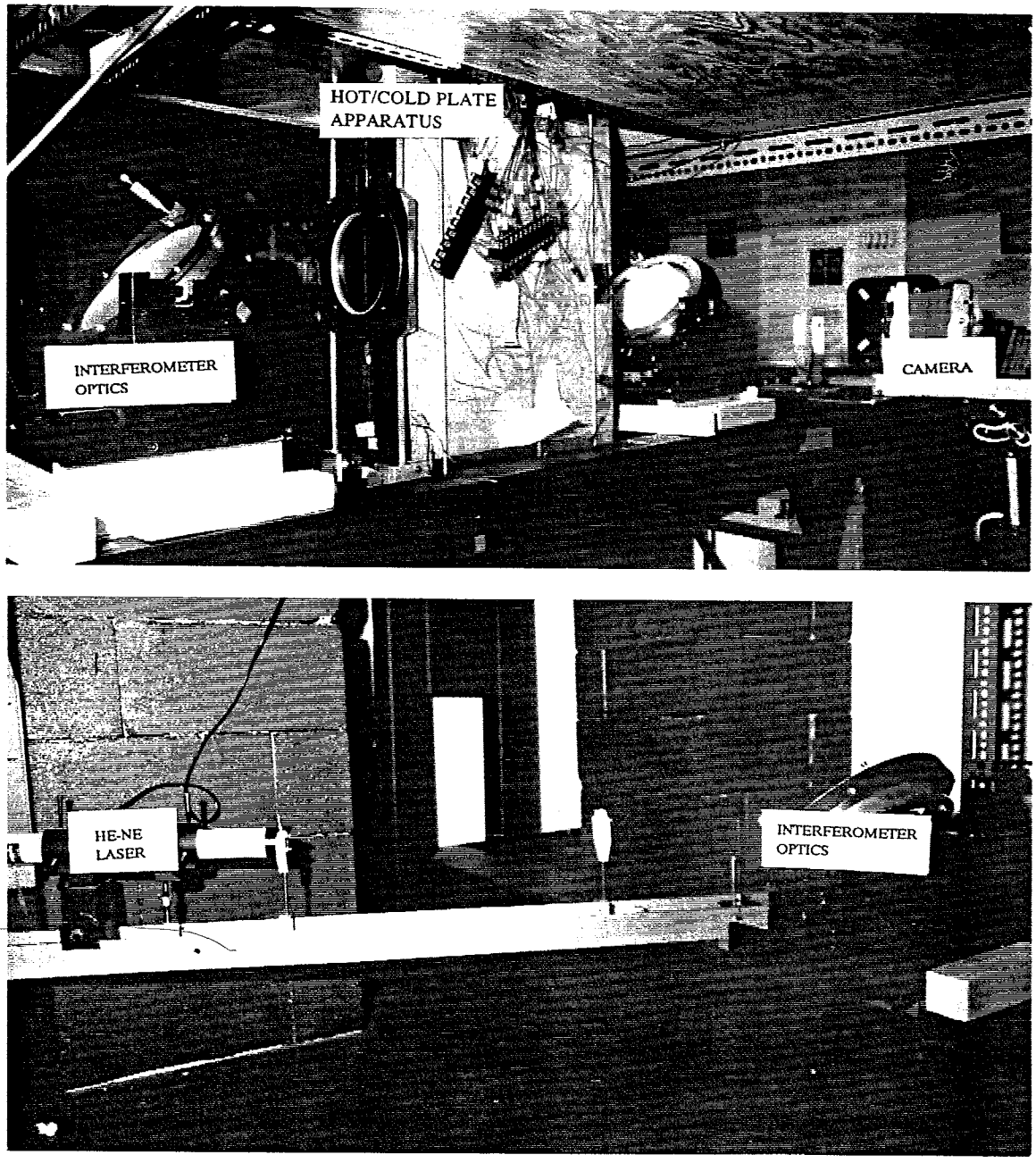

Fig. 2.5 Experimental Facility Showing Hot/Cold Plate Apparatus Integrated With Interferometer

in this report. The small scale hot-cold plate apparatus was used in the present study instead of the full-scale Guarded Hot Box apparatus described in the previous section. This is due to the severe funding restraint placed on the purchase of large optical windows required for the full-scale hot box (see Figures i.a to c). The small scale hot-cold plate apparatus was designed for integration with the Mach-Zehnder laser interferometer (described in the next section) using the existing small optical windows (Figures 2.6a to c). This limited the scope of this study to internal convection study only. The external convection coefficients will be evaluated in the next phase of this research when the large optical windows become available. The present full-scale apparatus will be modified by installing a large optical window covering the warm side and cold side and the air gap of the slot thereby serving the dual purposes of providing insulation and allowing light transmission through the slot (see Figures i.a to c).

The hot plate of the hot-cold apparatus was constructed of two 6.4 mm (1/4") thick aluminum plates. A nichrome heating wire was carefully installed in the grooves machined on one of the two aluminum plates and used as a heating plate. The heating plate was fastened to the other aluminum plate on which 29 copper-constantan thermocouples (see Figure 2.7) were installed to monitor the hot surface temperature. A 10 cm (4") thick polyurethane insulation was fastened to the hot plate assembly. An exploded view of the hot plate assembly is shown in Figure 2.7.

The cold plate was made of 13 mm (1/2") thick copper plate with a multiple-pass heat exchanger installed behind the plate. On the cold plate were also installed 29 copper-constantan thermocouples to monitor the cold surface temperature. The cold plate assembly was insulated with a 10 cm polyurethane. The exploded view of the cold plate is shown in Figure 2.8.

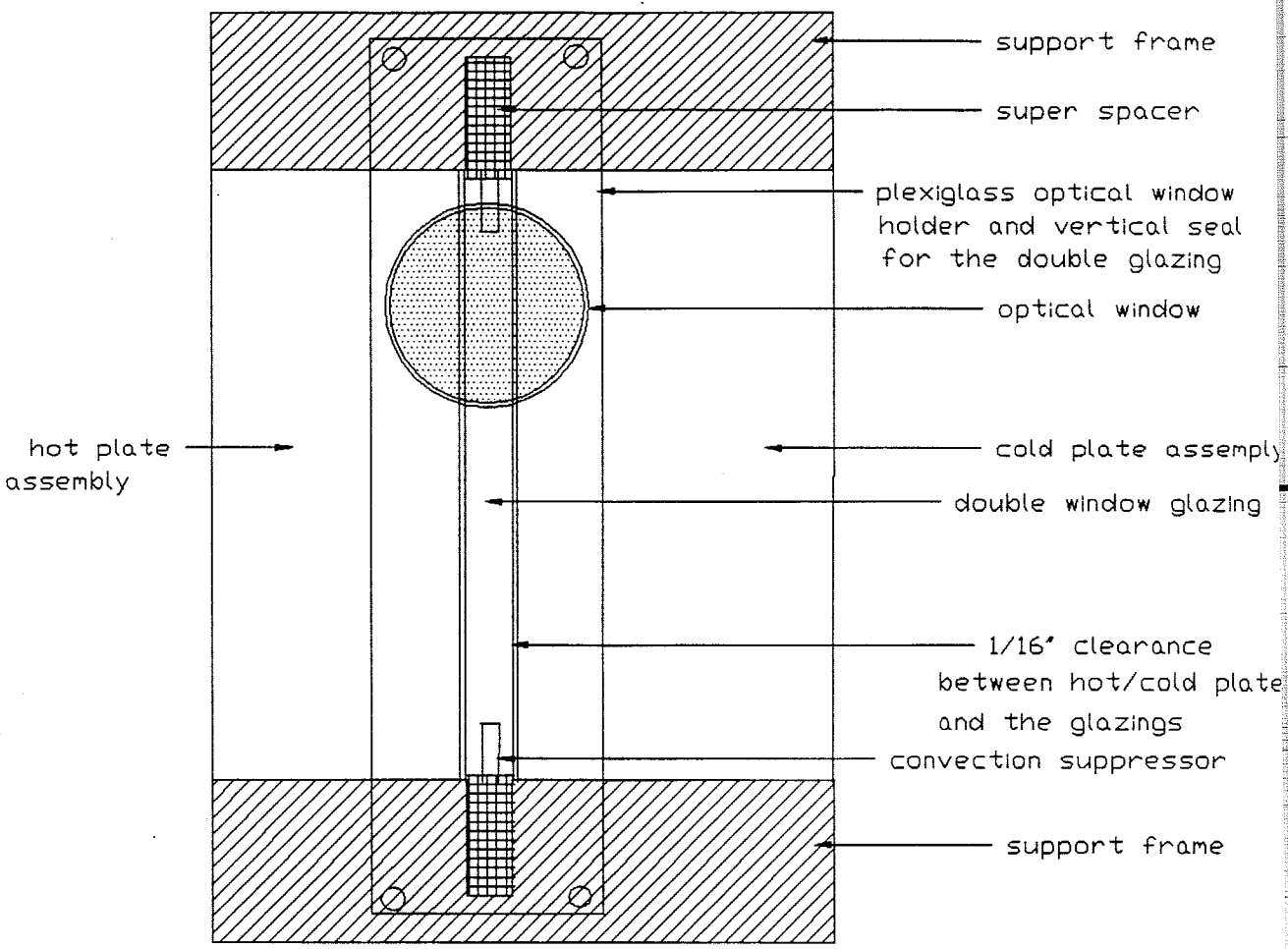

Fig. 2.6a Front View of the Hot-Cold Plate Apparatus Showing the Small Optical Window [Large Optical Window For Future Experiment is Shown in Fig. 6.1]

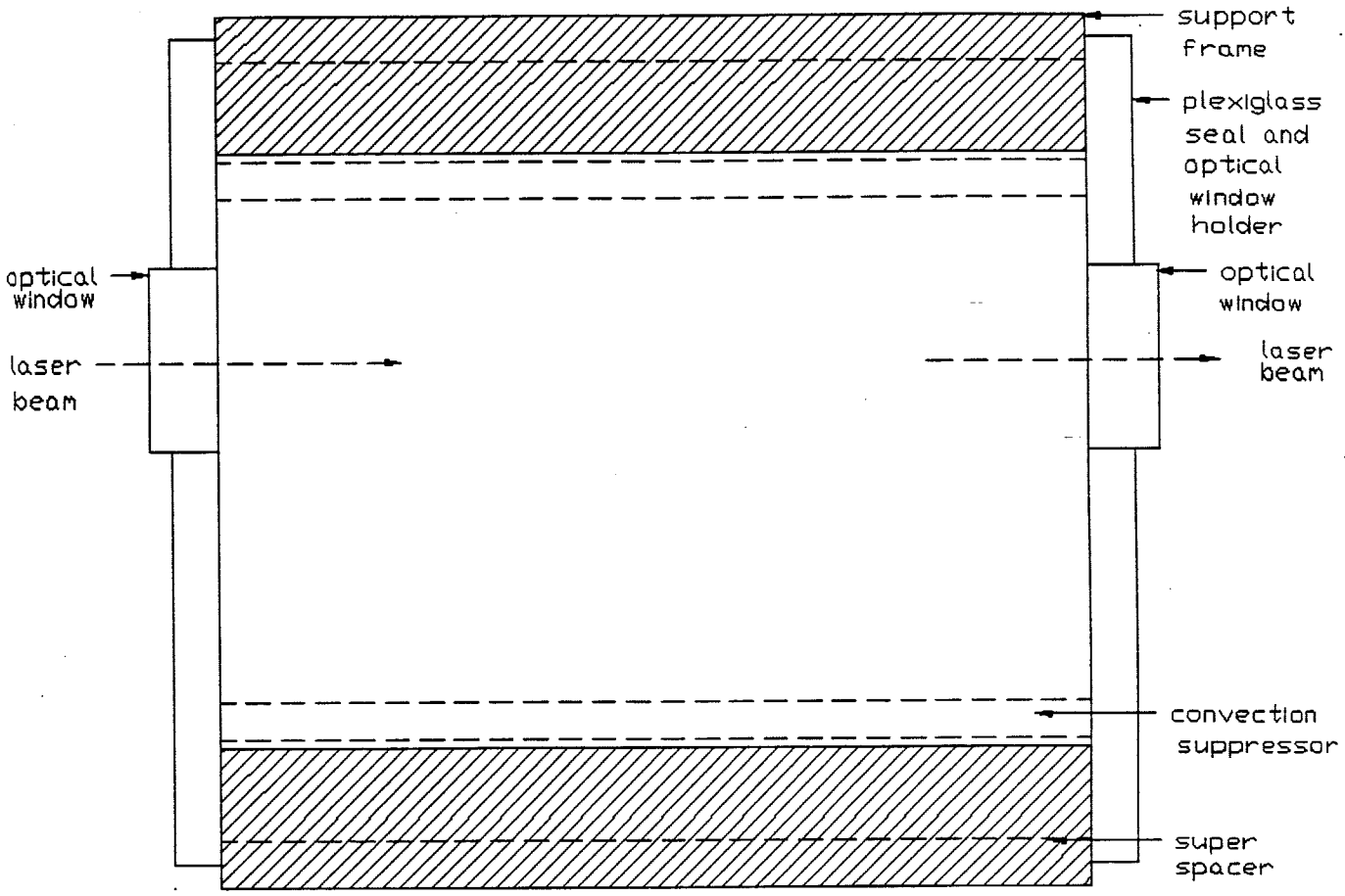

Fig. 2.6b Side View of the Hot-Cold Plate Apparatus Showing the Small Optical Window

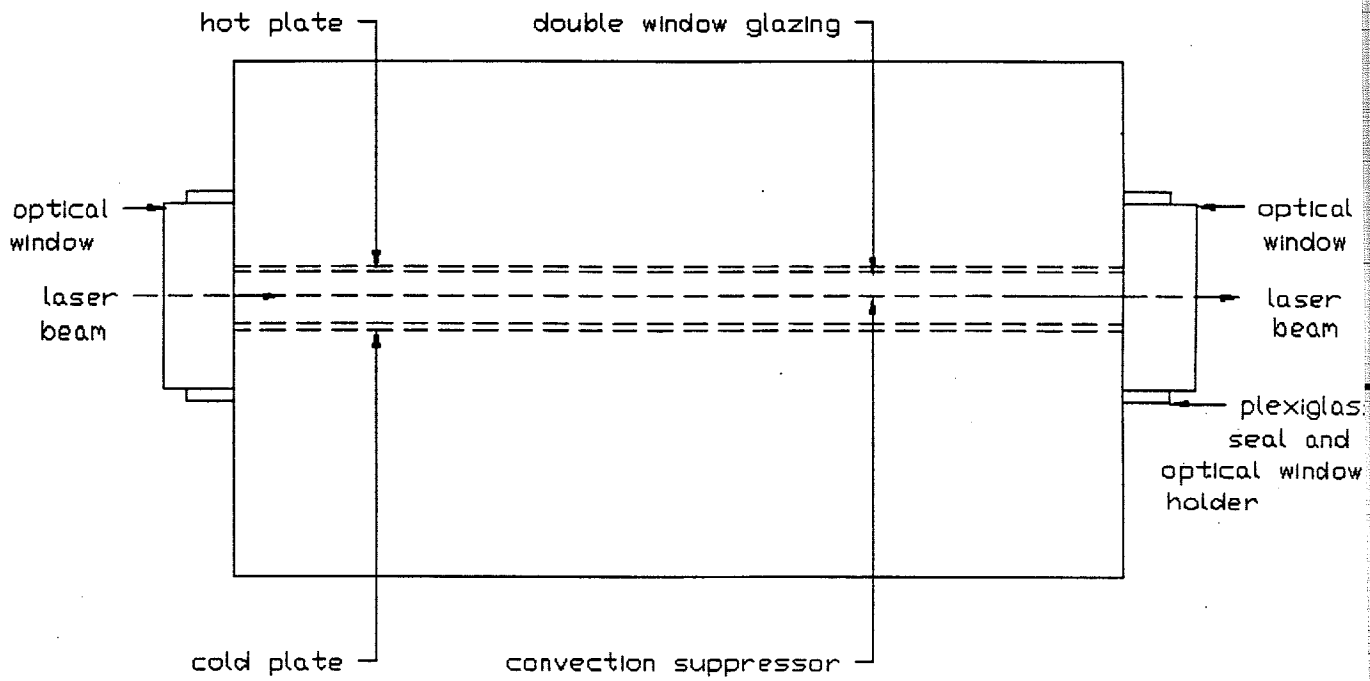

Fig. 2.6c **Top View of the Hot-Cold Plate Apparatus Showing the Small Optical Window**

The working-fluid of the heat exchanger is a solution of tri-ethylene glycol (TEG). The TEG solution was cooled and circulated through the heat exchanger by means of a 1/3 h.p. single phase recirculating pump. The hot and cold plate assemblies were installed on a traversing device which permits the up and down traversing of the entire hot-cold plate apparatus to which a pair of optical windows have been fastened (see Figure 2.5). The double window glazing to be tested was equipped with thermocouples to monitor the hot and cold glass surfaces temperature and then sandwitched between the hot aluminum and cold copper plates **allowing only 1.6 mm clearance between each plate and the double window glazing.** This is to ensure uniform temperature is achieved on the glazing surfaces. The hot-cold plate assembly with the double glazing serves as the test apparatus utilized in this study to evaluate the thermal performance characteristics of double window glazing.

2.3 MACH-ZEHNDER INTERFEROMETER

The Mach-Zehnder interferometer arrangement utilized in this study is shown in Figures 2.9a and b. The interferometer is capable of measuring the temperature field in a transparent medium such as in a confined air gap of a double window glazing. The present study is limited to the investigation of the internal heat transfer coefficient. Future studies will include the study of coupled internal and external film coefficients. A schematic of a Mach-Zehnder interferometer showing the direction of laser beam is shown in Figure 2.10. The light source of the interferometer is a continuous 5 mW linearly polarized and single mode Helium-Neon laser. The laser is capable of producing a monochromatic beam required for the operation of

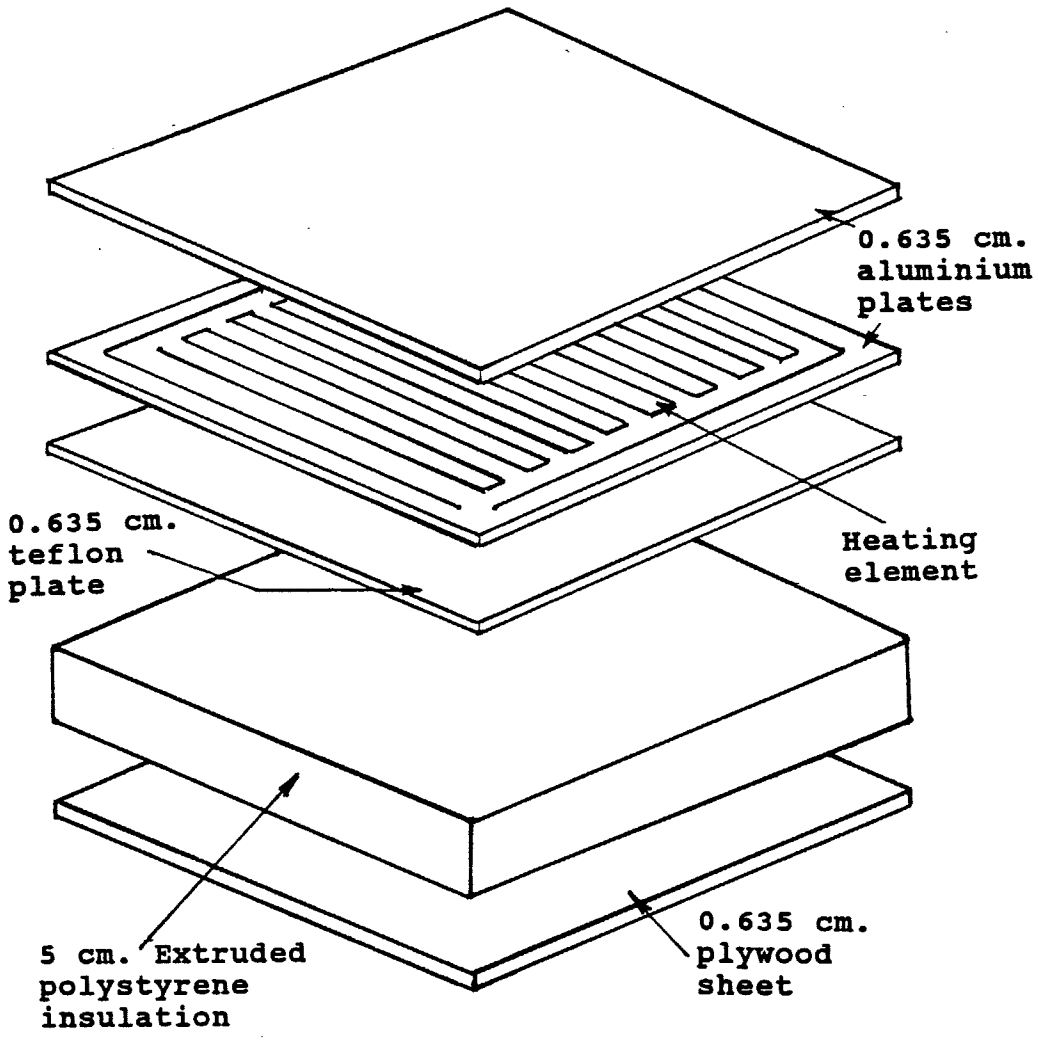

Fig. 2.7 Exploded View of the Hot plate Assembly

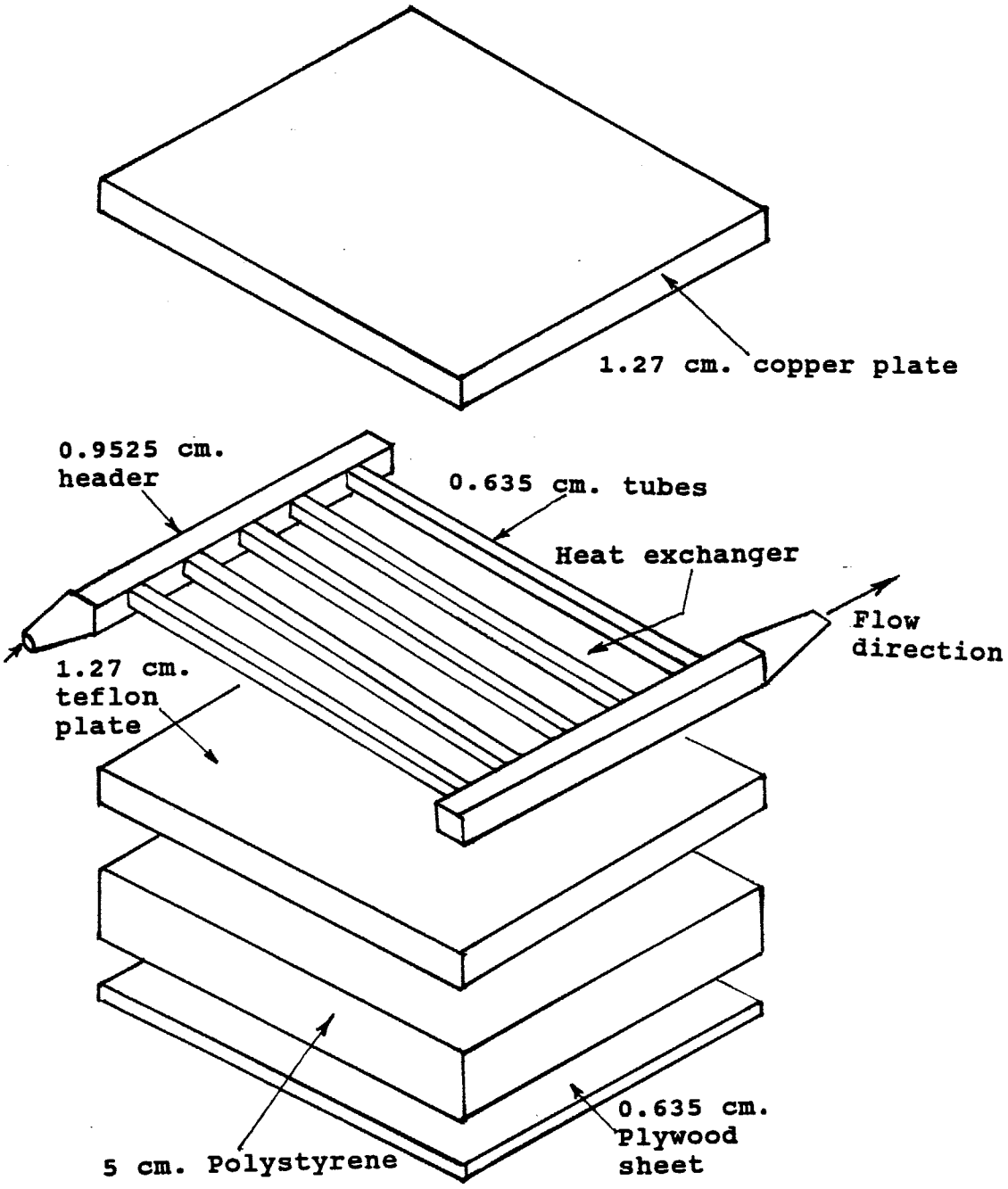

Fig. 2.8 Exploded View of the Cold Plate Assembly

the interferometer. Along the path of the laser beam are two double convex lenses of diameter 1.0 cm and 3.5 cm and focal length 1.5 cm and 20 cm respectively. The two lenses are used as collimators to expand and focus the laser beam onto a small 50 mm diameter plane mirror. The plane mirror reflects the beam onto a 20 cm diameter parabolic mirror which in turn reflects a parallel beam into the core optics of the interferometer. The core of the interferometer consists of two plane mirrors and two beamsplitters. All the core optics are 20 cm in diameter. The beamsplitters are half-silvered, and thus reflect and transmit equal portions of the incident beam. The plane mirrors are full-silvered and reflect practically all of the incident beam. The accuracy of the interferometer measurements depends largely on the quality of the core optics. Therefore, the core optics used here are made of a high quality industrial quartz with refractive index of 1.52 at 5461 A°. The optics are specified to be flat to 1/20 wavelength on the reflecting surface and 1/10 wavelength on the back surface. The surfaces are parallel to within 2.54×10^{-3} cm.

2.3.1 Operating Procedure Of Mach-Zehnder Interferometer

As shown in Figure 2.10, the parallel beam emanating from the parabolic mirror H enters the core optics of the interferometer at the first beamsplitter D where it splits into two equal beams. One half of the beam (the test beam) is reflected to mirror E which in turn reflects the beam such that it traverses the air gap region of a double window glazing unit placed at the test-section of the interferometer. The other half (the reference beam) passes through the undisturbed air in the room to incident on mirror G which reflects it such that it recombines with

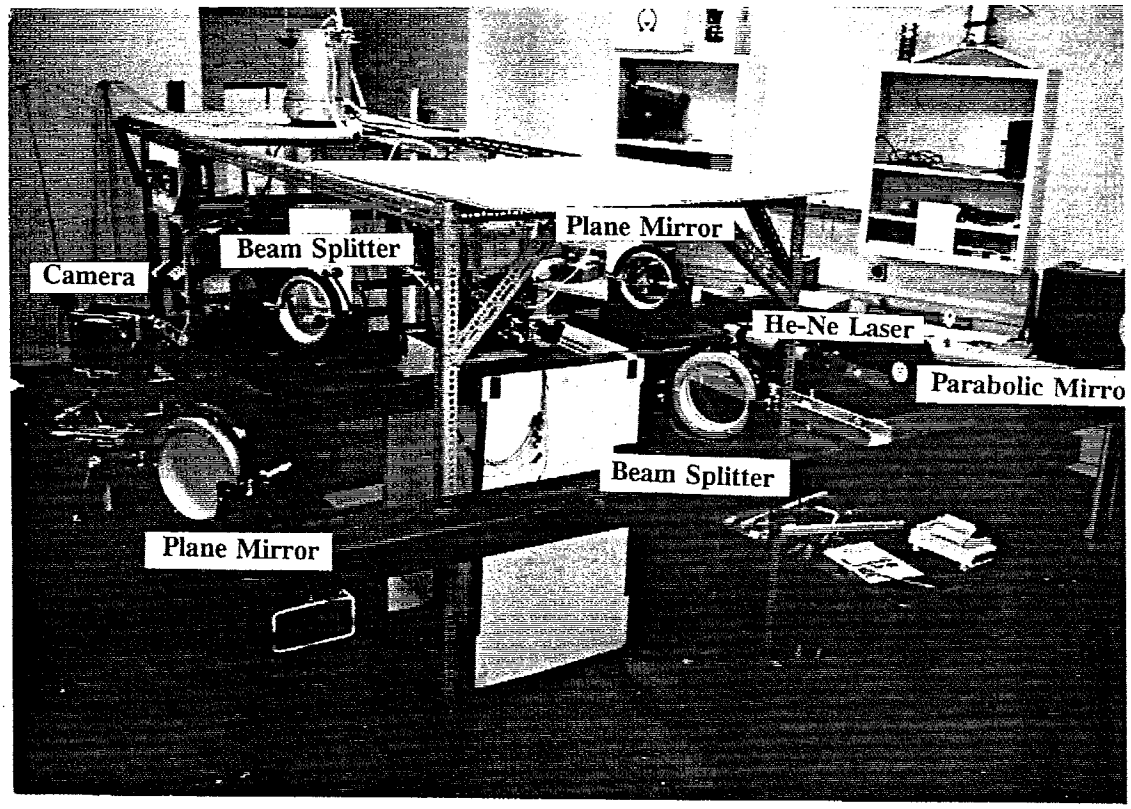

Fig. 2.9a Mach-Zehnder interferometer Showing the Optical Arrangement

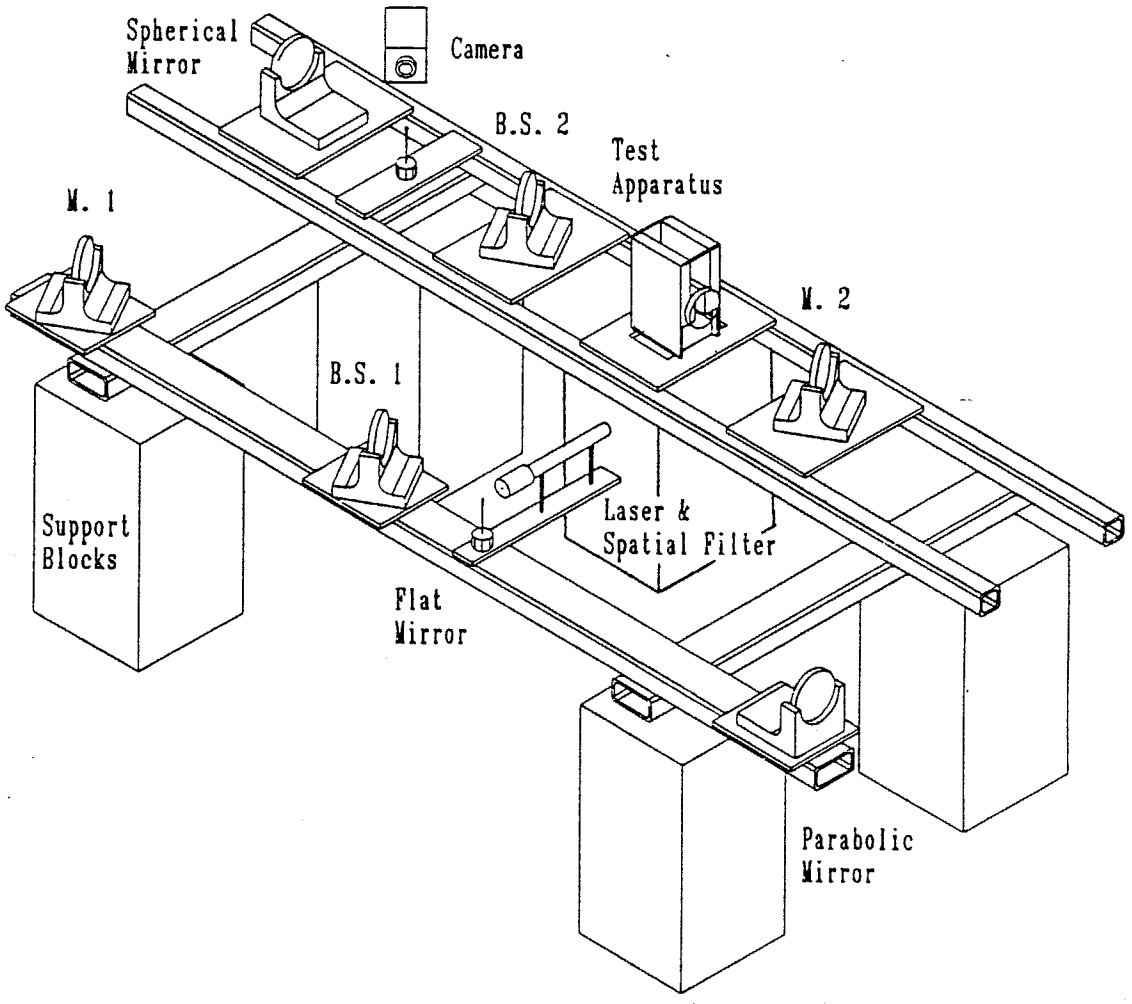

Fig. 2.9b Layout of Interferometer Showing Major Components

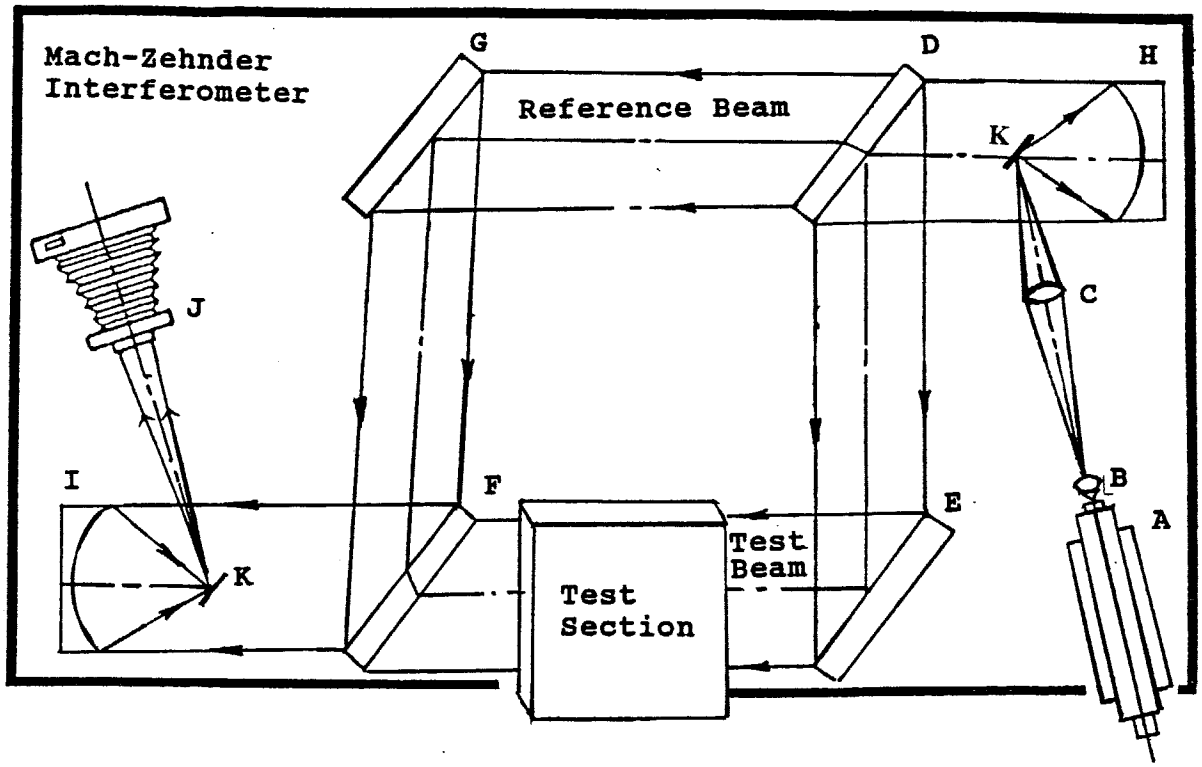

A. He-Ne 5mW laser
B. Expanding lens } Collimating lenses
C. Condensing lens
D. First beam splitter (20.3 cm. diameter)
E. First plane mirror (20.3 cm. diameter)
F. Second beam splitter (20.3 cm. diameter)
G. Second plane mirror (20.3 cm. diameter)
H. Parabolic mirror (20.3 cm. diameter, 162.5 cm. focal length)
I. Spherical mirror (20.3 cm. diameter, 78.70 cm. focal length)
J. Calumet Copal N.3 Polaroid camera
K. Diagonal mirror (1.0 cm. diameter)

Fig. 2.10 A Schematic of the Mach-Zehnder Interferometer Showing the Direction of the Laser Beam

the first half beam at the second beamsplitter F. The recombined beam produces an interference fringe pattern. The interference beam is then focused onto a small plane mirror K by the spherical mirror I. The plane mirror reflects the interference beam onto an object screen for visualization or onto the polaroid camera J where the interference pattern is instantly recorded and kept for post-processing.

When the optical components of the core region (the two full and the two half-silvered mirrors) of the interferometer are exactly parallel to each other, the field on the screen is either uniformly dark or bright depending on whether the lengths of the optical paths of the two equally divided beams differ by an even or odd number of half wavelength respectively. When the lengths of the optical paths of these two beams differ by an even number of half wavelength, the light waves of the two beams are in phase and there is an amplification. If the length of the optical paths are differ by an odd number, then the two beams are out of phase and they extinguish each other. This phenomenon is referred to as an **infinite fringe condition**, Figure 2.11. If two of the four core optics are turned through a slight angle such that the two equally divided beams recombine at an angle to each other, then a succession of dark and bright fringes appears. This succession of dark and bright fringes is due to the difference in the lengths of the optical paths of the two beams, which unlike in the infinite case, varies continuously (from place to place). This new setting is referred to as a **finite fringe condition**, Figure 2.12. Further details of this phenomenon can be found in (Goldstein, 1976) and (Showole, 1988). Either of these two fringe settings can be used for analysis. The choice of the fringe setting depends on the medium and the boundary conditions under investigation. Both fringe settings have advantages and disadvantages. These are given below:

Fig. 2.11 Infinite Fringe Interferogram

Fig. 2.12 Finite Fringe Interferogram

2.3.2 Advantages Of Finite Interferograms

* finite fringe interferograms can be easily obtained, so a constant monitoring or adjustment of the interferometer optics is not necessary

* small thermal gradients (ie small number of fringes) or fringe distortions can be analyzed accurately

* finite fringe interferograms can be used to analyze thermal gradients in irregular objects and large models

* finite fringe patterns are less sensitive or vulnerable to minor vibrational disturbances

* higher accuracy can be achieved due to a well defined reference fringe shift

2.3.3 Disadvantages Of Finite Interferograms

* a reference fringe shift must be calculated before analysis

* a finite fringe shift does not represent an isotherm

* finite fringes do not in general demonstrate clearly the flow patterns and cannot be used for flow visualization or a qualitative study except by a well trained personnel

2.3.4 Advantages Of Infinite Interferograms

* fringe shift field directly represents isotherm or constant temperature map

* flow pattern can be inferred from the infinite fringe field where the Prandtl number (ν/α) is close to unity (ie infinite fringe field can be used for flow visualization or a qualitative study)

2.3.5 Disadvantages Of Infinite Interferograms

* infinite fringe interferograms cannot be easily obtained, so a constant monitoring or adjustment of the optics is necessary to maintain interference

* infinite fringe setting is sensitive to slight vibration and minor disturbances
* number of fringes in the field must be at least five or more to be good for analysis
* infinite fringe interferogram is not as accurate as finite fringe field

2.3.6 Interferometric Equations For Temperature Determination

In this project, the finite fringe interferograms were used for analysis (or quantitative) study while the infinite interferograms were employed for the temperature visualization (or qualitative) study. The fringe shift, ε, obtained from the analysis of the finite interferogram (see Appendix A) was related to the index of refraction of the window air gap medium as follows

$$\varepsilon = L/\lambda_o \, (\eta_r - \eta) \tag{2.1}$$

where λ_o = wavelength in vacuum and η_r is the refraction index in the reference medium and η the refraction index in the heated air gap medium, **L** is the length of the air gap.

According to the Lorenz-Lorentz relation (see Goldstein, 1976) the index of refraction of a homogeneous transparent medium, as in the present study, is primarily a function of density, ρ, given as

$$(\eta^2 - 1)/\rho(\eta^2 + 2) = \text{Constant} \tag{2.2}$$

For gases the refractive index is close to unity (η_{air} = 1.0002716), therefore, Equation (2.1)

reduces to

$$2(\eta - 1)/3\rho = G(\lambda) \qquad (2.3)$$

where $G(\lambda)$ is called the Gladstone-Dale constant whose value is given as 1.51×10^{-2}. By combining Equation (2.3) with the ideal gas law, $\rho = P/RT$, yields

$$2(\eta-1)RT/3P = G(\lambda) \qquad (2.4)$$

Substitution of Equation (2.4) into Equation (2.1) gives

$$\varepsilon = (3G(\lambda)LP)/2R\lambda.(1/T - 1/T_r) \qquad (2.5)$$

By rearranging Equation (2.5) yields

$$T = T_r/(1+(2RT_r/3LPG(\lambda))\lambda\varepsilon) \qquad (2.6)$$

Equation (2.6) is a relationship between the fringe shift and the temperature. The technique used for the evaluation of fringe shifts from a finite interferogram was described in Appendix A.

2.4 THE COMPARATOR (TRAVELLING MICROSCOPE)

The measurement of fringe shifts in an interferogram is made with an optical comparator

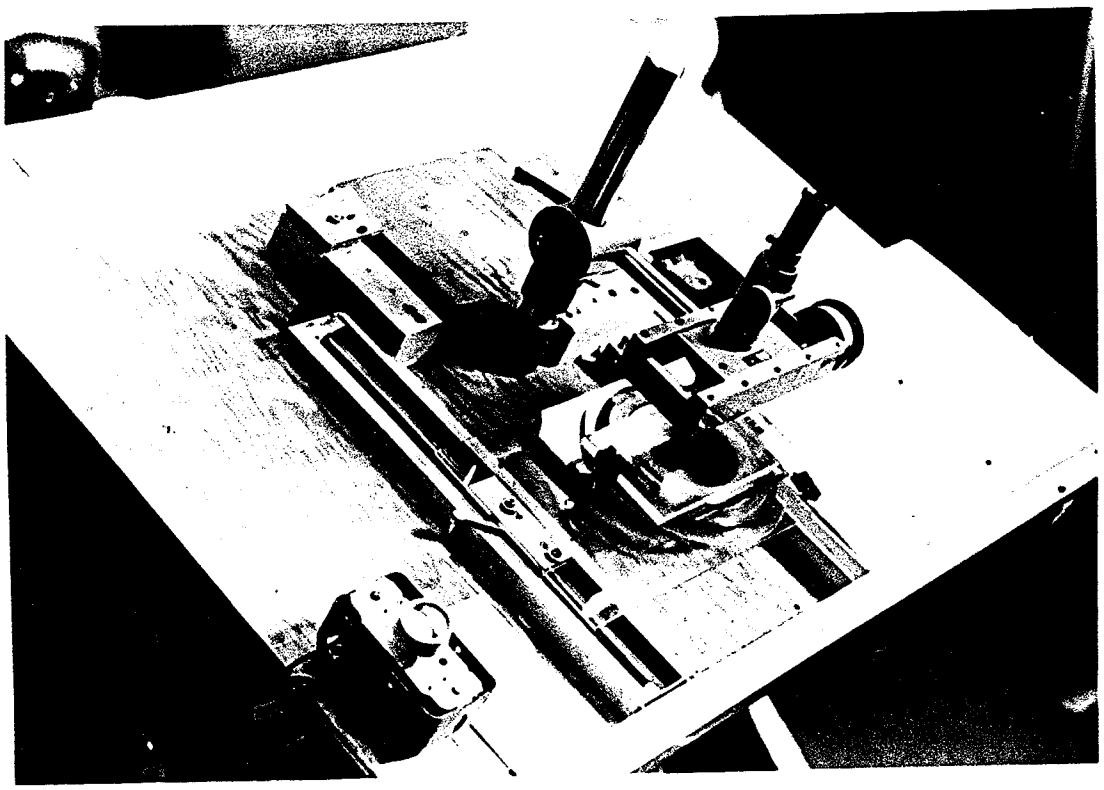

Fig. 2.13 The comparator- The fringe reader arrangement showing the travelling microscope, the jig-mount and the vernier scale

- a travelling microscope. A comparator shown in Figure 2.13 consists of a projection bulb, lens and mirror arrangement which projects interferograms onto a ground screen. Two glass plates mounted in a holder attached to the comparator table are used to clamp in position the interferometric picture to be analyzed. The comparator table could be translated in the horizontal and vertical directions by means of micrometer dials which are graduated in .00001" increments. The comparator can be used to measure both the finite and infinite fringe shifts, but the analysis techniques for the two fringe shifts are different.

2.5 THE DOUBLE WINDOW GLAZING MODEL

The double window glazing model used in this study was constructed of one plane glass and one low-e coated glass on the surface facing the air gap. The glasses and super spacer were supplied by Edgetech Limited, Ottawa Ontario. The glass dimensions are 43.18 cm (17") by 45.72 cm (18") and the thickness is 2.5 mm (1/10") (see Figure 2.14). The supper spacer separating the glazing and forming the top and bottom end wall surfaces of the slot has a dimension of 6.35 mm (1/4") high, 1.27 cm (1/2") wide and 45.72 cm (18") long. The super spacer was made of a desiccant material and therefore capable of absorbing the moisture in the air gap. The removal of the condensing moisture from the air gap is absolutely necessary for efficient operation of the interferometer.

Figures 2.14 and 2.15 show different features of an assembled double window glazing. The inside surface of the warm glass was selectively coated with Low-e material and was

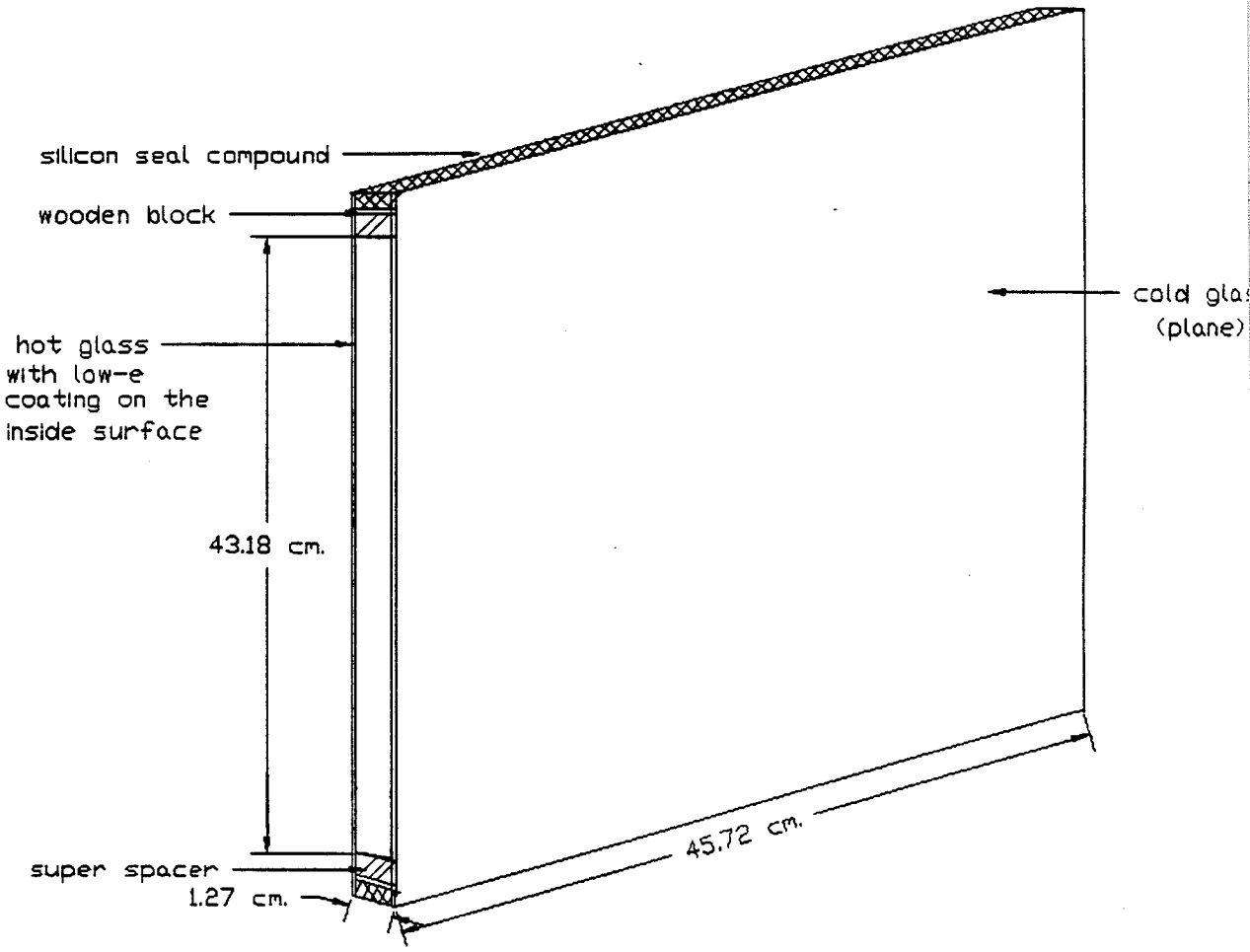

Fig. 2.14 Double Window Glazing Assembly Without Suppressor

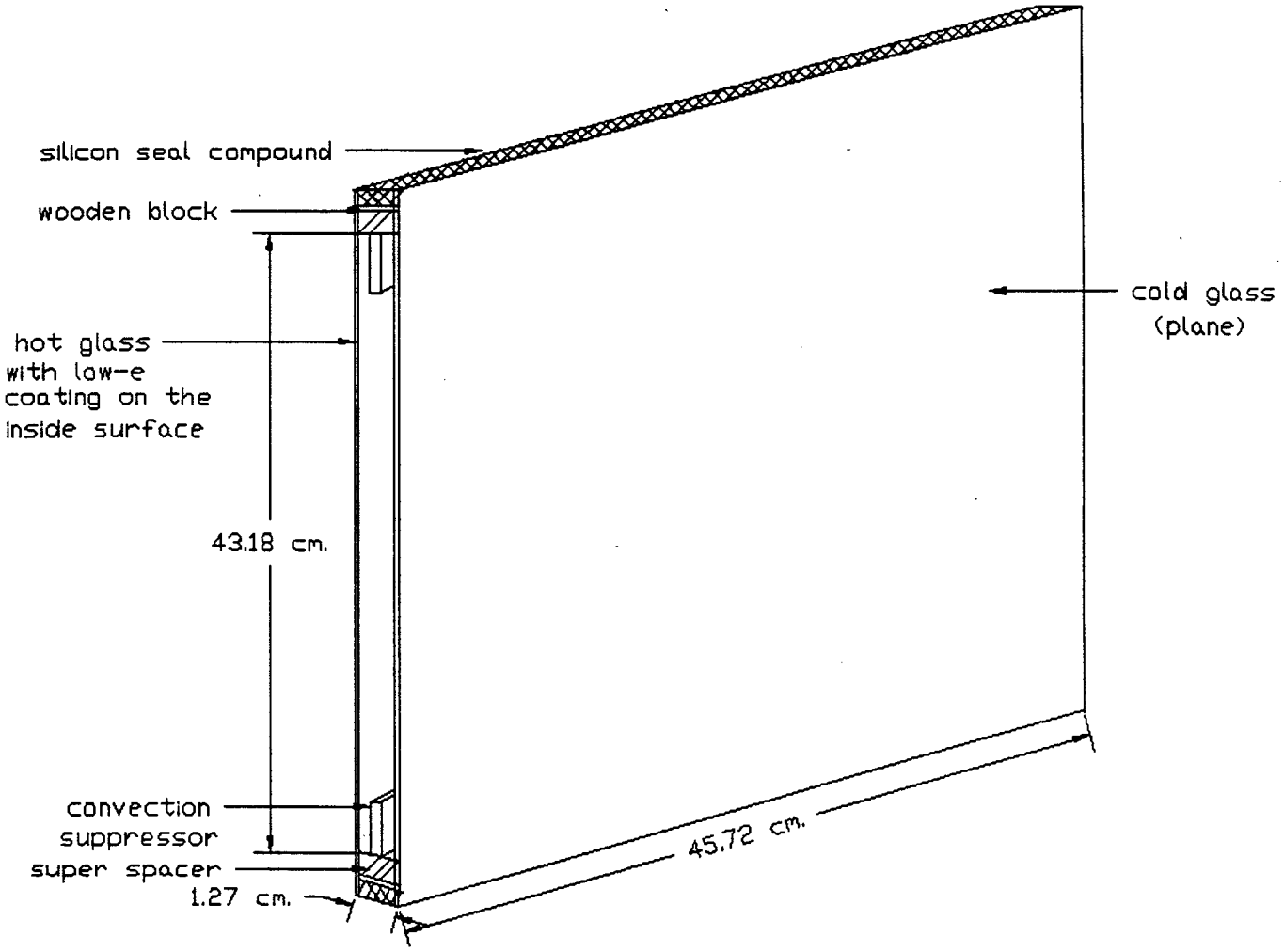

Fig. 2.15 Double Window Glazing Assembly With Convection Suppressor

separated from the uncoated plane cold glass by a super spacer. The super spacer is flexible and therefore supported by a wooden spacer block from behind to maintain rigidity (see Figures 2.14 and 2.15). The rigidity makes the inside surface of the spacer flat and straight. The straightness is necessary to prevent distortion of the interferometer laser beam passing through the air gap. The top and bottom edges were sealed with a silicon compound and allowed to cure before assembling the window glazing and the hot-cold plate apparatus. The air gap opening was sealed with a plexiglas face-plate which holds the optical window (see Figures 2.5 and 2.6). The gasket between the plexiglas face-plate and the double glazing provides a tight seal.

3. MEASUREMENT PROCEDURE

The primary objective of the interferometric experiment is to measure the temperature gradients, $dT/dx\,|_w$, at the surfaces of the hot and cold glazings and the top and bottom end walls of a double-glazing. The temperature gradients are then used to determine local heat transfer coefficients under varying hot and cold glass temperatures. In this section the measurement procedures that were used to accomplish this objective are described. The interferometer/window glazing alignment, the test run procedure, the interferometric data reduction procedures, and the procedure for obtaining the heat transfer results are described and discussed.

3.1 TEST RUN PROCEDURE

After the operating procedure described in section 2.3.1 was accomplished, the test

section holding the window glazing to be tested was properly aligned relative to the rays of the interferometer light beam (see Figure 3.1). The test section was mounted on a traversing device and was advanced to its lowest position for the first of five pictures required to cover the entire height of the window slot. The height of the slot was 43.2 cm (17") and the interferometer light beam was only 20 cm in diameter.

The first step in the measurement procedure was to bring the hot and cold glass surfaces to the desired temperatures. For the hot glass, this is simply accomplished by switching on the power supply to the heating plate. With the aid of a temperature controller which could be pre-set to the desired temperature, the steady state generally takes approximately 15 minutes. In the case of the cold glass the procedure was rather tedious. The temperature of the triethylene to be circulated to cool the cold plate was maintained at 10 to 20 degree below the cold plate temperature. This generally required the cold temperature bath be turned on 48 hours before the experiment. With a temperature controller replacing the thermostat of a domestic deep freezer used as the cold temperature bath in the experiment, the TEG could be cooled to -30°C. The TEG circulator was turned on and allowed to stabilize at the desired cold temperature. After this, the heating was turned on. When the temperature equilibrium was attained in the entire system, the interferograms pictures were taken. As mentioned earlier, the procedure was to advance the test section holding the window glazing at approximately 8.6 cm (3.4") intervals between picture taking. The positions at which the pictures were taken were pre-determined by attaching thin needles to the edge of the warm surface at these positions. The needles protrude into the air gap and cast their shadows on the interferometric pictures. A record was maintained of the pictures and the respective test positions. After observing from the interferogram on the

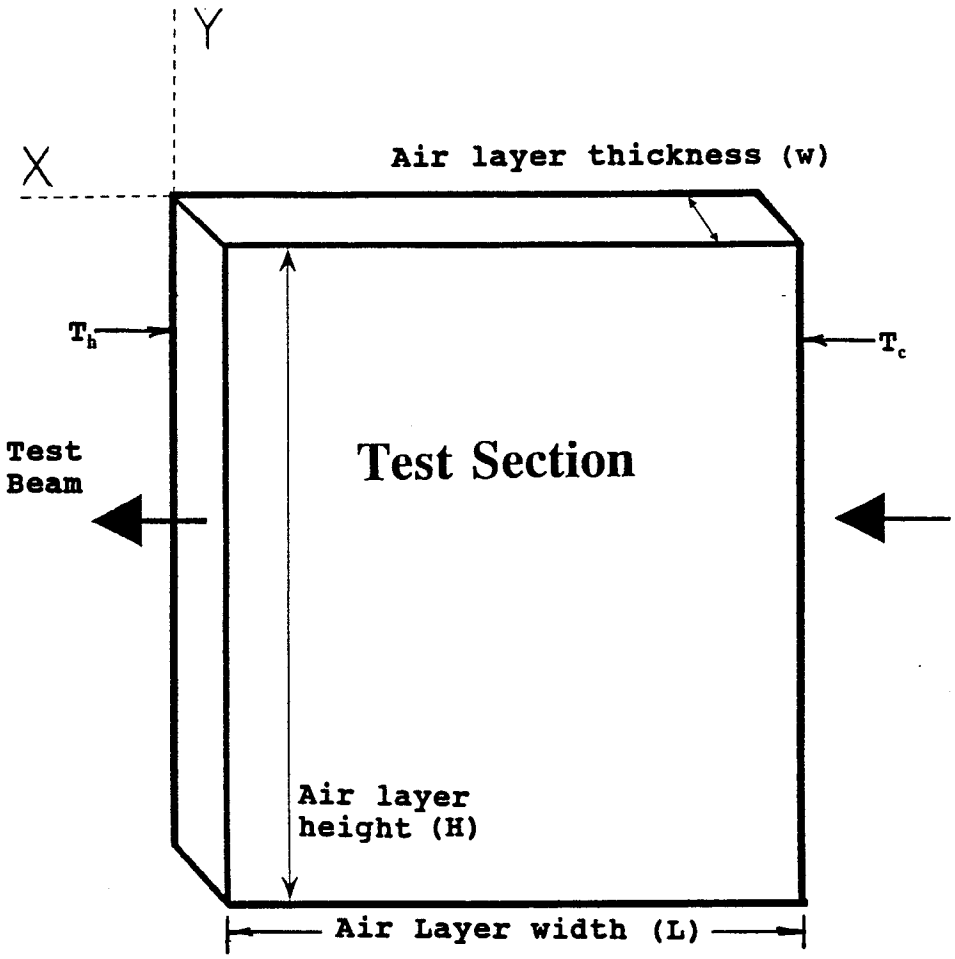

Fig. 3.1 **Schematic Showing the Laser Beam Traversing the Air Gap of a Double Window Glazing Unit**

screen that the vibration has been adequately subsided and the steady equilibrium state of all components maintained, the interferogram pictures were taken. If the fringes were observed to be completely steady only one picture was taken. If slight movement of the fringes due to the unsteady nature of the natural convection process is observed, three pictures were taken so that the best of the three could be chosen. As mentioned in the previous section, both finite and infinite fringe interferograms were taken. The finite fringe interferograms were analyzed, but the infinite fringe interferograms were taken only to provide a descriptive qualitative record of the temperature contours and were not analyzed. All the interferogram pictures were taken with 10.14 cm x 12.7 (4" x 5") type 55 polaroid film and 1/25 second shutter speed.

As soon as the interferogram pictures had been taken the following important measurements needed for analysis were made:

* The temperatures of the heating and cooling plates and of the hot and cold glass surfaces were recorded by the copper-constantan thermocouples imbedded in the plates or attached to the glass surfaces.

* The temperature in the laboratory room was measured by a thermocouple attached to the digital thermometer and a mercury in glass thermometer. Each of these devices were located in the opposite sides of the room. The average of the two readings was taken as the true room temperature.

* The wet bulb temperature was measured by a standard sling psychrometer. The relative humidity of the laboratory room was also determined.

* The atmospheric pressure of the laboratory room was recorded by a mercury barometer.

The interferograms were developed few minutes after the test run to separate the negative and positive parts of the polaroid film . The positive was examined immediately to determine if the test run was to be repeated. If the test proved valid, the negative was kept for analysis

otherwise would be discarded and the experiment repeated.

3.2 DATA REDUCTION PROCEDURE

As mentioned earlier, the goal of an interferometric experiment is to evaluate the temperature gradient, dT/dx, on the boundary surfaces of the air layer in window slot. The local conductive heat flux on these wall surfaces can then be expressed as

$$q'' = -k_w \, dT/dx \Big|_{wall} \qquad (3.1)$$

where k_w is the thermal conductivity of air evaluated at the wall temperature.

The standard approach is to present the heat transfer results in a non-dimensional form defined as

$$Nu_y = hW/k_m \qquad (3.2)$$

where, Nu_y = local Nusselt number

h = local heat transfer coefficient

W = width of the air gap along the x-axis

k_m = thermal conductivity evaluated at the mean air gap temperature, $(T_h + T_c)/2$.

The local heat transfer coefficient is defined as

$$h = q''/(T_h - T_c) \qquad (3.3)$$

By combining equations (3.1), (3.2) and (3.3) we express local Nusselts number as

$$Nu_y = -(k_w/k_m) \cdot W/(T_h-T_c) \cdot dT/dx \Big|_{wall} \qquad (3.4)$$

The temperature gradient at the glass surface can be expressed in non-dimensional form as

$$dT/dx = (T_h-T_c)/W \cdot dT^*dx^* \qquad (3.5)$$

where, $T^* = (T - T_c)/(T_h - T_c)$

$x^* = x/W$

Substitution of Equation (3.5) into (3.4) yields

$$Nu_y = -(k_w/k_m)\, dT^*/dx \Big|_{wall} \qquad (3.6)$$

The average Nusselt number was then calculated as follows

$$Nu_{ave} = 1/H \int_0^H Nu_y \, dy \qquad (3.7)$$

where H is the height of the enclosure along the y-axis.

A computer analysis program based on a method of a least squares regression using a third order polynomial equation was developed. By using this computer program and the

interferometric raw data from the comparator, the coefficients of the polynomial equations were obtained. With these coefficients, local temperature was then calculated at any point desired in the enclosure. The temperature gradients at the surface were evaluated and used to calculate the local Nusselt numbers. The average Nusselt number was then obtained by integrating the local Nusselt numbers over the surface. The computer program is available upon request.

To calculate the thermal resistance due to the convection coefficient, the average Nusselt number obtained above can be related to the thermal conductivity, k, of the air in the enclosure and the effective thermal conductivity, k_e, defined as

$$Nu_{ave} = k_e/k \tag{3.8}$$

The effective thermal conductivity can be related to the thermal resistance, R-value, by the following expression:

$$R = W/k_e \tag{3.9}$$

where W is the thickness of the air layer between the glazings.

The contribution of convection thermal resistance to the overall thermal transmittance, U-value can be estimated as:

$$U_{conv.} = 1/(R + R_h + R_c) \tag{3.10}$$

where R_h and R_c are the external film resistances on the hot and cold glass surfaces and can also be obtained by measuring the heat transfer coefficients on the external surfaces using the

interferometric technique as demonstrated above for the internal heat transfer coefficient. To evaluate R_h and R_c the external film coefficients h_h and h_c on the hot and cold glass surfaces must be measured. This measurement will be carried out in future studies when a large optical window (see Figure i.a to c) becomes available. Because of the experimental limitation imposed by the presently available small optical window the measurements of h_h and h_c are not possible and hence the evaluation of R_h and R_c are not covered in this report.

4. TEST RESULTS AND DISCUSSION

An interferometric technique was employed in this study particularly for the visualization and the analysis of natural convection heat transfer characteristics in the air layer enclosed between two differentially heated window panes. Following the determination of the heat transfer characteristics, a convection barrier was introduced to suppress convection eddies occurring in the bottom and top corner regions of the slot to reduce heat losses or convection cooling in the region and consequently to eliminate window condensation.

A total of 16 test runs were made with the double window glazing subjected to varying conditions. The results of these test runs are summarized in Table 4.1 and shown graphically in Appendix B. The finite and infinite interferograms as well as the calculated isotherms for the 16 test runs are also shown in Appendix B. Because of the space limitation only the top, central and bottom sections are shown in Appendix B for each of the finite and infinite interferograms. However, the calculated isotherms from the analysis of the interferograms shown on the same

Table 4.1

Summary of Results

Test Run No.	T_h °C	T_c °C	ΔT	W cm.	AR	H_s/H	Gr_w x10^3	Gr_H x10^8	Nu_{cc}	Nu_{ave}
1	23	9	14	1.27	34	0	4.2	1.7	.9924	1.114
2	20	3	17	1.27	34	0	5.6	2.2	.9899	1.153
3	20	0	20	1.27	34	0	6.6	2.6	.9852	1.178
4	20	-3	23	1.27	34	0	7.8	3.1	.9897	1.212
5	18	-6	24	1.27	34	0	8.6	3.4	1.053	1.249
6	19	-9	28	1.27	34	0	10.	4.0	1.065	1.279
7	20	-6	26	.953	45	0	3.8	3.6	.9866	1.003
8	20	-9	29	.953	45	0	4.4	4.1	.9824	1.009
9	20	-9	29	1.59	27	0	20.	4.1	1.454	1.655
10	19	-9	28	1.91	22	0	34.	4.0	1.538	1.809
11	19	-6	25	1.27	34	0.056	8.8	3.5	1.078	1.229
12	20	-6	26	1.27	34	0.118	9.2	3.6	1.059	1.272
13	19	-6	25	1.27	34	0.235	8.8	3.5	1.099	1.263
14	18	-6	24	1.27	34	0.471	8.5	3.3	1.871	1.195
15	20	-6	26	1.27	34	0.056*	9.1	3.6	1.066	1.315
16	21	-9	27	1.91	22	1.0**	36.	4.2	1.486	1.553

H_s/H = Suppressor height to Cavity height ratio

* Suppressor on top and bottom sections of the slot

** H_s/H = 1 (Full partition or tripple glazing).

CC (centre cell)

plate covers the entire height of the vertical slot. For the purpose of clarity the discussion of the results are presented in two parts. The first part (runs 1 to 10) covers the natural convection heat transfer characteristics in window slot without convection suppressor or barrier. The second part (runs 11 to 16) considers the cases where convection barriers had been introduced into the slot to suppress convection eddies.

The parameters studied can be expressed as a function of the average Nusselt number given as

$$Nu_{ave} = f(Gr_W, Pr, W/H) \tag{4.1}$$

where Gr = Grashof number defined as:

$$Gr_W = g\beta W^3(T_h - T_c)/\nu^2 \tag{4.2}$$

and Pr = Prandtl number defined as:

$$Pr = \nu/\alpha \tag{4.3}$$

The Rayleigh number, Ra, can then be defined as:

$$Ra_w = Gr_w \times Pr \tag{4.4}$$

The above parameters except the height, H, and the Prandtl number, Pr, were varied over the range permitted by the present experimental apparatus. The effects of the parameters were determined. The height, H, was fixed and the range of aspect ratio, $22 \leq H/W \leq 45$ was

covered. This is equivalent to a variation of the air gap width between 0.95 cm (3/8") and 1.9 cm (3/4"). The Gr_W was varied by varying both the air gap width, W, and the temperature difference, ΔT. But the former allowed a wider coverage of Gr_W to include cases of unicellular and multicellular natural convection to be discussed later.

It is of importance at this point to indicate that the work presented in this report is not an energy balance on the differentially heated air layer in the two-dimensional slot. This work is devoted only to the natural convection characteristics which constitutes a portion of the total heat transfer. The total heat transfer which is beyond the scope of this study is the sum of the conductive, convective and radiative heat transfer. But an understanding of the convective heat transfer characteristics is pertinent to the development of advanced energy efficient window system, and is the focus of the present study.

4.1 NATURAL CONVECTION IN WINDOW AIR GAPS WITHOUT SUPPRESSOR

The natural convection in window air gaps without suppressor is a practical case of the problem of a long vertical slot heated from one side. This problem and that of a horizontal slot heated from below have been widely studied in the past with little or no variation in the boundary conditions. In the case of the horizontal slot commonly referred to as the "Benard cell" problem the fluid in the slot is completely stationary (dead air) when the Rayleigh number is less than the critical, that is, $Ra_c < 1708$. The Ra_c for horizontal slot has been given by [Chandrasekhar, 1961] to be 1708. In contrary to the horizontal slot the fluid motion occurs in the vertical window slot at any finite Rayleigh number. Batchelor [1954] and many researchers

have reported similar observation in long slender vertical slot heated from one side. Because fluid motion exists at a relatively smaller Rayleigh number in vertical slot (including the conduction regime) as compared to the horizontal slot, the results and discussion of the heat transfer characteristics in this study are subdivided into three regimes: (i) conduction regime ; (ii) flow instability and transition regime; and (iii) boundary layer flow regime as illustrated in Figure 4.1(a). To investigate the three regimes the aspect ratio of the vertical slot must satisfy the following relation given by Gill and Davey [1969]:

$$A > 30 \times Pr \qquad (4.5)$$

For air with Pr = 0.71, the aspect ration should be greater than 21 for the fluid motion to cover the three regimes. The aspect ratio of the vertical window slot considered in this study ranges between 22 and 45. Therefore, this study covers all of the above flow regimes.

4.1.1 Conduction and Flow Instability

The fluid motion which exits in the vertical slot at low Rayleigh number consists of one large stable cell which fills the cavity with the fluid rising on the hot wall, falling on the cold and turning at the top and bottom end walls. No convective heat transfer occurs as a result of this motion which is characterized by conduction heat transfer in the central region of the slot between the two vertical glass panes (see Figure 4.1a). This motion is generally believe to be stable and orderly until hydrodynamic instability occurs.

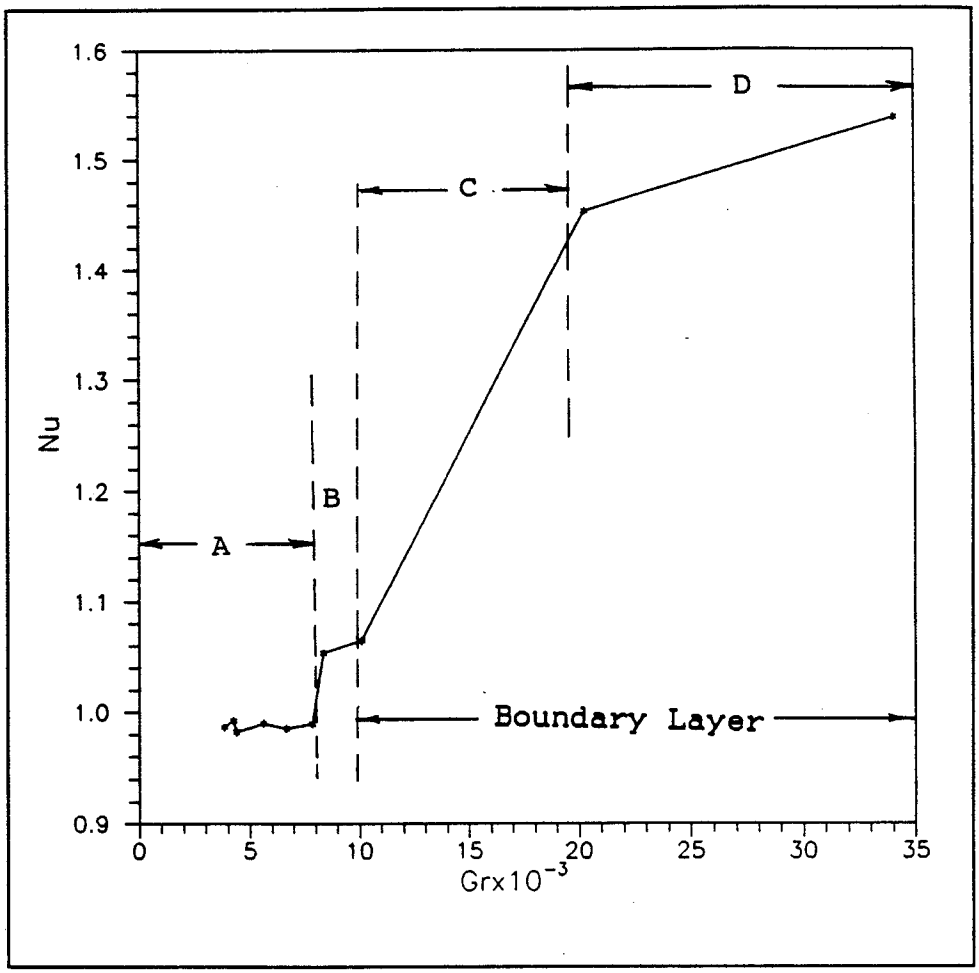

A. Conduction
B. Transition and on-set convection
C. Unicellular convection
D. Multicellular convection

Fig. 4.1a Various Heat Transfer Regimes in the Air Layer

The stable and orderly motion in conduction regime mentioned above seems to have been disputed by Korpela et al [1982] who show that in conduction regime, there exists a transition from unicellular fluid motion to multicellular and then to unicellular at transition zone when the Grashof number (Gr_H) based on the height of the slot is fixed while the aspect ratio of the slot is varied. This phenomenon was only possible when all the dimensionless parameters (Gr and Nu) are based on the height of the cavity, that is, when the height of the slot is used as the characteristic dimension. In all other works reported in the literature including a later work by Yee and Korpela [1983] the width of the vertical slot was used as the characteristic dimension, and the above phenomenon was not observed or reported. They have all generally observed a change from conduction to transition and to convection (or boundary layer) regimes as Grashof number (Gr_w) based on the width of the slot is increased while the aspect ratio is fixed. Yee and Korpela have also reported in their later work that as the Gr_w increases the fluid motion has progressively developed from unicellular at conduction to unicellular and multicellular convection flows with growing boundary layer as the Grashof number is increased further. This is the phenomenon we observed in the present study and is found to be in agreement with the observation of Eckert and Carlson [1961]. The transition of fluid motion from unicellular to multicellular in conduction and back to unicellular at transition reported by Korpela et al [1982] is open to criticism as this contradicts their later work on the same subject. Their use of the height of the vertical slot as characteristic dimension in order to carry out their objective of analyzing fluid motion in the conduction regime may also be open to criticism. The use of the height of the slot as characteristic dimension with fixed Grashof number and variable aspect ratio may produce a false or unrealistic picture of fluid motion in conduction regime which may not

be possible to validate experimentally. The multicellular flow pattern in conduction regime described by Korpela et al [1982] may not represent a physical phenomenon. The so called multicellular flow in conduction regime has not actually been observed or reported in the literature by any other researcher.

The instability of the low Rayleigh number flow based on the width of the vertical slot has been studied and analyzed by several workers including Gershuni [1953], Vest and Arpaci [1969], Kurzweg [1970], Unny [1972], and Hart [1971].

At the critical condition when the flow in the slot first becomes unstable or at the instance of hydrodynamic breakdown Vest and Arpaci [1969] found this critical condition to be dependent on Grashof number and independent of Prandtl number. However, for Pr = 0.71, Vest and Arpaci gave the critical or transition Grashof number of 7880. Other studies such as Eckert and Carlson [1961] obtained a critical Grashof number of approximately 8000, but Unny [1972] and Holland and Konicek [1973] and Lee and Korpela obtained a critical Grashof number of approximately 11000. In all these studies the boundary conditions on the vertical walls are the same with a slight variation on boundary condition at the top and bottom end walls where the condition is either adiabatic or linear temperature profile.

In the present study the boundary conditions are different from those assumed in the previous studies in that the vertical walls are non-isothermal and the top and bottom end walls are neither adiabatic nor imposed with linear temperature profile. Nevertheless, the present problem is basically the same as in the previous studies and therefore exhibits similar flow and heat transfer characteristics.

In examining the flow instability and obtaining the critical Grashof number we employ

the **linear theory of hydrodynamic instability**. The procedure of the **linear theory of hydrodynamic instability** is to determine the Grashof number at which the fluid particle in the center cell of the air layer first becomes unstable. In this study, the values of the Nusselt number Nu_{cc} corresponding to the Grashof numbers at the center cells (Gr_{cc}) when the fluid particles first become unstable is shown in Table 4.1. and plotted in Figure 4.1b. The Grashof number at the center cell corresponding to Nu = 1.0 is referred to as the critical Grashof number, Gr_c. In this study our critical Grashof number was found to lie between 7800 and 8600 (see Table 4.1), that is:

$$7800 \leq Gr_c \leq 8600$$

The linear theory of hydrodynamic instability was also used by Lee and Korpela [1983] to obtain their centre cell Nusselt numbers versus Grashof numbers plot shown in Figure 4.1b. We found good agreement between the value of our Gr_c and those obtained by Eckert and Carlson [1961], Vest and Arpaci [1969] and many other studies which range between 7880 and 8000. However, there is no agreement between our Gr_c and those obtained by Holland and Konicek [1973], Unny [1972] and Lee and Korpela [1983] which range between 10000 and 11000. The discrepancy is thought to be due mainly to the variation in the boundary conditions, (particularly at the top and bottom end walls of the vertical slot) and the range of Grashof numbers. The work of Eckert and Carlson was an experimental study and as is the case in this study, they did not take a deliberate measure to impose a specific boundary condition (even though adiabatic condition was assumed) at the top and bottom end walls leaving that condition to manifest itself. This is the approach we took in this study which was considered to be non-

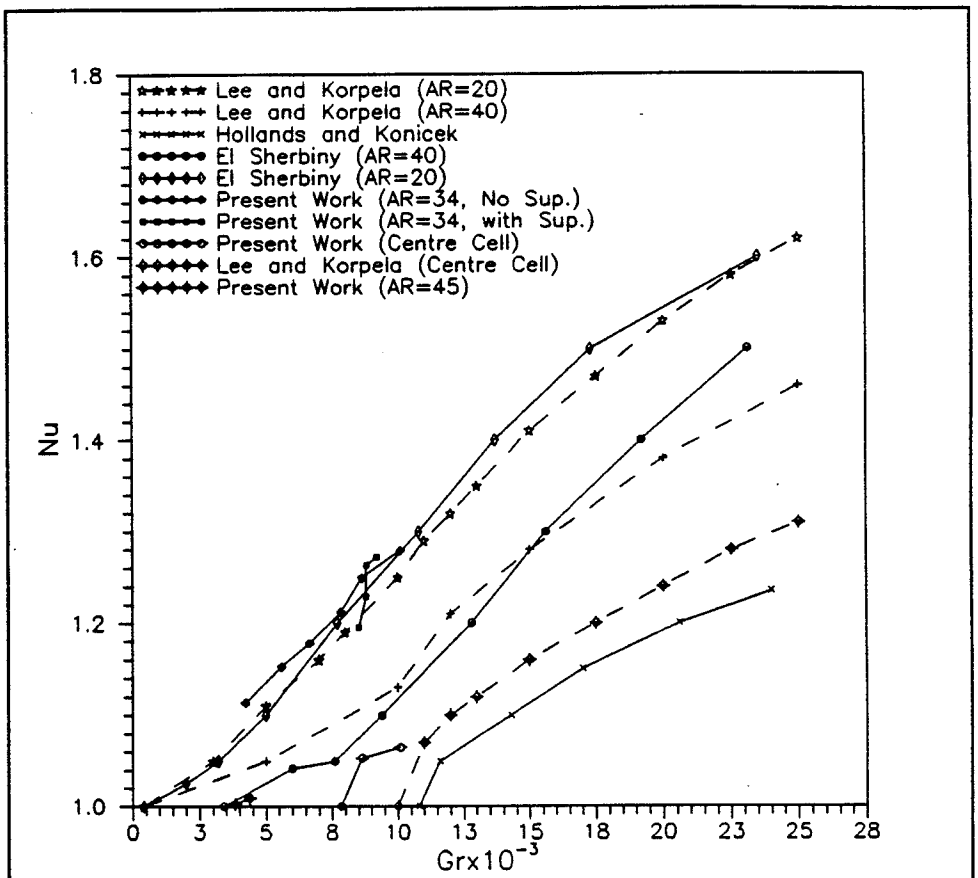

Fig. 4.1(b) Nusselt number as a function of Grashof number

Fig. 4.1b Comparison of the Present Results with the Results of Previous Researchers

adiabatic as evident from our results. The works of Holland and Konicek, Lee and Korpela and others whose studies were based on theoretical grounds or on numerical assumptions while this study and that of Eckert and Carlson inclined more towards practical reality with real world boundary conditions.

4.1.2 The Transition and On-set of Convection

The fringes (Fig. 4.1c) and the temperature profile along the vertical centre line of the air layer (Fig. 4.2) indicate linear temperature drop exists in the entire air gap except at the very bottom corner of the hot surface and top of the cold surface where the distortion of the fringes shows an indication of a transition to convection. The temperature profile (Fig. 4.3) from the analysis of the interferogram also shows linear temperature drops in the centre of the enclosure from the hot to the cold glass surface. This is a strong indication that conduction predominate in the air layer. Although the linear temperature drop suggests heat is transferred by conduction in the central region of the air layer, this does not necessarily mean that no fluid motion exists but that no thermal energy transport is connected with the fluid motion in the central region, but weak convection may coexist with the conduction as illustrated in Figure 4.1a. Only a very sophisticated method such as the interferometry used here could detect the weak convection.

Figure 4.4 shows the local Nusselt number distribution along the hot and cold surfaces in the transition regime. As seen in the figure, the local Nusselt number is considerably larger than unity at the bottom corner of the hot surface and top corner of the cold surface where

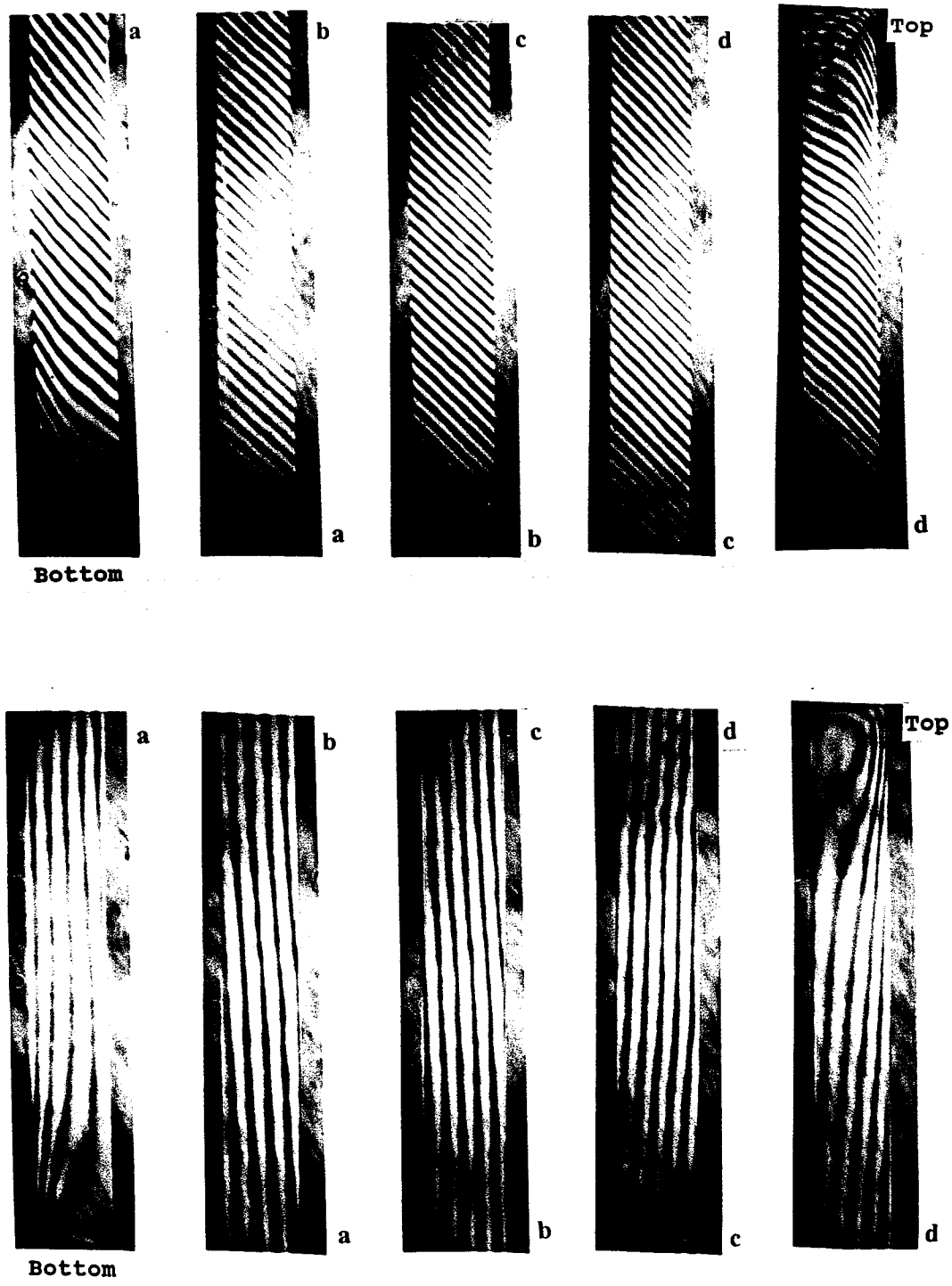

Fig. 4.1(c) Finite and infinite interferograms ($Gr_w = 4.2x10^3$)

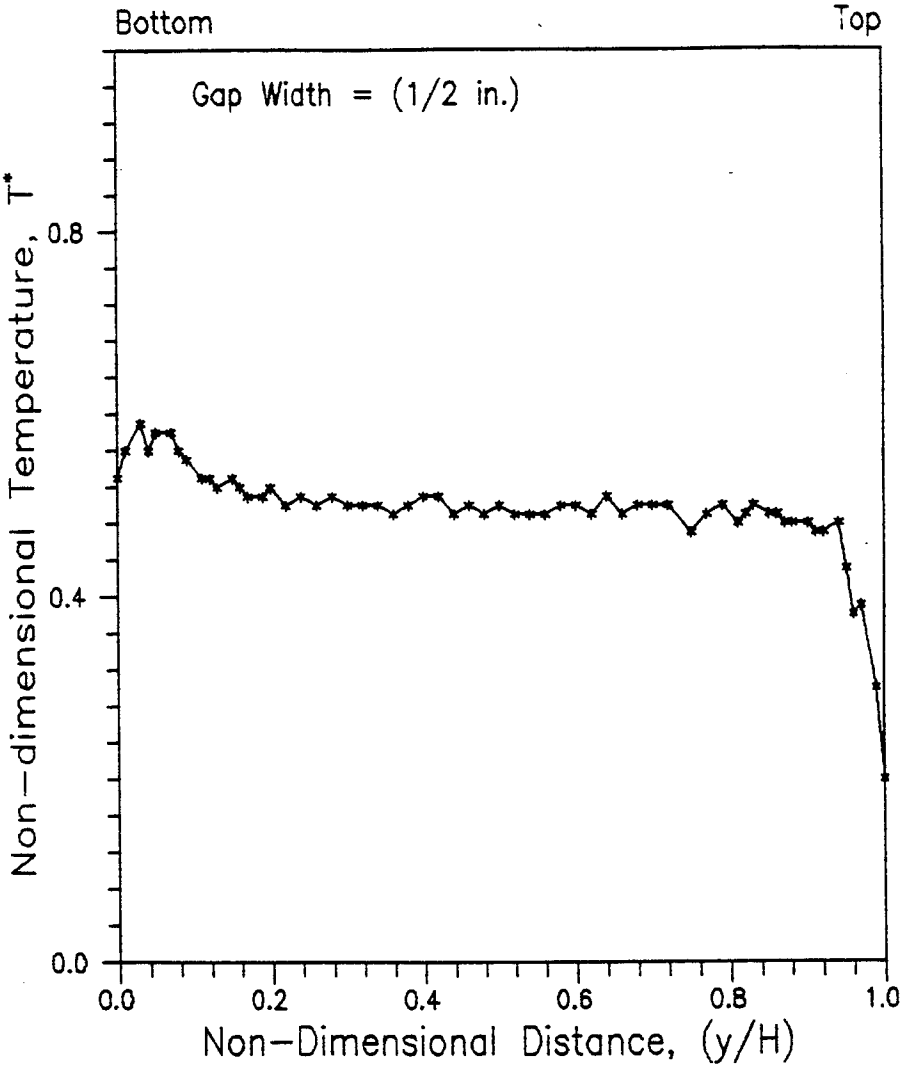

Fig. 4.2 Temperature Profile Along the Vertical Centre Line of The Air Gap (Gr_w = 4.2 x 10^3)

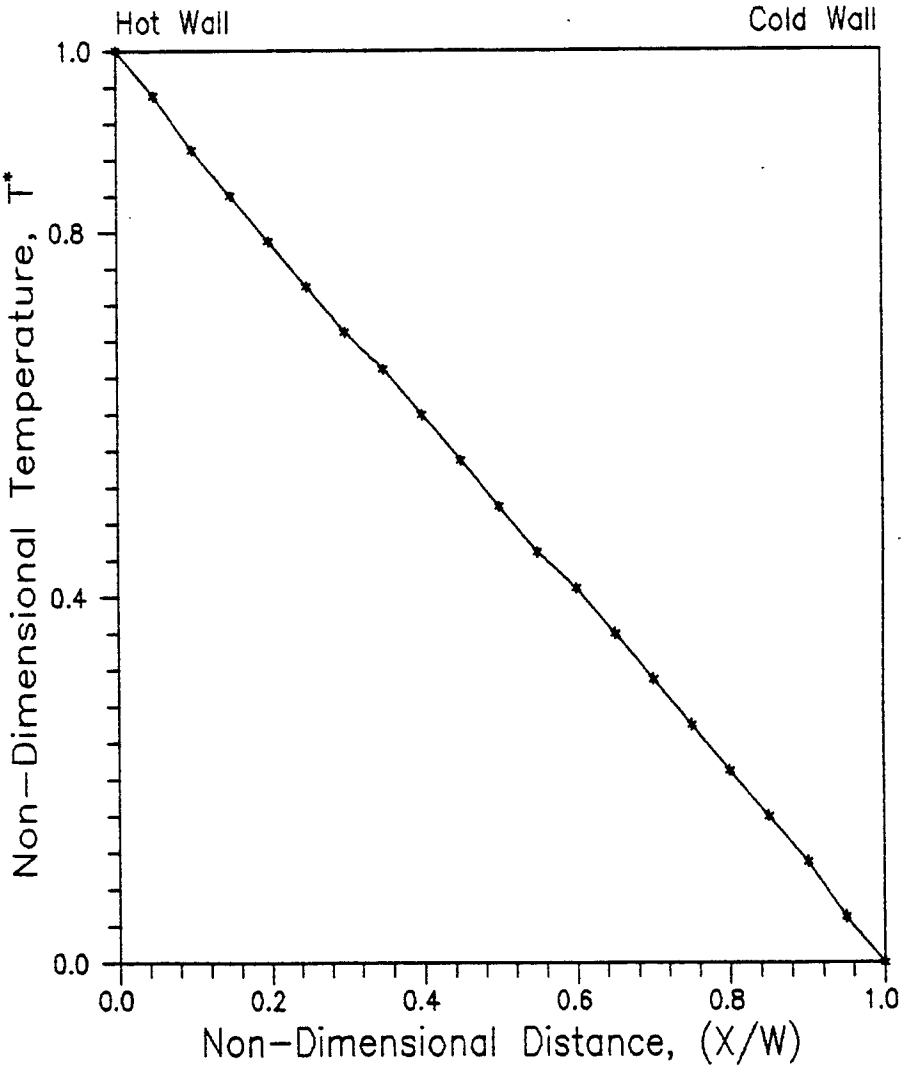

Fig. 4.3 Temperature Profile Along The Horizontal Centre Line of The Air Gap (Gr_w = 4.2 x 10^3)

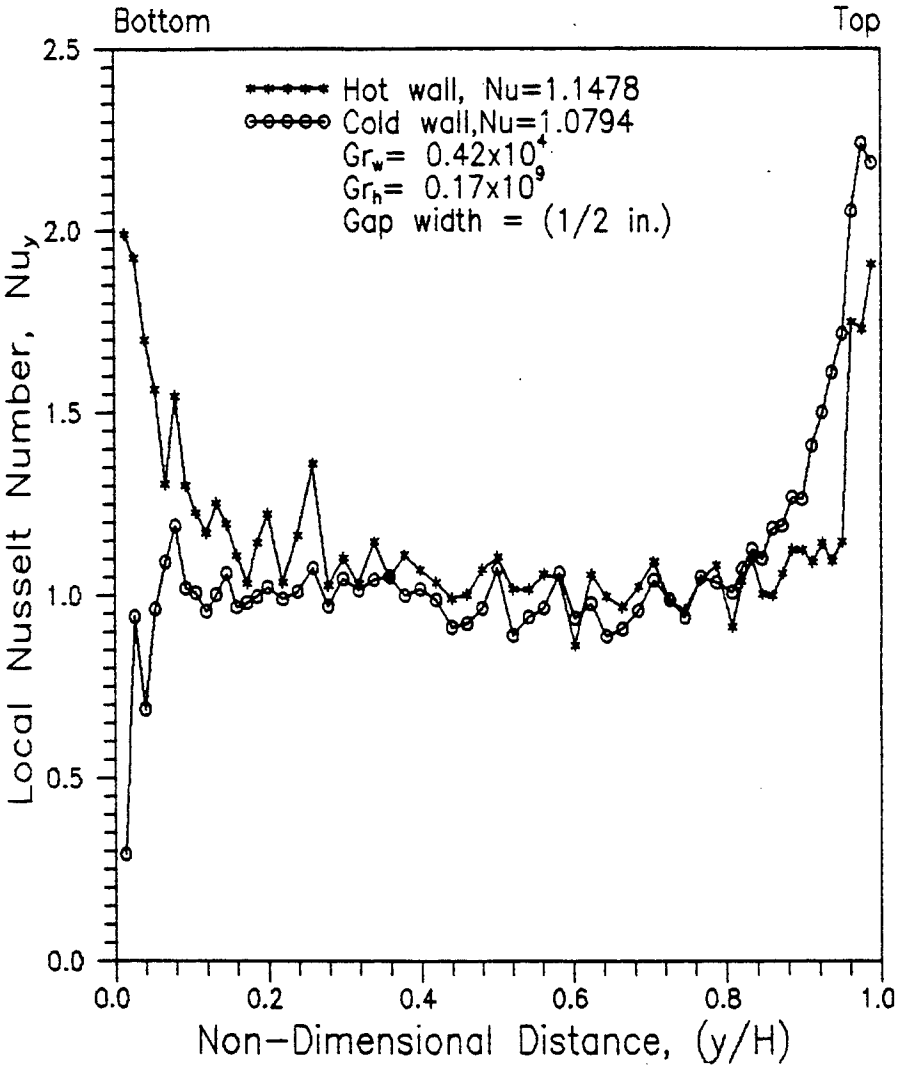

Fig. 4.4 Local Heat Transfer on Hot and Cold Glass Surfaces ($Gr_w = 4.2 \times 10^3$)

strong convection exist. In contrast at the top corner of the hot and bottom corner of the cold surfaces the local Nusselt number is lower than unity. Although there is a slight fluctuation in the centre, the local Nusselt number allowing for the scattering of the data, is generally close to unity.

For an air gap width of 0.95 cm (3/8") the heat transfer is essentially by conduction (see Table 4.1). But the difference in heat transfer between the 3/8" and 1/2" air gap enclosure as noted in Appendix B, is that for 3/8" air gap Nu is greater than unity on the hot surface and less than unity on the cold surface while Nu is approximately unity on both hot and cold surfaces in 1/2" air gap enclosure. As will be discussed later an air gap greater than 1/2" could lead to multicellular convection eddies in the cavity. This phenomenon may explain why 1/2" air gap is usually considered as an optimum width for an insulated double glazing.

Figures (4.5) and (4.6) show the temperature and the local heat transfer profiles on the top and bottom seals. In contrast to the general assumption in many previous studies where boundary conditions at the seals were taken to be adiabatic or at the best linear, this result revealed that the real world temperature boundary condition was non-adiabatic and the temperature profile was non-linear. As seen in Appendix B, the boundary conditions at the top and bottom end walls (the seals) varied considerably according to the characteristics of the heat transfer in the air layer. For example in the conduction regime the temperature distribution on the top was found to be higher than at the bottom seal. In other cases shown in Appendix B, there was a wide variation in the mechanism of heat transfer to or from the seals. Therefore, there is variation in the heat transfer characteristics and the temperature profiles.

The sign convention adopted for the local Nusselt number distribution on the seals (see

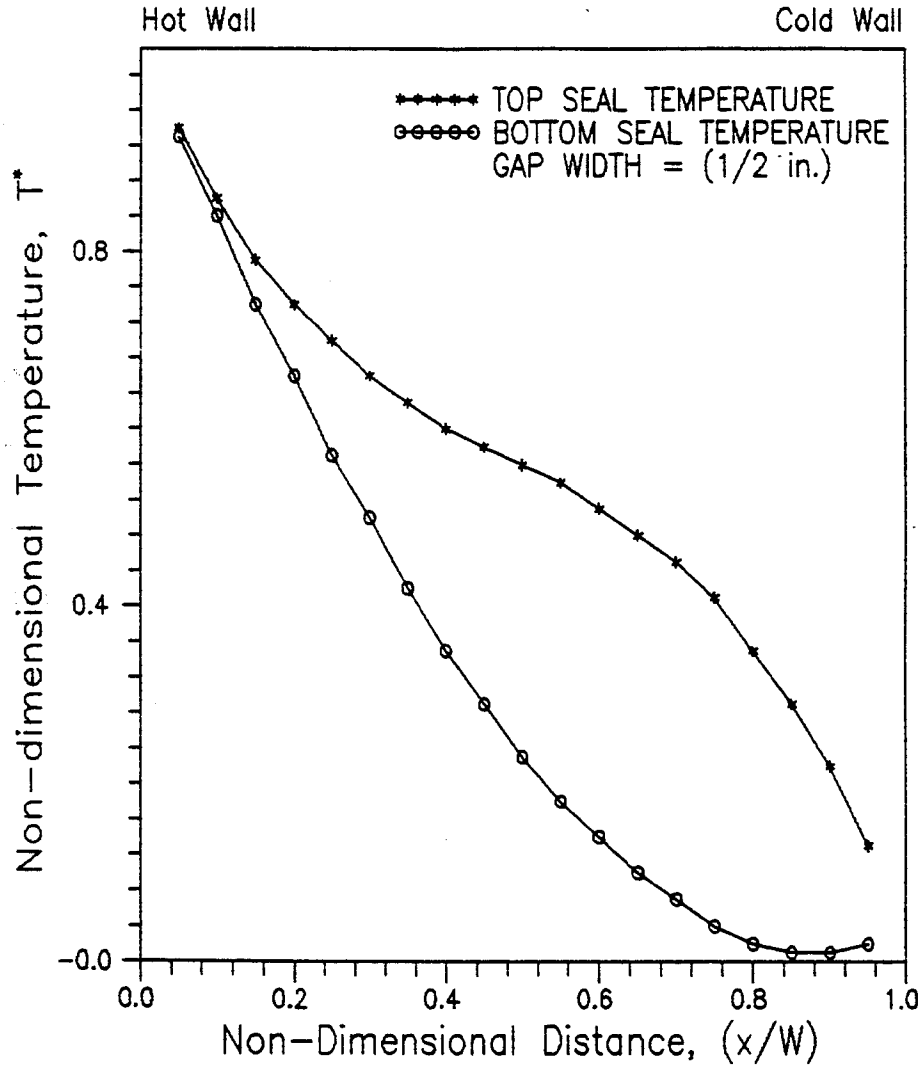

Fig. 4.5 Temperature Profiles on Top and Bottom Surfaces of The Air Gap (Gr_w = 4.2 x 10^3)

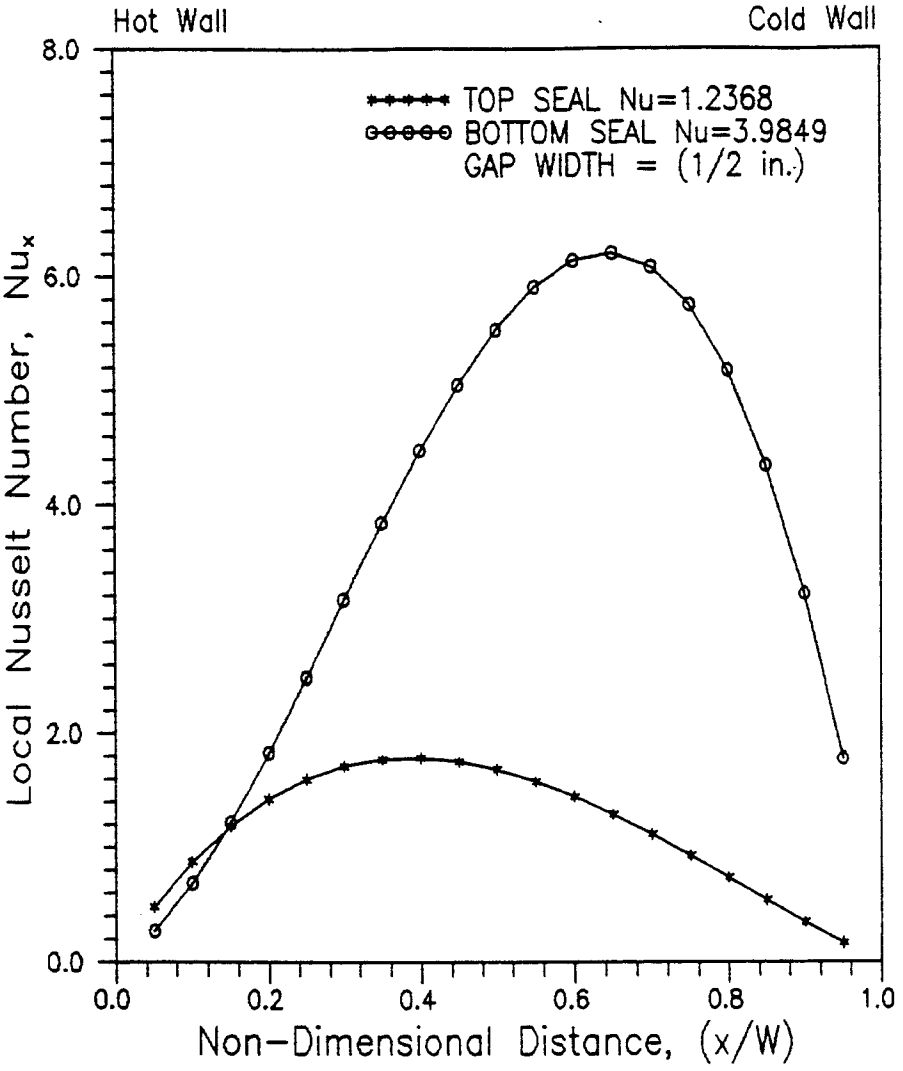

Fig. 4.6 Local Heat Transfer on Top and Bottom Surfaces of The Air Gap (Gr_w = 4.2 x 10^3)

Appendix B) is such that the positive sign indicates heat is transferred from the fluid to the seal and the negative sign indicates heat transfer is from the seal to the fluid. Using this sign convection, the local heat transfer distribution (Fig.4.6) indicates heat was transferred from the fluid to the top and bottom seals. The transfer of heat was higher on the bottom than on the top seal.

The finite and infinite interferograms (Figure 4.7) and the calculated isotherms (Test run #5 in Appendix B) revealed a development of boundary layers on the hot and cold glass surfaces. At the on-set of convection two modes of heat transfer co-exist. In the developing boundary layers along the vertical hot and cold surfaces, heat is transported by convection while conduction heat transfer still predominate across the centre of the air layer. This observation is supported by Figures 4.8 and 4.9 which show considerable linearity of the horizontal and vertical centerline temperature profiles. A close look at the infinite interferogram in Figure 4.7 revealed two possible flow patterns in the transition regime. At T_c = 0°C to -6°C or at low Grashof numbers, the thermal and hydrodynamic boundary layers on the hot and cold glass surfaces grew thicker until they merged possibly at the centre of the enclosure. As the Grashof number increased the infinite fringe or the calculated isotherms revealed that the thermal boundary layer thickness increased gradually and continually from the bottom to the top of the hot surface. At the higher Grashof number (say at T_c < -6°C) the growing thermal boundary layers on the hot and cold did not merge at the centre but continue from the bottom to the top of the hot surface. The resistance to heat transfer occurred in the thin layer attached to the wall surface. The fluid in the region outside the boundary layers was motionless and heat transfer was transferred across this region by conduction. From the above observation, it can be

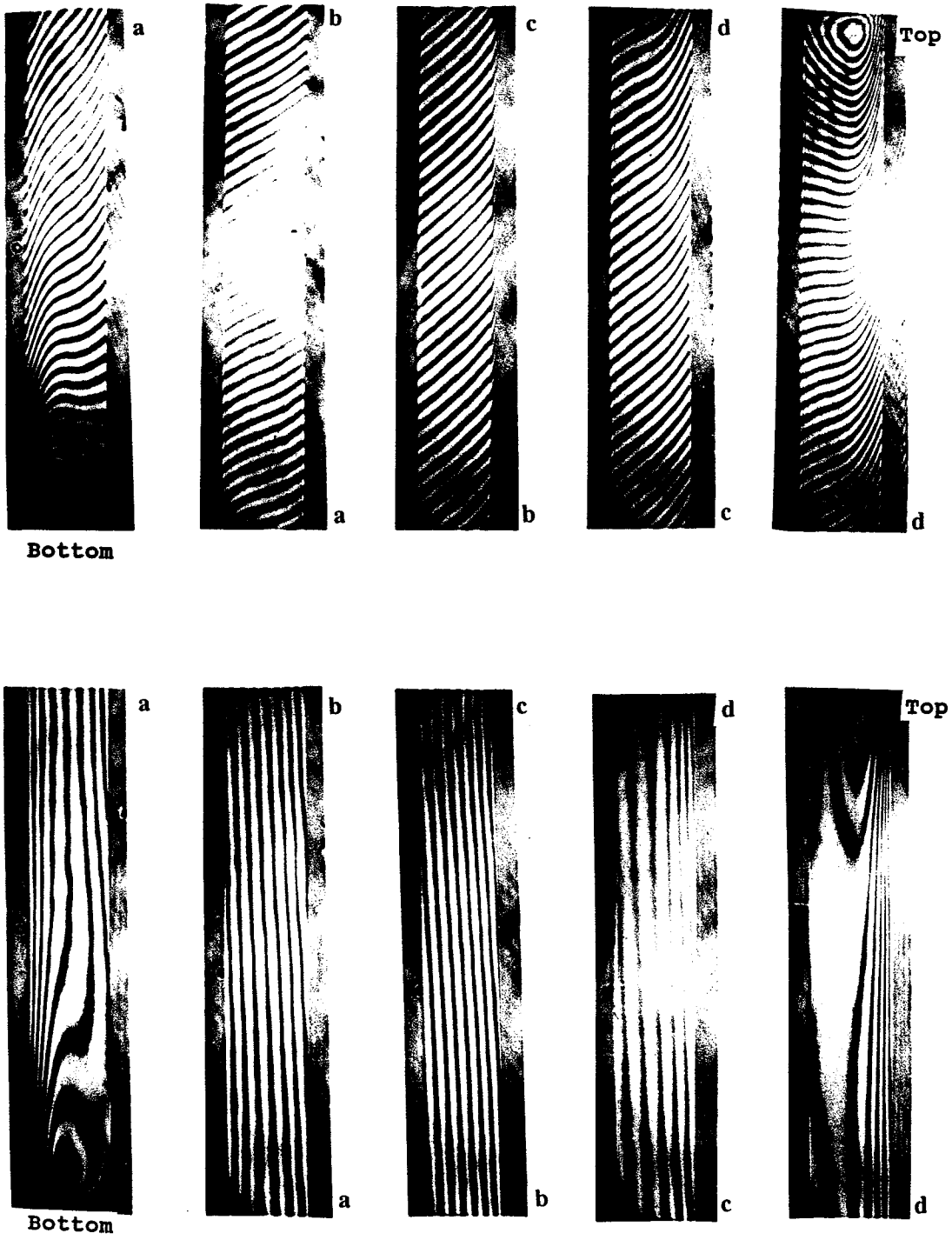

Fig. 4.7 Finite and infinite interferograms ($Gr_w = 8.6 \times 10^3$)

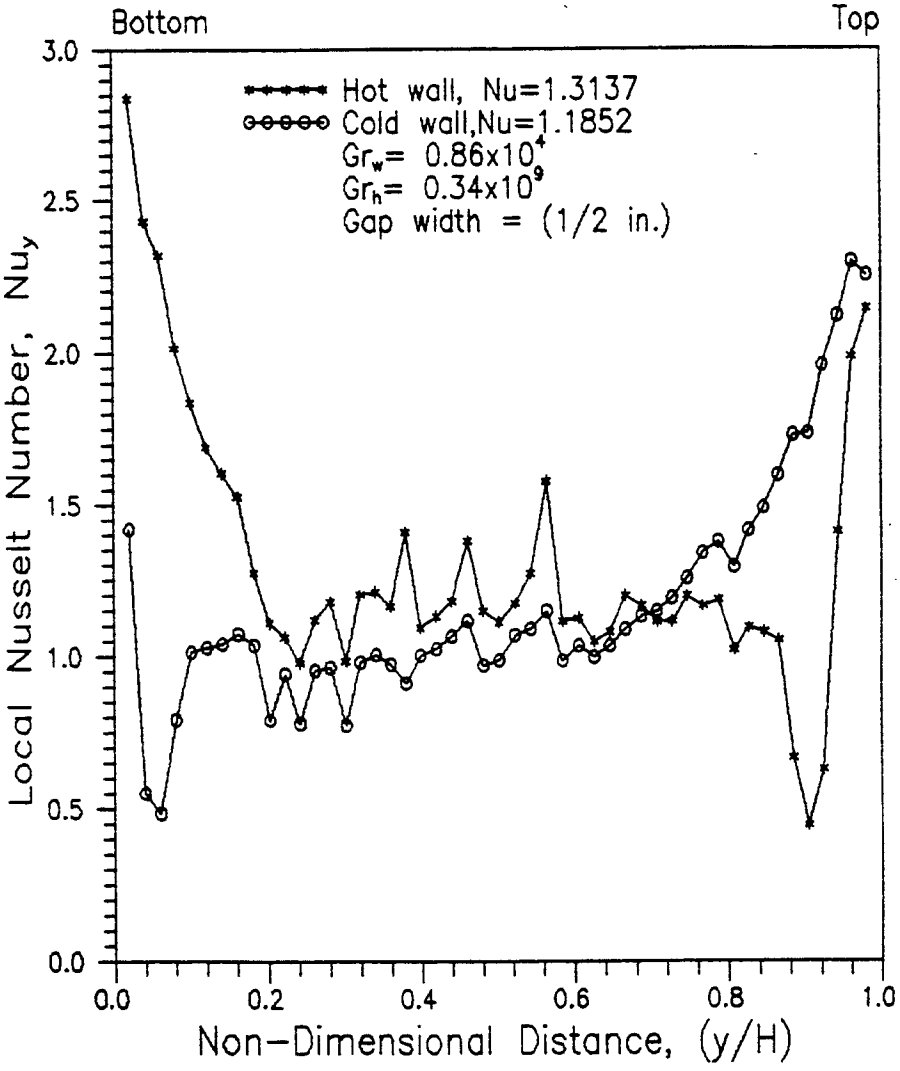

Fig. 4.8 Local Heat Transfer on Hot and Cold Glass Surfaces ($Gr_w = 8.6 \times 10^3$)

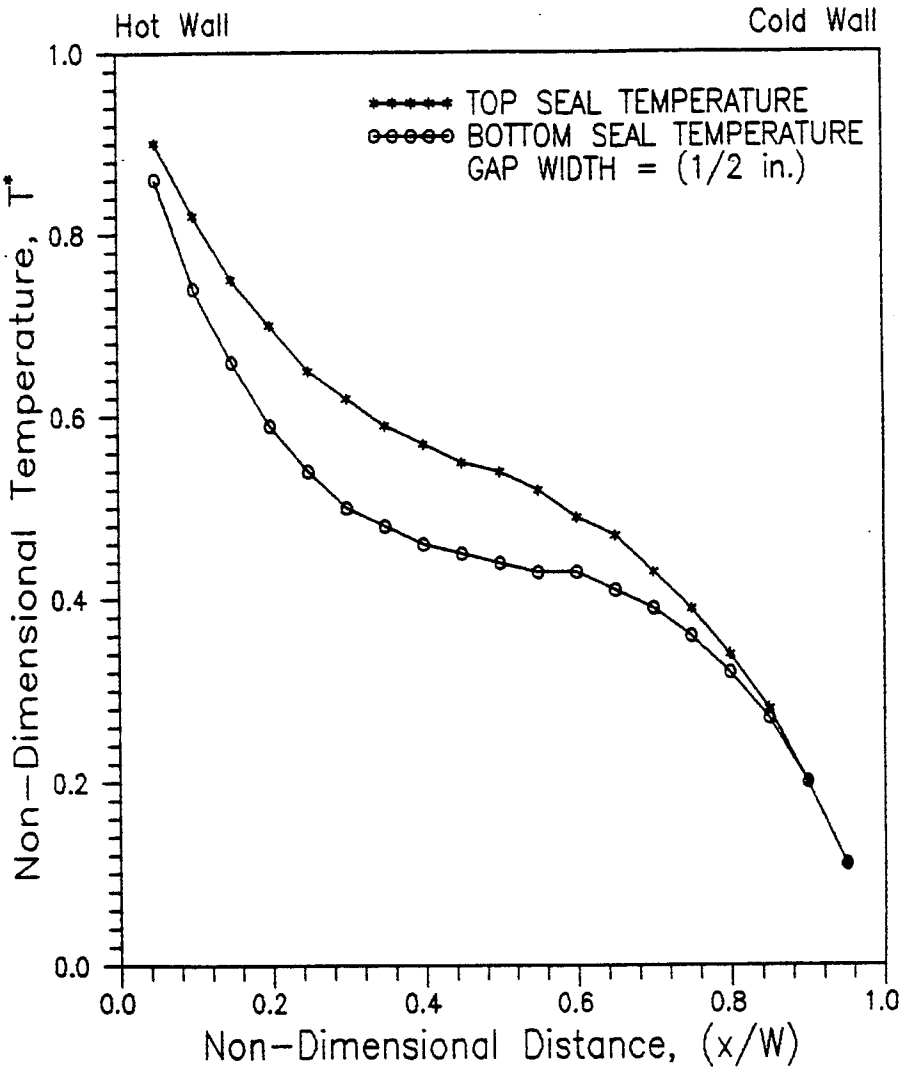

Fig. 4.9 Temperature Profiles on Top and Bottom Surfaces of The Air Gap (Gr_w = 8.6 x 10^3)

concluded that in the transition regime, the flow is governed by boundary layers which continues to grow along the surface. This led to an increase in thermal resistance and a decrease in heat transfer coefficient from bottom to the top of the hot surface as shown in Figure 4.8. The temperature profiles on the top and bottom seals (Figures 4.9) are non-linear but indicated a drop in temperature from the highest near hot surface to the lowest at the cold wall. As shown in Figure 4.10, heat transfer occurred from the fluid to the top seal, but over 75% of the bottom seal from the cold surface heat was transferred from the seal to the fluid and from fluid to the seal in the remainder portion.

4.1.3 Unicellular Heat Convection

As the Grashof number increased further the flow in the enclosure was increasingly fluctuating and becoming unsteady. This resulted in fully developed laminar boundary layer. As shown in the centre of the interferograms Figure 4.11 and the calculated isotherms of (Test run #6), local instabilities in form of vortices appeared in the core region. These vortices might have separated from the growing boundary layers on the vertical hot surface. As noted in the bottom and top regions of the infinite interferogram, it appears that the instabilities leading to the formation of vortices first occurred at these corner regions due to sudden and unstable deceleration of fluid particles. These instabilities as a result of buoyancy effects propagated to the core region of the enclosure. These convective eddies have a direct relationship with the Grashof number, and as the Grashof number was increased beyond the inception of the eddies, the intensity of the instabilities increased. The consequence of these instabilities is an increase

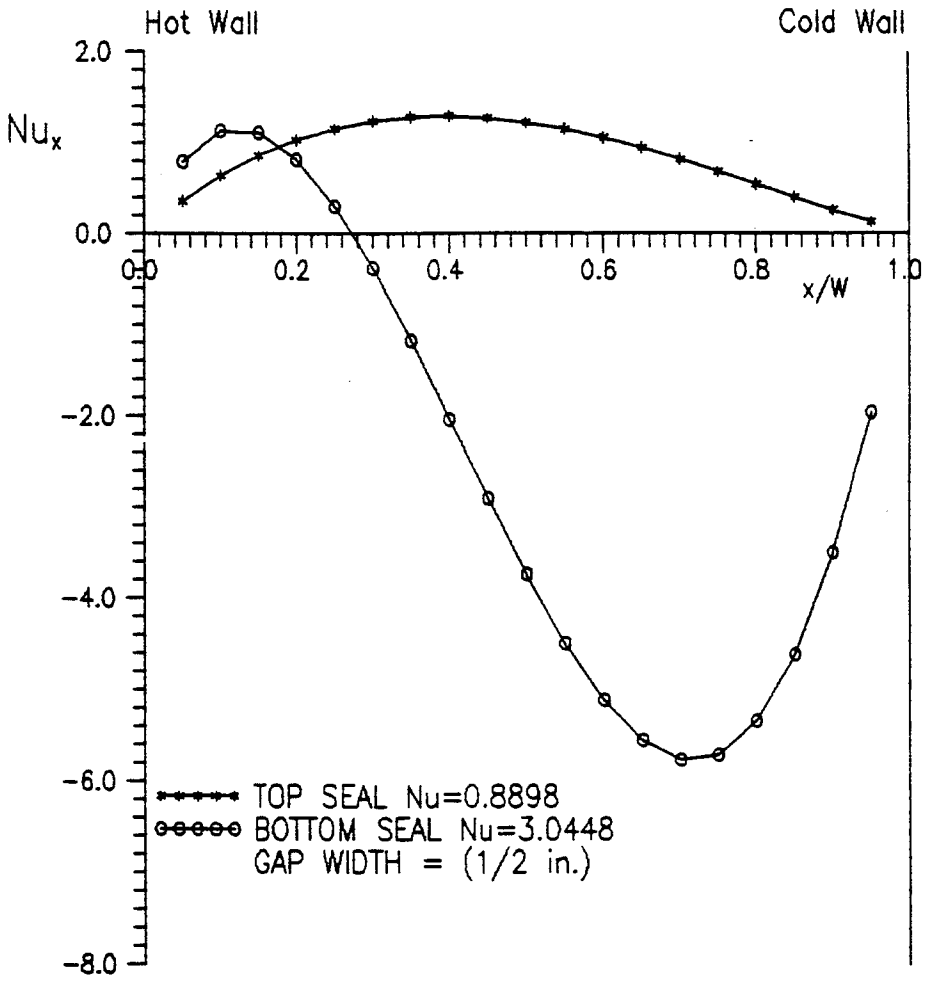

Fig. 4.10 Local Heat Transfer on Top and Bottom Surfaces of The Air Gap (Gr_w = 8.6 x 10^3)

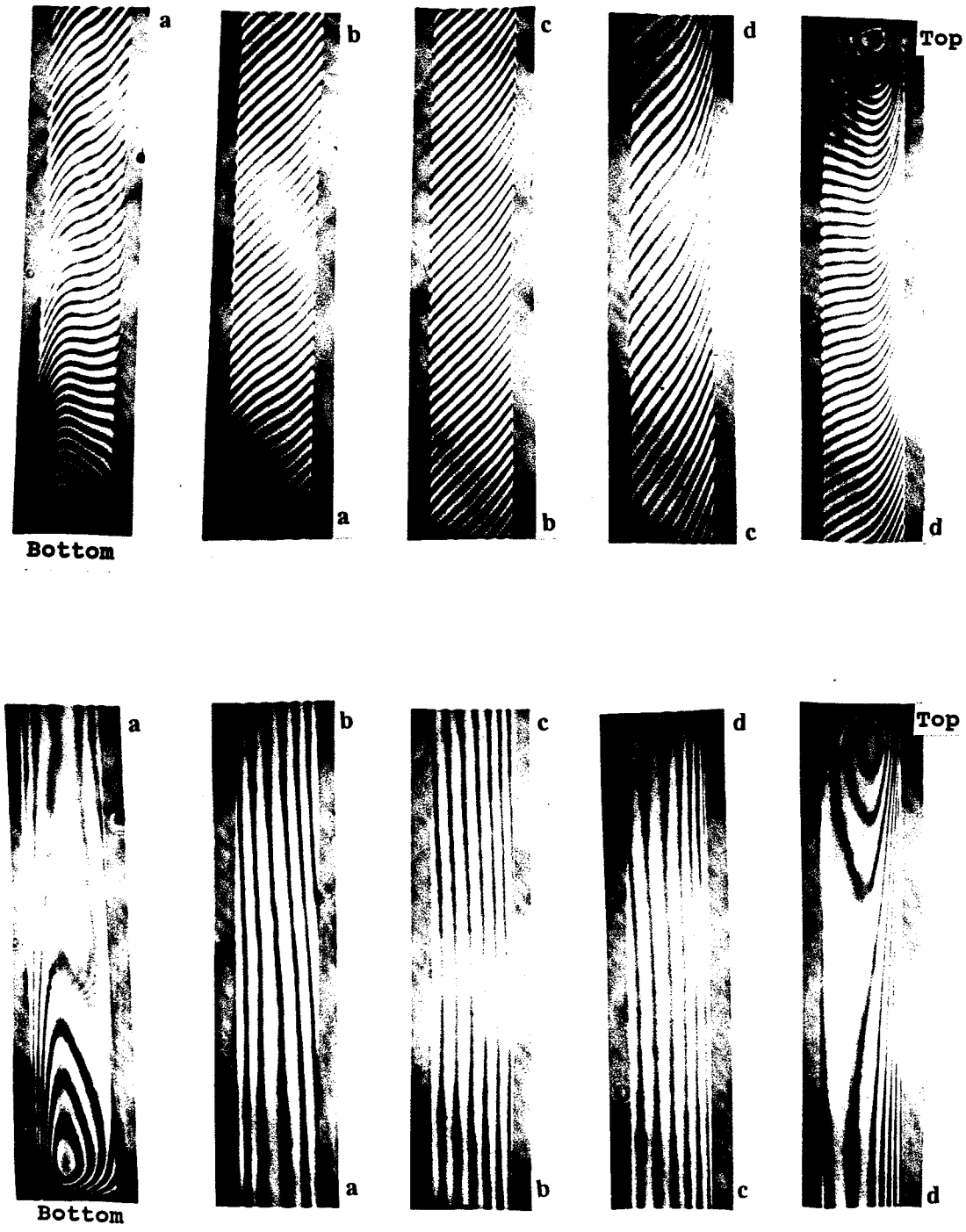

Fig. 4.11 Finite and infinite interferograms ($Gr_w = 1.01x10^4$)

in heat loss by convection through the enclosure. The heat transfer characteristics associated with these instabilities are shown in Figures 4.12, 4.13 and 4.14. The plot of the average Nusselt number versus the Grashof number is shown with the results of other researchers in Figure 4.1b. The comparison of the present results with results obtained by previous researchers shown in Figure 4.1b will be discussed in section 4.4.

4.1.4 Multicellular Heat Convection

As the Grashof number increased further, the unsteadiness in the flow resulted in series of concentric eddies referred to as multicellular convection. This is depicted in the interferometer pictures in Figure 4.15 and test run #9. In order to simulate the multicellular convection ΔT must be very high, that is, T_c must be less than -40°C. Since our experimental apparatus could not support such a low temperature, the remedy was to consider a window slot with a larger air gap width to achieve higher Grashof number, Gr_w equivalent to the low temperature. The appropriate air gaps are 1.59 cm. (5/8") and 1.9 cm. (3/4"). As seen in the interferometer pictures and the calculated isotherms (Fig. 4.15), the fringes appear to be parallel to the surface and the isotherms appear to be very steady. This is an indication that the boundary layers were still laminar while the centre of the enclosure was fully mixed by eddy diffusion. The eddies separated randomly from the outer edges of the boundary layer and resulted in large scale perturbations of the temperature profiles near the boundary layers. The temperature profile across the cavity gap as seen in Figure 4.16 was non-linear. Other heat transfer characteristics in the multicellular convection regime are shown in Figures 4.17 and 4.18.

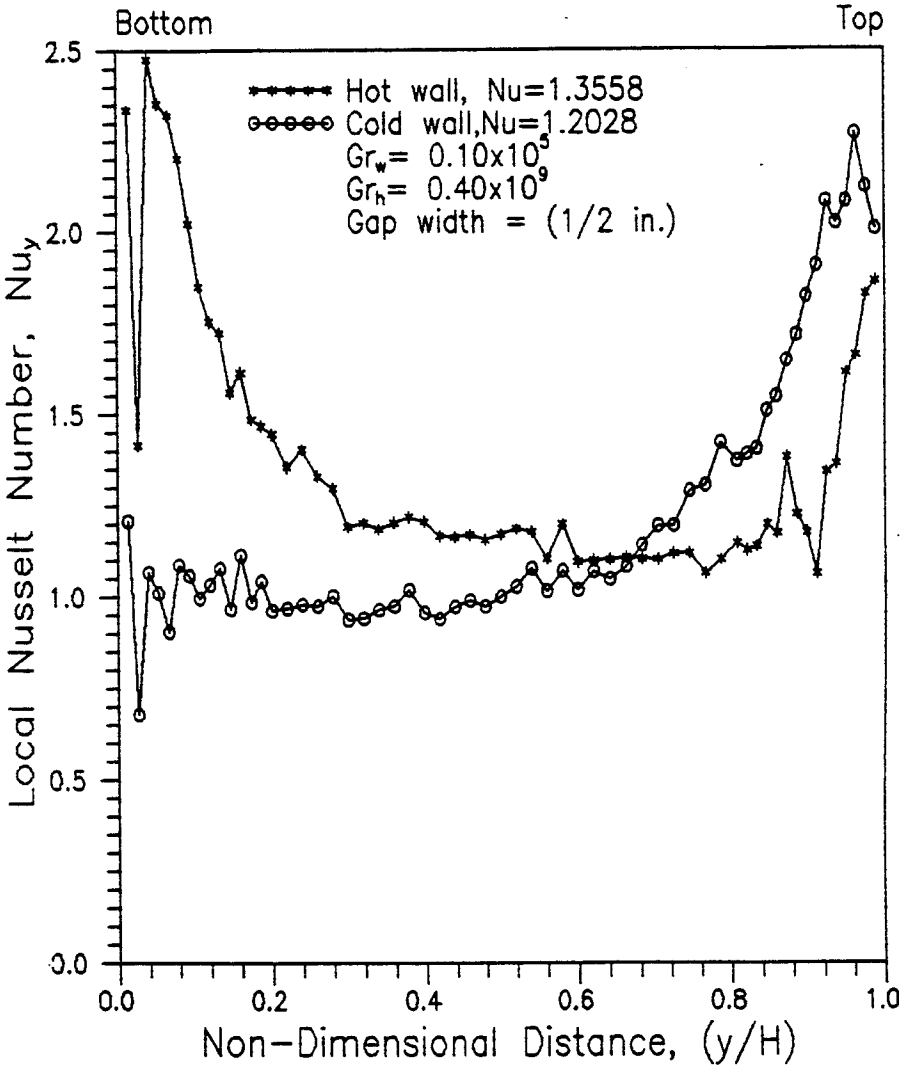

Fig. 4.12 Local Heat Transfer on Hot and Cold Glass Surfaces (Gr_w = 1.0 x 10^4)

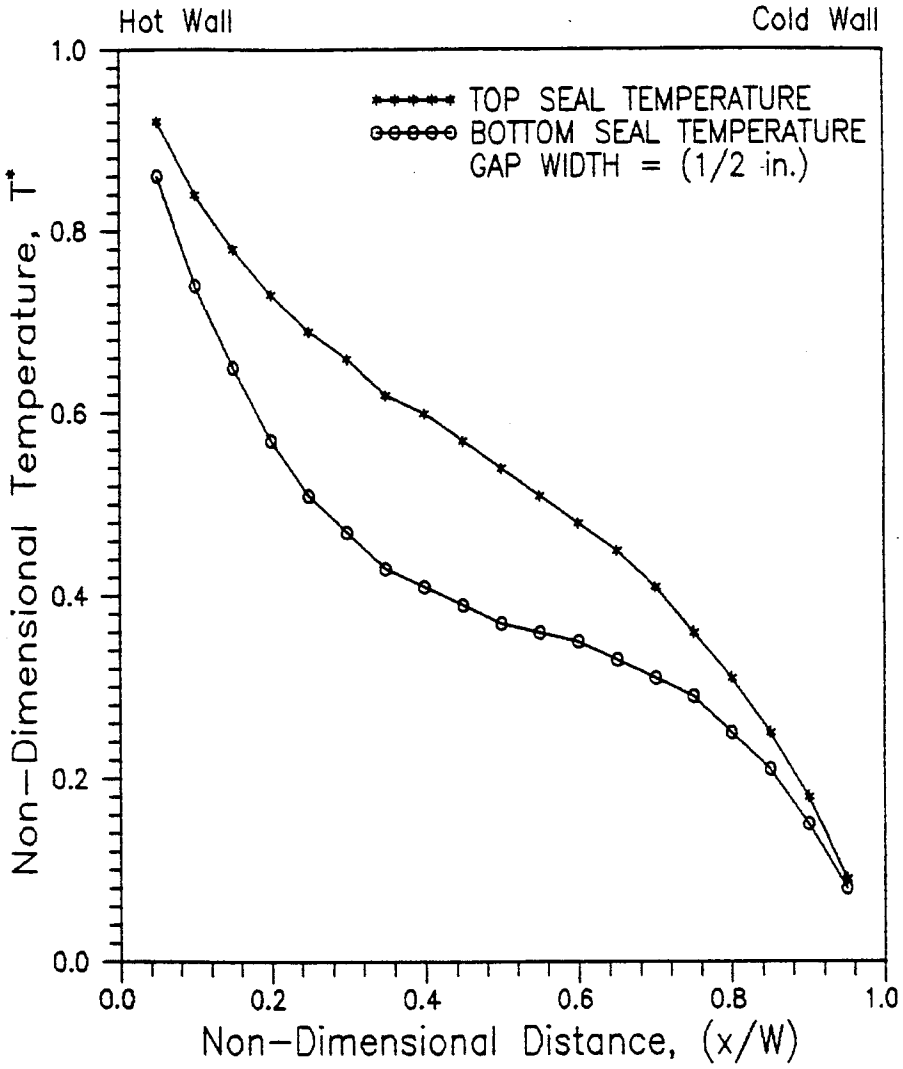

Fig. 4.13 Temperature Profiles on Top and Bottom Surfaces of The Air Gap (Gr_w = 1.0 x 10^4)

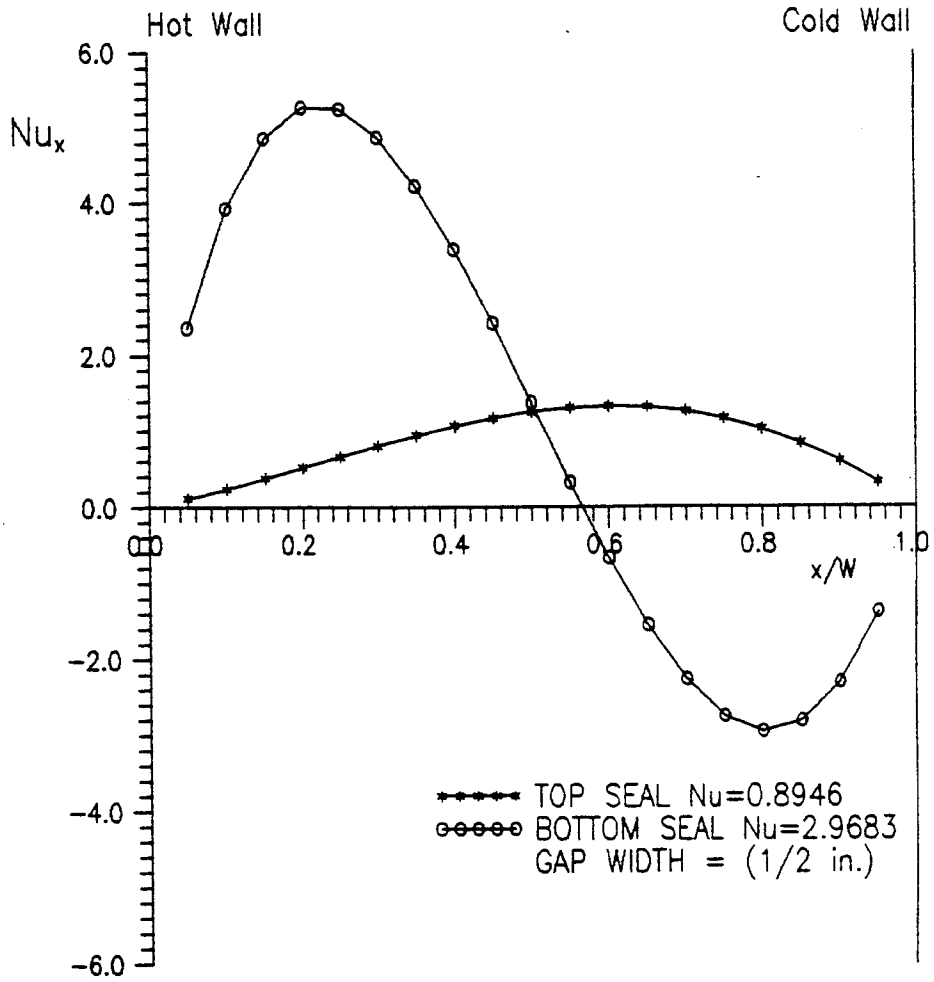

Fig. 4.14 Local Heat Transfer on Top and Bottom Surfaces of The Air Gap (Gr_w = 1.0 x 10^4)

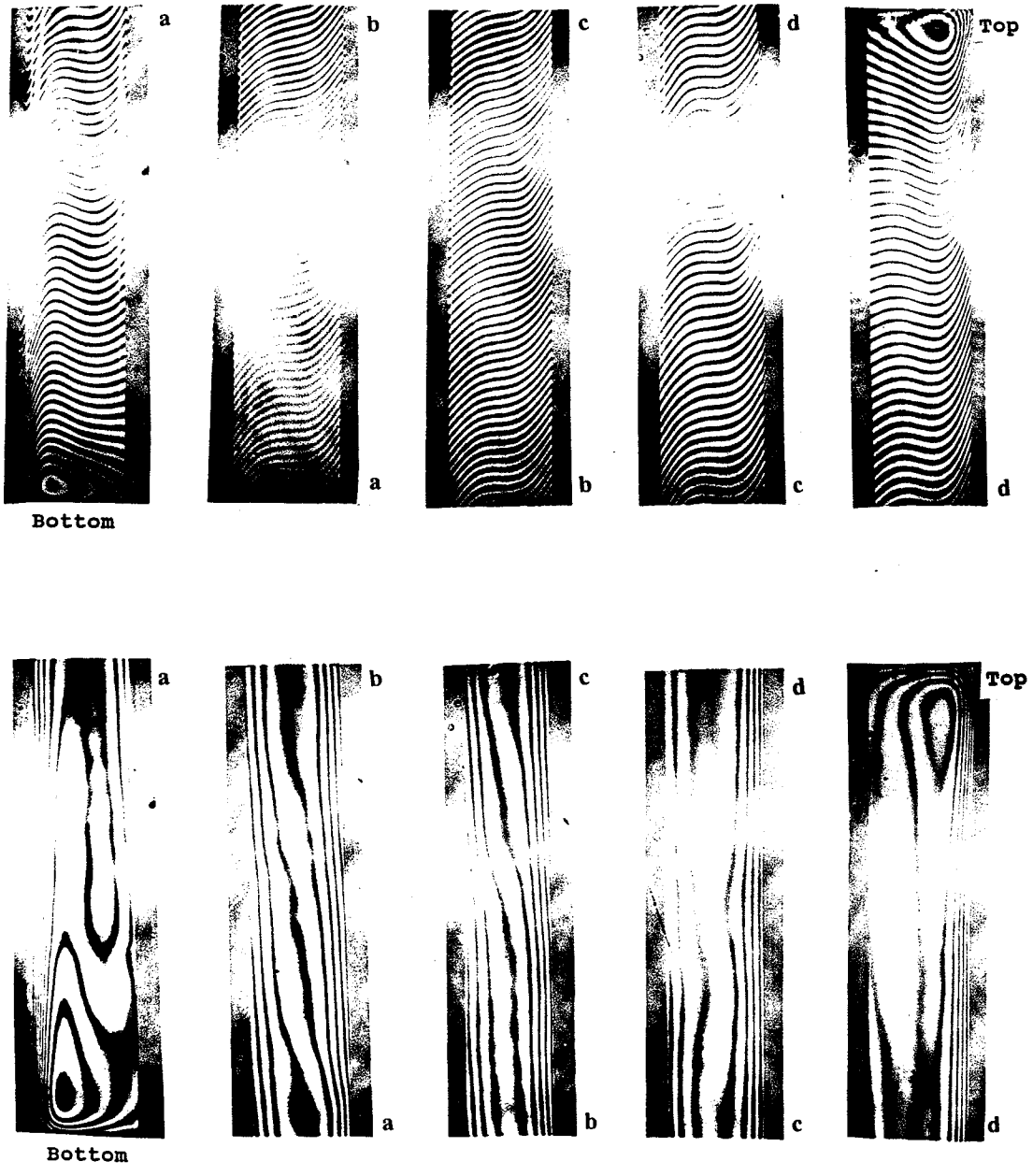

Fig. 4.15 Finite and infinite interferograms ($Gr_w = 3.4 \times 10^4$)

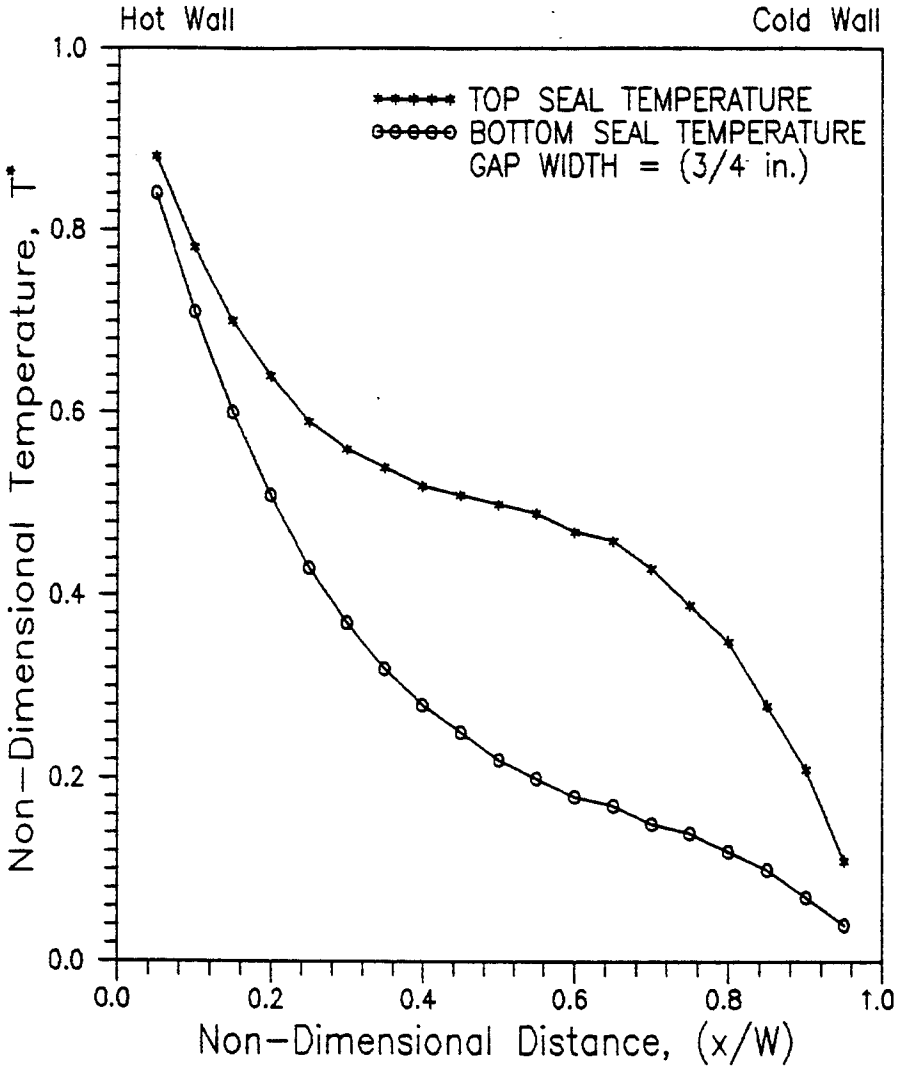

Fig. 4.16 Temperature Profile Along The Horizontal Centre Line of The Air Gap (Gr_w = 3.4 x 10^4)

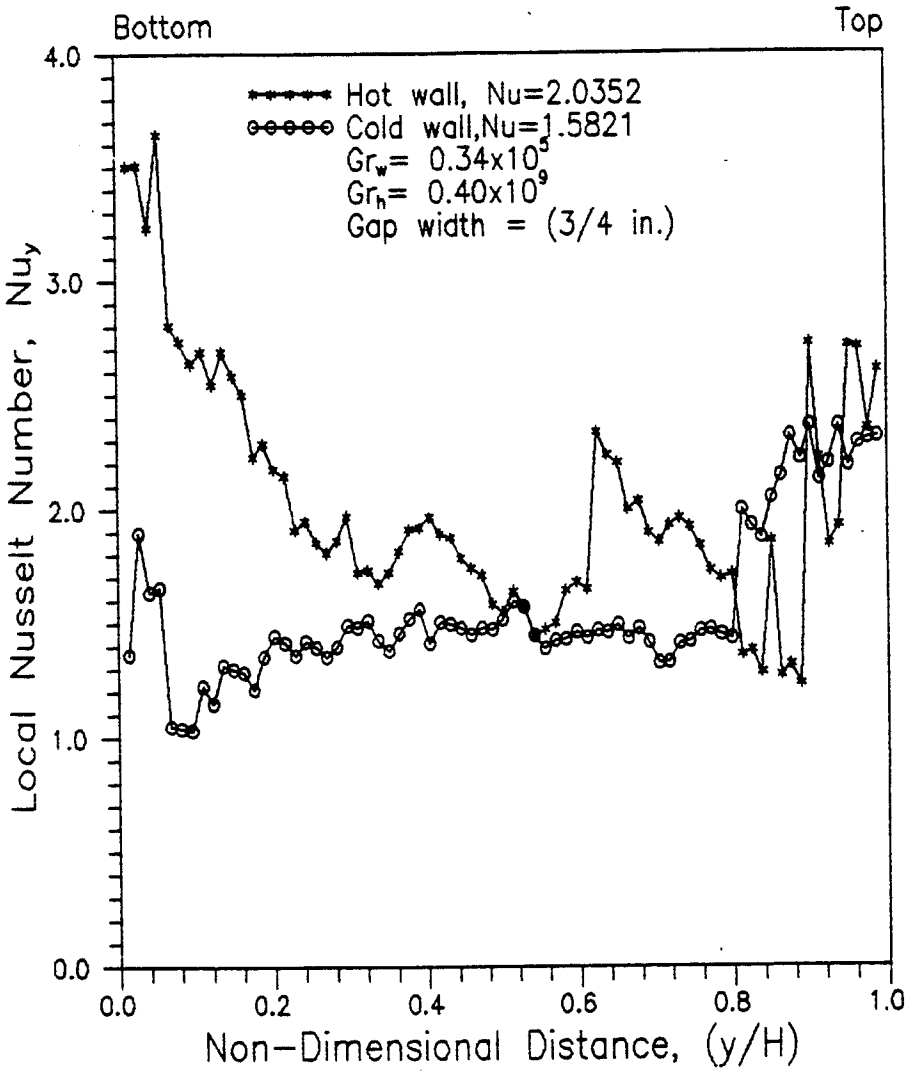

Fig. 4.17 Local Heat Transfer on Hot and Cold Glass Surfaces (Gr_w = 3.4 x 10^4)

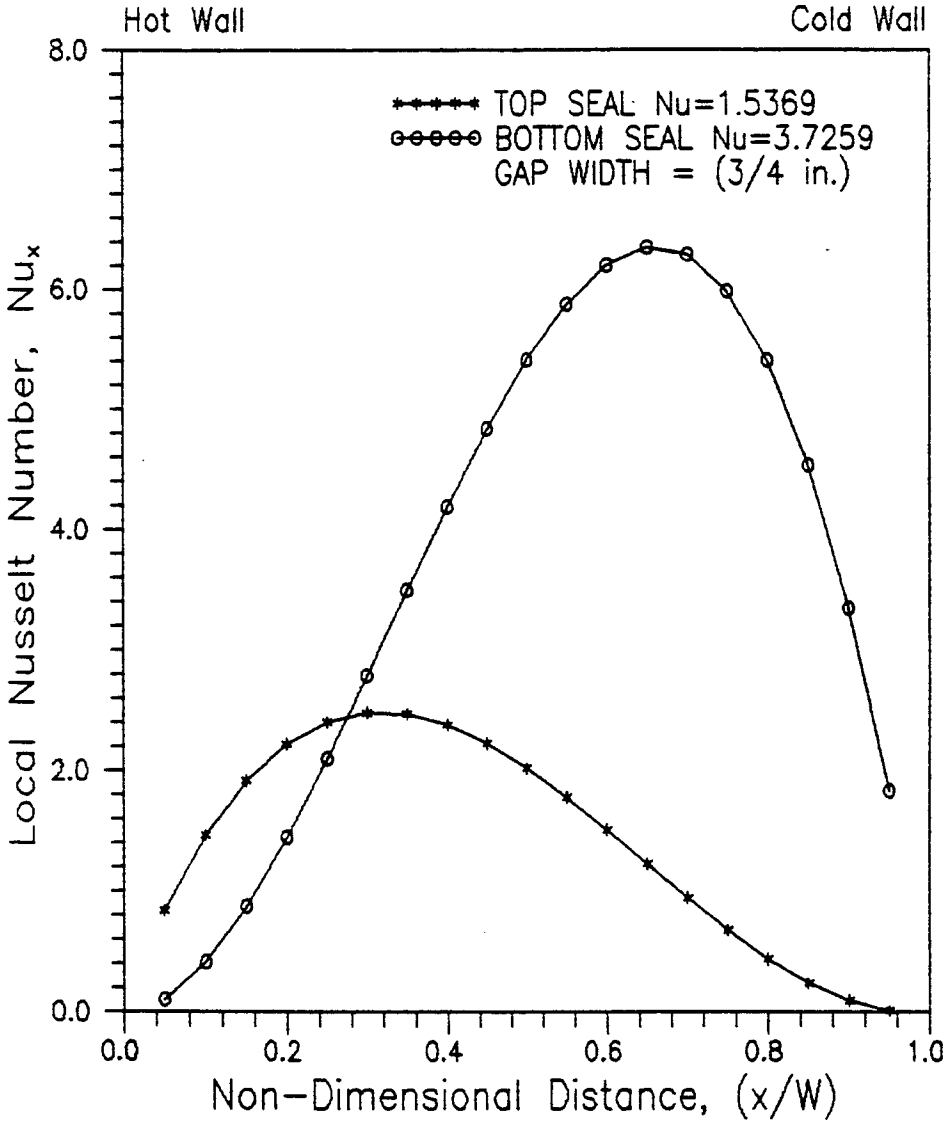

Fig. 4.18 Local Heat Transfer on Top and Bottom Surfaces of The Air Gap (Gr_w = 3.4 x 10^4)

The eddies at higher ΔT or Grashof number across the air gap could be responsible for higher energy transport from the hot to the cold surface of the cavity. In the next section, discussion will focus on the use of suppressor to suppress the eddies and reduce energy transfer from the hot to the cold wall. The average Nusselt number versus Grashof number for the multicellular convection is shown in Table 4.1. Further discussion of the multicellular convection in relation to the unicellular convection and the results of other researchers will be found section 4.4.

4.2 CONVECTION SUPPRESSOR

An introduction of suppressor in the bottom or top corner regions of the vertical enclosure results in the suppression and/or displacement of the convection eddies occurring at these regions. Suppressor height of 2.54 cm. (1"), 5.08 cm. (2"), 10.16 cm. (4"), 20.32 cm. (8") and full partitions (ie a third glazing) which are equivalent to suppressor heights to cavity height ratios, L/H of 0.056, 0.118, 0.235, 0.471, and 1.0 were considered in this study. Typical interferograms and calculated isotherms for a case with suppressor height of 5.08 cm. (2") in the bottom section of the air gap are shown in Figure 4.19. As shown in the infinite interferograms, the eddy which formerly located in the bottom section of the enclosure was displaced upward to the tip of the suppressor. The higher the suppressor the higher the displacement of the eddy. When the suppressor tip corresponds to the mid-section of the cavity as in test run number 14 (see Table 4.1), the local heat transfer becomes the highest at the mid-point. This is a situation that must be avoided in the selection of the suppressor.

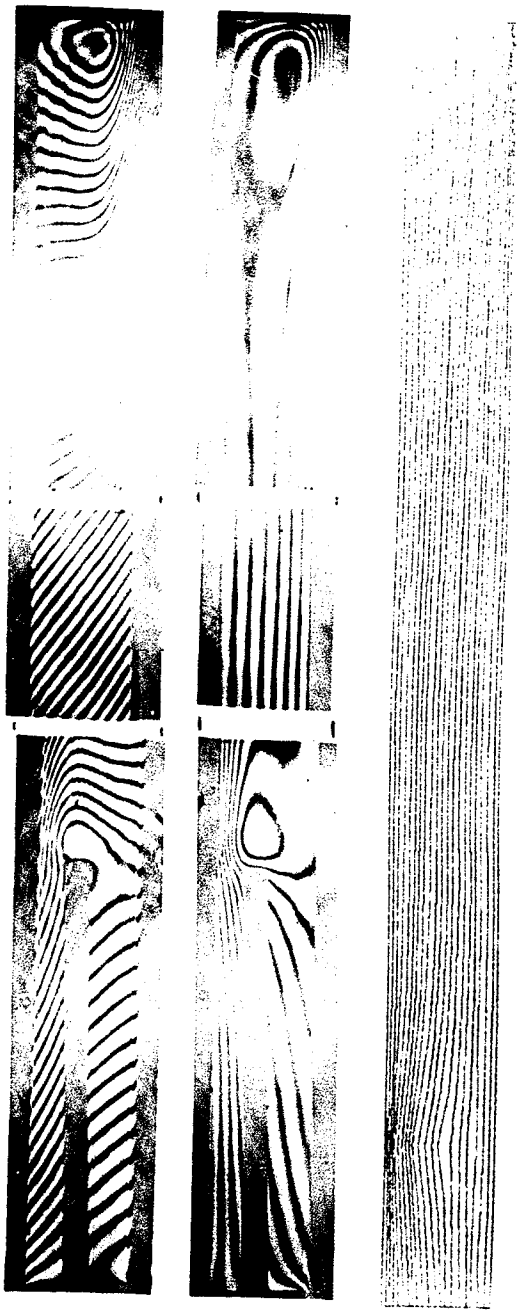

Fig. 4.19 Finite and infinite interferograms with convection suppressor (Suppressor height, H_s = 5.08 cm. (2")), ($Gr_w = 9.2 \times 10^3$)

A close look at the local heat transfer distribution (Fig. 4.20) reveals that the peak of the local Nusselt number, Nu_y, has also been shifted from the bottom corner to a location on the hot wall corresponding to the tip of the suppressor. The value of Nu_y at the bottom corner dropped considerably. This is an indication that the convection heat transfer in the bottom section of the slot has been drastically suppressed. However, the results summarised in Table 4.1 and presented in Figure 4.1b show that the average heat transfer in the cavity does not change considerably with the introduction of the suppressor except in the cases where the suppressor height to cavity height ratio is 1/2 and 1. For these cases the average heat transfer drops by 4% and 14% respectively from the case of cavity with no suppressor. But for cases where the suppressor height to cavity height is less than 1/2 the results (see Figure 4.1b) show that average heat transfer rate may be slightly enhanced with introduction of the suppressor particularly when the cavity aspect ratio is smaller. A similar observation has been reported by Bajorek and Lloyd [1982], Chang, Lloyd and Yang [1982] and Ciofalo and Karayiannis [1991]. However, for the case of a 1.9 cm. (3/4") air gap the result in Table 4.1 show that for L/H = 1 the heat transfer rate dropped significantly from the case where L/H = 0. But what is of significance in this study is the displacement of the convection eddies from the corner region of the cavity where convection may induce glass surface condensation. This phenomenon is discussed in detail in the next section. More results on the convection suppression are presented in Figure 4.1(a), Table 4.1, and Appendix B. The correlation of the Nu versus the Grashof number for the range of the L/H covered in this study is discussed in section 4.5.

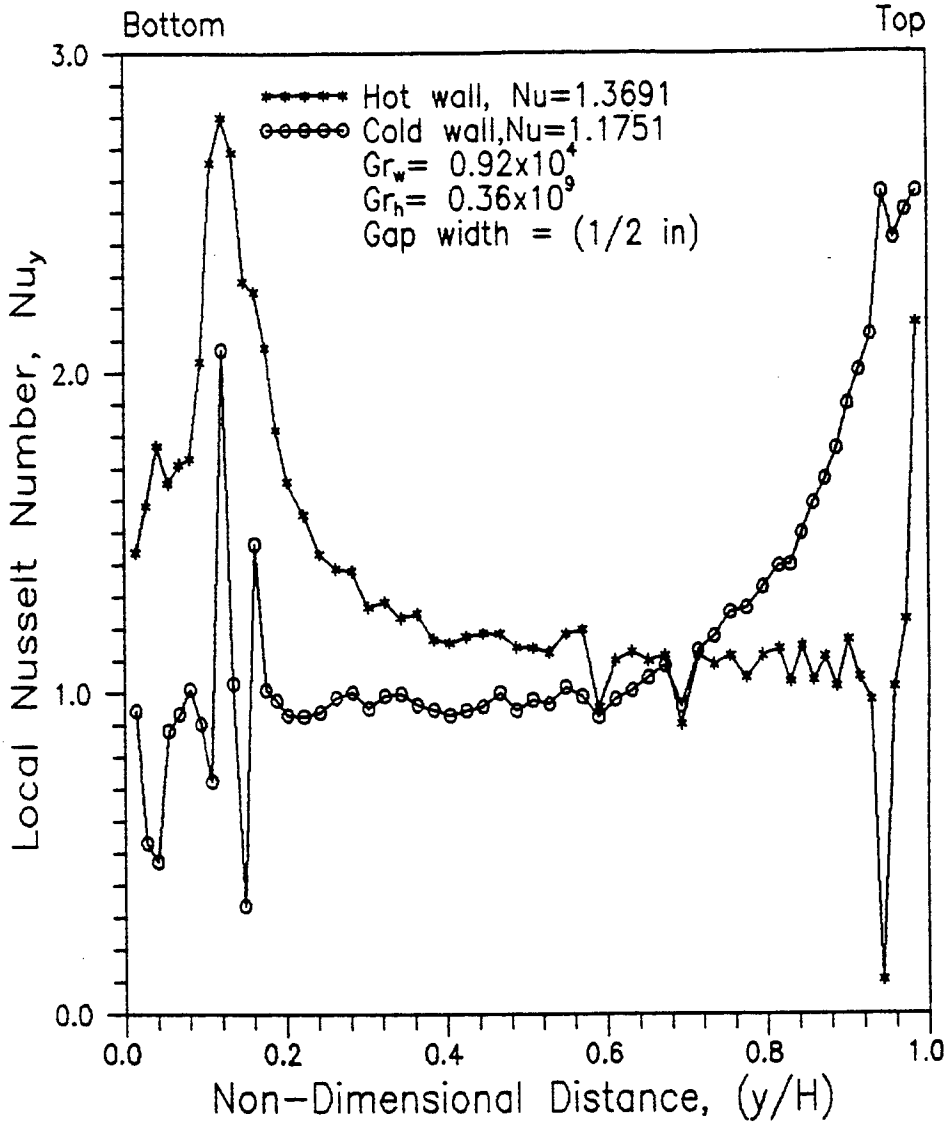

Fig. 4.20 Local Heat Transfer on Hot and Cold Glass Surfaces (Gr_w = 9.2 x 10^3)

4.3 MECHANISM FOR THE SUPPRESSION OF WINDOW SURFACE CONDENSATION

The convection eddies discussed above are more prominent in the bottom and top sections of the air layer between double window glazing subjected to high temperature difference across the air layer. The strong activities of these eddies may result in high energy transport across the air layer from the hot glass to the cold glass. This results in convection cooling of the bottom and top sections of the hot glass surface. The convection cooling effect may cause the temperature of the bottom and/or top sections of the hot glass surface to drop below the **Dew point temperature** of the indoor air near the hot surface. When this occurs there is a formation of condensation on the bottom and/or top section of the hot surface. The detail of the surface condensation is discussed in Appendix C. An introduction of convection suppressor in the bottom and top section of the slot could suppress the convection eddies (see Figure 4.19), eliminate convection cooling, and thereby maintain the hot glass surface temperature above the indoor dew point temperature and consequently prevent the formation of surface condensation.

To investigate the above phenomenon thermocouples were installed to monitor the surface temperatures at the bottom section of the hot glass of a double glazing with and without convection suppressor in the air gap. These temperatures are 15°C and 8°C respectively. The temperature and the relative humidity (R.H) of the indoor air near the hot glass surface are 20°C and 60% respectively. Under this condition the dew point temperature of the indoor air is 12.3°C. Therefore surface condensation will occur on the bottom section of the hot glass as illustrated by the psychometric chart in Appendix C. When suppressor is inserted in the air gap

the hot glass surface temperature becomes higher than the dew point temperature of the surrounding indoor air and the surface condensation disappears. Further studies using a large scale window glazing and the full-size hot box with humidity control system will be required to validate the above phenomenon. The full scale study will be developed in the proposed next phase of this work to have a better understanding and provide more information and design data and correlation equations on the convection-condensation phenomenon. We shall be able to determine the optimum ratio of the suppressor height to cavity height required to suppress surface condensation.

4.4 COMPARISON OF THE PRESENT RESULTS WITH PREVIOUS RESULTS PUBLISHED IN LITERATURE ON NATURAL CONVECTION IN VERTICAL SLOTS

As mentioned in the introductory section of this report, several studies dealing with the classical problem of differentially heated air layer enclosed between vertical walls have been reported in the literature. Until recently, the boundary conditions of isothermal vertical walls and adiabatic top and bottom end walls have usually been the subject of investigation. Holland and Konicek [1973] investigated the stability of differentially heated inclined air layers with isothermal hot and cold vertical walls. To maintain linear temperature profile on the top and bottom end walls surfaces, Holland and Konicek covered these surfaces with aluminum foil. Elsherbiny et al [1982] also considered similar boundary condition in their study of natural convection in inclined and vertical air layer. Lee and Korpela [1983] assume the classical boundary conditions of isothermal walls and adiabatic end walls in their numerical study. Except

for the difference in boundary conditions the present study and those mentioned above are similar. Therefore comparisons are drawn between them.

The results obtained in the above mentioned studies are presented in Figure 4.1(b). Starting with the heat transfer results at the center cell of the cavity which we employ to analyze and determine the critical Grashof number and the onset of convection, the present results are generally higher than those obtained by Lee and Korpela. However, there is a good agreement between the present study and the work of Eckert and Carlson and that of Vest and Arpaci (not shown in Figure 4.1b). This agreement forms the basis for the validation of the present experimental technique. The discrepancy between our center cell results and that of Lee and Korpela indicates that natural convection occurs at lower Grashof number in our study than experienced by Lee and Korpela. This may due to the influence of the boundary conditions at the top and bottom end walls which in our case are conducting and considered to be non-adiabatic. Lee and Korpela assume the boundary conditions at these surfaces to be adiabatic.

Considering the effect of aspect ratio in Figure 4.1b, there appear to be a close agreement with the result of Elsherbiny and Lee and Korpela at aspect ratio of 20. Our results for aspect ratio H/W = 34, compare favourably with the results of Elsherbiny et al and Lee and Korpela for aspect ratio of 20. This again reiterate our earlier observation that convection occurs much earlier than observed in previous studies. Again the results of Elsherbiny and Lee and Korpela for aspect ratio 40 are reasonably comparable. At low Grashof number there appear to be a good agreement between our results at aspect ratio 45 and the result of Elsherbiny at aspect ratio 40. The general trend indicated in Figure 4.1b is that the rate of natural convection heat transfer is inversely proportional to the aspect ratio.

4.5 DATA CORRELATION

In this study the height of the enclosure was fixed. Since the optimum air gap width for double glazing has been established and generally accepted to be 1/2", the data used for correlation are those based on 1/2" air gap. Therefore, the aspect ratio, H/W, was fixed. The Nu_{ave} is a function of Ra only and can be expressed as

$$Nu = aGr^n \tag{4.6}$$

The correlation was carried out using a least square linear regression analysis.

4.5.1 Correlation equation for the enclosure without convection suppressor

The correlation equation of the average Nusselt number for the hot glass surface is

$$Nu = .186Gr^{0.215} \tag{4.7}$$

and for the cold glass surface

$$Nu = .46Gr^{0.105} \tag{4.8}$$

For the cavity the correlation equation of the overall average Nusselt number is expressed as

$$Nu = .302Gr^{.15} \tag{4.9}$$

The above equations are valid for $4.233x10^3 \leq Gr \leq 1.01x10^4$, $H/W = 34$

4.5.2 Correlation Equations For The Bottom And Top Seals

As mentioned above, the boundary conditions on the top and bottom seals are non-adiabatic. Various heat transfer characteristics were observed at the top and bottom seals for various cases studied. Therefore, we considered appropriate to develop a correlation equation for the various heat transfer data obtained in this study for the top and the bottom seal. **For the bottom seal the correlation equation is**

$$Nu = 5.7\ Gr^{-0.1} \qquad (4.10)$$

This equation is valid for $4.233x10^3 \leq Gr \leq 1.01x10^4$, $H/W = 34$

and **for the top seal is**

$$Nu = 5.45Gr^{.206} \qquad (4.11)$$

This equation is valid for $4.233x10^3 \leq Gr \leq 1.01x10^4$, $H/W = 34$

4.5.3 Correlation Equation for the Enclosure with Convection Suppressor

For the cavity with convection suppressor the correlation equation of the average Nusselt number is given either in term of Grashof number or in term of the ratio of the height of the suppressor to the height of the slot (H_s/H):

In term of the Grashof number, the correlation equation is given as:

$$Nu = 0.00123Gr^{0.76} \qquad (4.12)$$

This equation is valid for $8.5x10^3 \leq Gr \leq 9.2x10^3$, and $.056 \leq H_s/H \leq 0.471$

In term of the ratio of the suppressor height to the cavity height (H_s/H) the correlation equation of the average Nusselt number is given as:

$$Nu = 1.2107(H_s/H)^{-0.013} \qquad (4.13)$$

This equation is valid for the range of H_s/H, $0.056 \leq H_s/H \leq 0.471$ and $Gr = 8.5x10^3$

5. CONCLUSION

Heat loss by convection in confined air layer of a double window glazing is a complex phenomenon which require a thorough understanding of the energy transport mechanisms in order to be able to design high energy efficient windows or to accurately evaluate thermal and condensation performance of insulated window. The complexity of this mode of energy transport is largely due to the interaction of the thermal and hydrodynamic boundary layers on the wall surfaces with the fluid in the core region of the enclosure. The confinement of the convective heat transfer in the enclosure and its coupling with the external convective heat transfer further complicate the problem. The confinement of the air layer makes many traditional temperature and flow measuring instruments such as thermocouple and hot wire anemometer impossible to implement. Therefore, a remote measuring device becomes mandatory. The strong diffusion and flow instabilities make the analytic solution of the thermally coupled partial differential equations of the problem also impossible without imposing over-simplified boundary conditions and assumption which may lead to misleading results and inaccurate interpretation of the actual phenomenon. Moreover measurement and analysis of window pane surface condensation can be too complex for numerical or analytical approach.

To accomplish the above objective, a remote non-intrusive and unique interferometric technique was utilized to study the temperature field and by using heat as a tracer to visualize by inference the flow pattern in the confined enclosure. The parameters examined are the surface temperatures, the enclosure air gap width, the aspect ratio of the enclosure, and the Grashof or Rayleigh number.

Infinite and finite interferograms (interferometric pictures) were obtained. The infinite interferograms were utilized for qualitative study and by inference the flow visualization study. The finite interferogram were used for analyses. The analysis of the finite interferogram provided the temperature map of the enclosure. The data were used to calculate the local and average heat transfer coefficients. It was shown that the average Nusselt number can be related to the thermal Resistance (R-value) and the overall heat transfer coefficient (U-value).

The discussion of heat transfer covered the conduction, the transition, the unicellular and multicellular convection regimes.

The temperature and the heat transfer distribution on the non-adiabatic top and bottom edge seal surfaces of the enclosure were presented and discussed in detail. In contrast to assumption in previous studies where boundary conditions at the seals were considered adiabatic, it was revealed in this study that the real world temperature boundary condition was non-adiabatic and the temperature profile was non-linear. The real world boundary condition at the seal varied with the heat transfer characteristics in the enclosure. The use of the non-adiabatic boundary condition revealed new phenomena and heat transfer results here-to-fore not been reported in literature.

In this study the range of our critical Grashof number, Gr_c, is $7800 \leq Gr_c \leq 8600$. This

value was in the range of Gr_c given by Vest and Arpaci [1969] and Eckert and Carlson [1961]. This study also revealed that in the transition to convection regime, two modes of heat transfer co-existed. Heat was transported by convection in the developing boundary layer on the wall surface and by conduction across the air layer. It was found that as the Grashof number increased, the boundary layer thickness increased until at high Grashof number the boundary layers on the walls merged to develop into convection eddies at fully established convection regime. Further increase in Grashof number resulted in the flow developing into multi-cellular eddies. The convective eddies which was found to promote heat loss and induce surface condensation was suppressed by an introduction of convection suppressor into the enclosure cavity.

The following correlation equations were obtained

For the top edge seal surface

$$Nu = 5.45Gr^{-0.206}$$

This equation is valid for $4.233x10^3 \leq Gr \leq 1.01x10^4$, $H/W = 34$

For the bottom edge seal surface

$$Nu = 5.7\ Gr^{-0.1}$$

This equation is valid for $4.233x10^3 \leq Gr \leq 1.01x10^4$, $H/W = 34$

For hot glass surface

$$Nu = .186Gr^{0.215}$$

For cold glass surface

$$Nu = .46Gr^{.105}$$

For the entire air layer

$$Nu = .302Gr^{.15}$$

The above equations are valid for $4.233x10^3 \leq Gr \leq 1.01x10^4$, $H/W = 34$

For the cavity with convection suppressor the correlation equation of the average Nusselt number is given as:

$$Nu = 0.00123Gr^{0.76}$$

This equation is valid for 8.5x103 < Gr < 9.2x103, and $0.056 \leq L/H \leq 0.471$

For the ratio of the suppressor height to the cavity height (H_s/H) the correlation equation of the average Nusselt number is given as:

$$Nu = 1.2107(H_s/H)^{-0.013}$$

This equation is valid for the range of H_s/H, $0.056 \leq H_s/H \leq 0.471$ and

$8.5x10^3 \leq Gr \leq 9.2x10^3$

The correlation equations are strictly valid for the range of Grashof number and suppressor to cavity heights ratios specified. Interpolation between parameters are not recommended.

REFERENCES

Arasteh, D.K., Beck,F.A., Griffith, B.T., Byars, N., and Acevedo-Ruiz, M., "Using Infrared Thermography to Study Building Heat Transfer", ASHRAE Journal, October 1992.

Arasteh, D., Selkowitz, S., and Hartmann, J., 1985, "Detailed Thermal Performance Data on Conventional and Highly Insulating Window Systems", Proceedings of ASHRAE/DOE/BTECC Thermal Performance of the Exterior Envelopes of Buildings III, ASHRAE SP 49.

American Society of Heating, Refrigerating And Air-Conditioning Engineers, Inc., 1989, ASHRAE HANDBOOK of Fundamentals, 1989 Edition, S.I.Unit version.

Bailey, D.W., Cameron, A.M., "Infrared Assessment of Windows under Laboratory Conditions", Final Report to CANMET - Energy Mines & Resources Canada, under Contract No. 23284-7304/01-SQ

Bajorek, S.M. and Lloyd, J.R., 1982 "Experimental investigation of natural convection in partitioned enclosures", ASME J. Heat Transfer, vol. 104, pp. 527-532.

Batchelor, G.K., 1954, "Heat Transfer by Free Convection Across A Closed Cavity Between Vertical Boundaries at Different Temperatures", Quarterly Journal of Applied Mathematics, vol.xii, pp. 209-233.

Brown, W.P., Solvanson, K.R., and Wilson, A.G., 1961, "A Unique Hot-Box Cold-Room Facility", ASHRAE Transactions, Vol. 67, pp. 561-577.

Brown, W.P., and Solvanson,K.R., 1984, " A Calorimeter for Determining Heat Transmission Characteristics of Windows", ASTM Conference on Thermal Insulation, Materials and Systems, Dallas,USA.

Bowen,R.P. 1985, "DAR's Approach for Determining the Heat Transmission Characteristics of Windows", National Research Council, Division of Building Research, Building Research Note 234.

Chang, L.C., Lloyd, J.R., and Yang, K.T., 1982, "A finite difference study of natural convection in complex enclosures", Proc. 7th Int. Heat Transfer Conf., Munich, pp. 183-188.

Ciofalo, M. and Karayiannis, T.G., 1991, "Natural convection heat transfer in a partially- or completely- partitioned vertical rectangular enclosure", Int. J. of Heat and Mass Transfer, vol. 34, number 1, pp. 167-179.

Eckert, E.R.G., and Carlson, W.O., 1961, "Natural Convection in an Air layer Enclosed Between Two Vertical Plates With Different Temperature", Int. J. Heat and Mass Transfer, vol.2, pp. 106-120.

ElSherbiny, S.M., Raithby, G.D., and Hollands, K.G.T., "Heat Transfer by Natural Convection Across Vertical and Inclined Air Layers", J. Heat Transfer, Vol. 104, pp.96-102.

Gershuni, G.Z., and Zhukhovitskii, E.M., 1969, "Stability of Plane-Parallel Convective Motion With Respect to Spatial Perturbations", Journal of Applied Mathematics and Mechanics, vol. 33, No.5, pp. 855-860.

Gill, A.E., and Davey, A., 1969, "Instabilities of a buoyancy driven system", J. Fluid Mech. 35 (4) pp. 775-798.

Goldstein, R.J., 1976 "Optical Techniques for Temperature Measurements", Measurements in Heat Transfer, McGraw-Hill Book Company, New York.

Grange, T., and Owens, P., 1985, "Low Emissivity Glass", Proceedings of Building Research ISBN 91 540 4121X, Stockholm, Sweden.

Gray, D.D., "Convective heat loss from windows: A review of literature", West Virginia University, Morgantown, W V 26506-6101 Report, 1985.

Hart, J., 1971, "Stability of flow in a differentially heated inclined box", J. Fluid Mech., vol. 47, pp. 547-576.

Hollands, K.G.T. and Konicek,L., 1973, "Experimental Study of the Stability of Differentially Heated Inclined Air Layers", Inter. J. Heat and Mass Transfer, vol. 16, pp. 1467-1476.

Kurzweg, U.H., 1970, "Stability of Natural Convection Within an Inclined Cavity", J. of Heat Transfer, vol. 14, pp. 190-191.

Kusuda, T., and Collins, B.L., 1978, "Simplified Analysis of Thermal and Lighting Characteristics of Windows: Two Case Studies", National Bureau of Standards, BSS 109.

Lampert, C.M., 1981, "Heat Mirror Coatings for Energy Conserving Windows", Solar Energy Materials, Vol. 6, No.1.

Lawrence Berkeley Laboratory, Windows and Daylighting Group, Applied Science Division, 1988, "A PC Program (WINDOW 3.1) for Analyzing Window Thermal Performance", Lawrence Berkeley Laboratory, University of California, Berkeley, CA 94720, USA.

Lee, Y. and Korpela, S., 1983, "Multicellular Natural Convection in a Vertical Slot", J. Fluid Mechanics, Vol. 126, pp. 91-121.

Showole, R.A. 1988, "An Interferometric and Numerical Study of Free and Mixed Convective Heat Transfer From Open Rectangular, Semi-cylindrical and V-shaped Isothermal Cavities", Ph.D. Thesis, University of Western Ontario, London, Canada.

Unny, T.E., 1972, "Thermal instability in differentially heated inclined fluid layers", Applied Mechanics, vol. 39, pp. 41-46.

Vest, C.M. and Arpaci, V.S., 1969, "Stability of natural convection in vertical slot", J. of Fluid Mechanics, vol. 36, pp. 1-15.

Wilson, A.G., Solvanson, K.R., and Nowak, E.S., 1959, "Evaluation of Factory-Sealed Double-Glazed Window Units", National Research Council, Division of Building Research, Research Paper No. 85.

Wright, J.L.,and Sullivan, H.F., 1987, "VISION: A Computer Program for the Detailed Simulation of the Thermal Performance of Innovative Glazing Systems", International Conference on Building Management, Lausanne, Switzerland, vol. 4, pp. 5-12.

APPENDIX A

FRINGE SHIFT EVALUATION TECHNIQUE

As mentioned in section 2.4, the fringe shift positions were determined by measurements made with a travelling microscope. The fringe shift evaluation of finite and infinite fringes are similar in theory but technically different. The evaluation technique to be discussed here and which applies to the present study is for the finite fringe interferogram. The finite fringe evaluation technique may be used for infinite fringe interferogram, but the usual method for infinite fringe evaluation is not suitable for finite fringe evaluation.

A typical finite fringe interferogram for a vertical enclosure is shown in Figure A.1a. Following the alignment of the finite fringe interferogram with the cross hair of the comparator, using the hot surface as reference, the table of the comparator holding the interferogram was moved vertically to set the cross hair at predetermined locations on the reference walls where the fringe numbers were to be counted or where the temperature gradients on the wall were to be calculated. The fringes were then numbered consecutively from the hot to the cold surface and the corresponding horizontal positions (or fringe shift) including the positions of the walls were read from the micrometer dial of the comparator. The corresponding fringe numbers at the hot and cold walls were obtained by extrapolation. These values constitute the raw data for the interferometric analysis. A plot of the fringe numbers versus the horizontal positions of the fringes was made as shown in Figure A.1b.

The total fringe shift was computed from the known temperature T_h and T_c of the hot and

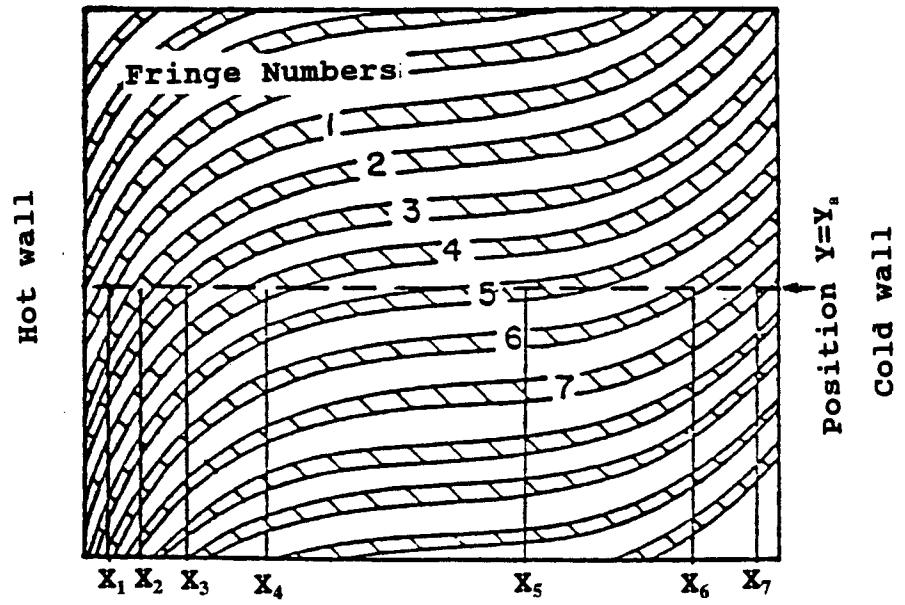

Fig. A.1a **A Sketch of a Typical Finite Fringe Interferogram Showing the Fringe Number**

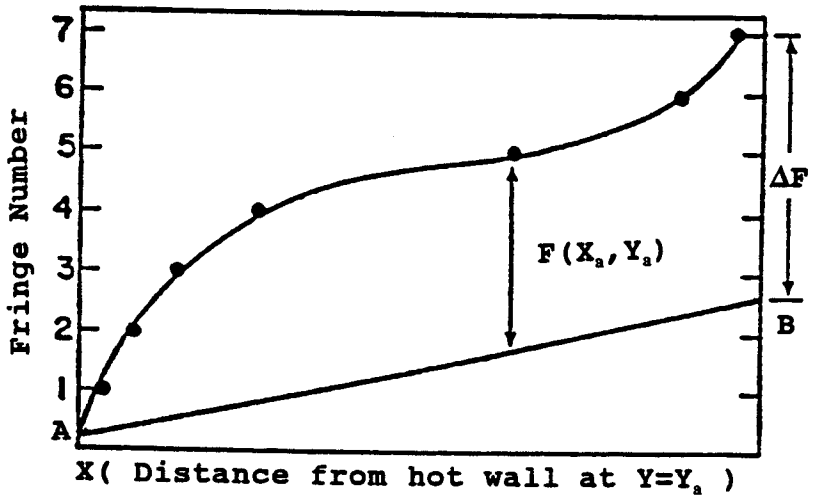

Fig. A.1b **Plot of the Fringe Numbers (Obtained from Fig A.1a at $Y=Y_a$) Versus the Horizontal Positions of the Fringes**

cold walls using Equation 2.5 in section 2. The total fringe shift was then subtracted from the extrapolated fringe number at the cold wall as shown in Figure A.1b. A straight line was then drawn from point A to B which represent the unknown reference fringe field necessary for analysis. A reference fringe was set before the enclosure was heated but disappeared after heating. So the reference fringe has to be re-established. The correct fringe shifts were then the vertical distances between the measured fringe field and the computed reference fringe field. For example, the true fringe number at (x_a,y_a) is F(xa,ya).

A computer analysis program was then developed. With the aid of this computer program the true fringe numbers at each horizontal positions were related to the actual temperatures existing at these positions. This was done by a third order polynomial (least square) method as follows

$$F(x_a,y_a) = a_1 + a_2x + a_3x^2 + a_4x^3 \qquad (A.1)$$

where a_1, a_2, a_3, a_4 are the coefficients of the polynomial equation.

Combining this equation with Equation (2.6), the local temperatures across the enclosure were obtained. All of the above steps were repeated at each horizontal position to obtain the temperature map in the enclosure. These were used to calculate the temperature profile and the temperature gradients and the local heat transfer coefficients on the hot and cold walls.

APPENDIX B

Results of the analysis

Note: Because of the space limitation only the top, central and bottom sections are shown in Appendix B for each of the finite and infinite interferograms. However, the isotherms contours shown on the same plate covers the entire height of the vertical slot. The isotherms contours were obtained from the analysis of five interferograms of the entire sections of the slot.

Table B.1

Results of the Analysis

Test Run No.	T_h °C	T_c °C	ΔT	w cm.	AR	H_s cm.	Gr_w x10^3	Gr_H x10^8	Nu_{cc}	Nu_{ave}
1	23	9	14	1.27	34	0	4.2	1.7	.9924	1.114
2	20	3	17	1.27	34	0	5.6	2.2	.9899	1.153
3	20	0	20	1.27	34	0	6.6	2.6	.9852	1.178
4	20	-3	23	1.27	34	0	7.8	3.1	.9897	1.212
5	18	-6	24	1.27	34	0	8.6	3.4	1.053	1.249
6	19	-9	28	1.27	34	0	10.	4.0	1.065	1.279
7	20	-6	26	.953	45	0	3.8	3.6	.9866	1.003
8	20	-9	29	.953	45	0	4.4	4.1	.9824	1.009
9	20	-9	29	1.59	27	0	20.	4.1	1.454	1.655
10	19	-9	28	1.91	22	0	34.	4.0	1.538	1.809
11	19	-6	25	1.27	34	2.54	8.8	3.5	1.078	1.229
12	20	-6	26	1.27	34	5.08	9.2	3.6	1.059	1.272
13	19	-6	25	1.27	34	10.16	8.8	3.5	1.099	1.263
14	18	-6	24	1.27	34	20.32	8.5	3.3	1.871	1.195
15	20	-6	26	1.27	34	2.54*	9.1	3.6	1.066	1.315
16	21	-9	27	1.91	22	Full**	36.	4.2	1.486	1.553

* H_s = 2.54 cm. (Suppressor on top and bottom sections of the slot).

** H_s/H = (Suppressor height to Cavity height ratio) = 1 (i.e Full partition or tripple glazing).

CC (centre cell)

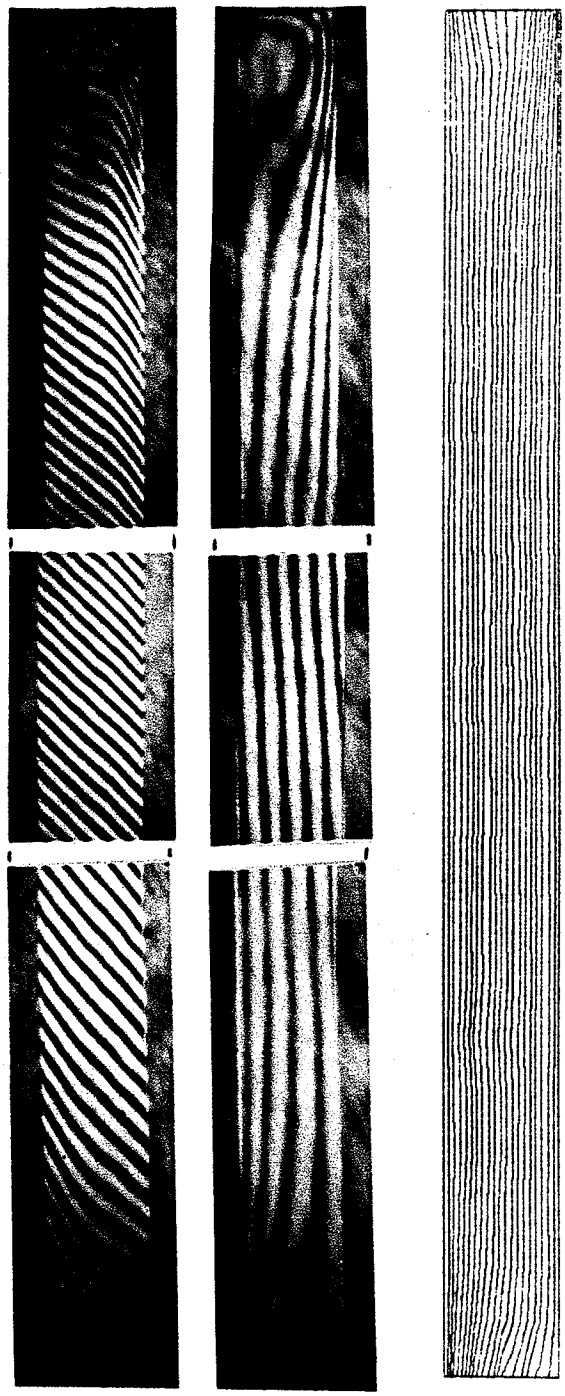

Test Run # 1

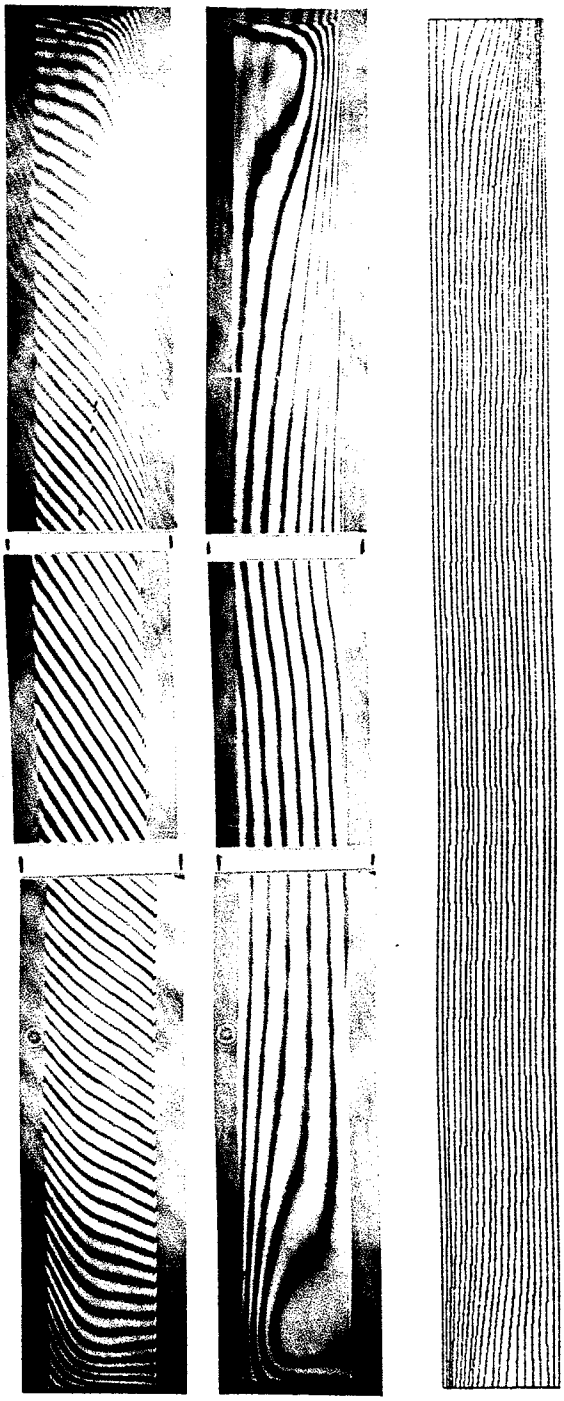

Test Run # 2

Finite and Infinite Interferograms and Calculated Isotherms

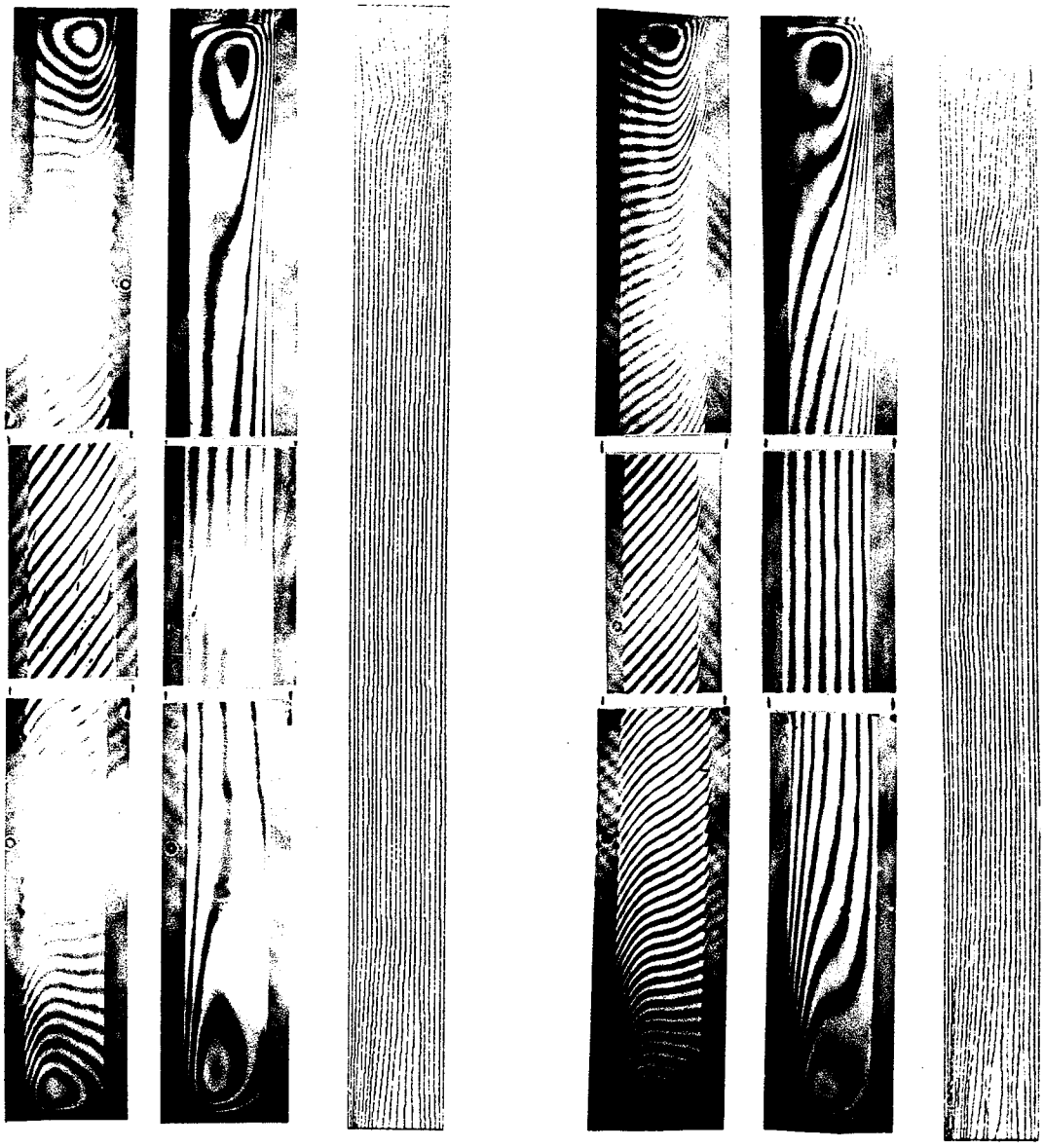

Test Run # 3

Test Run # 4

Finite and Infinite Interferograms and Calculated Isotherms

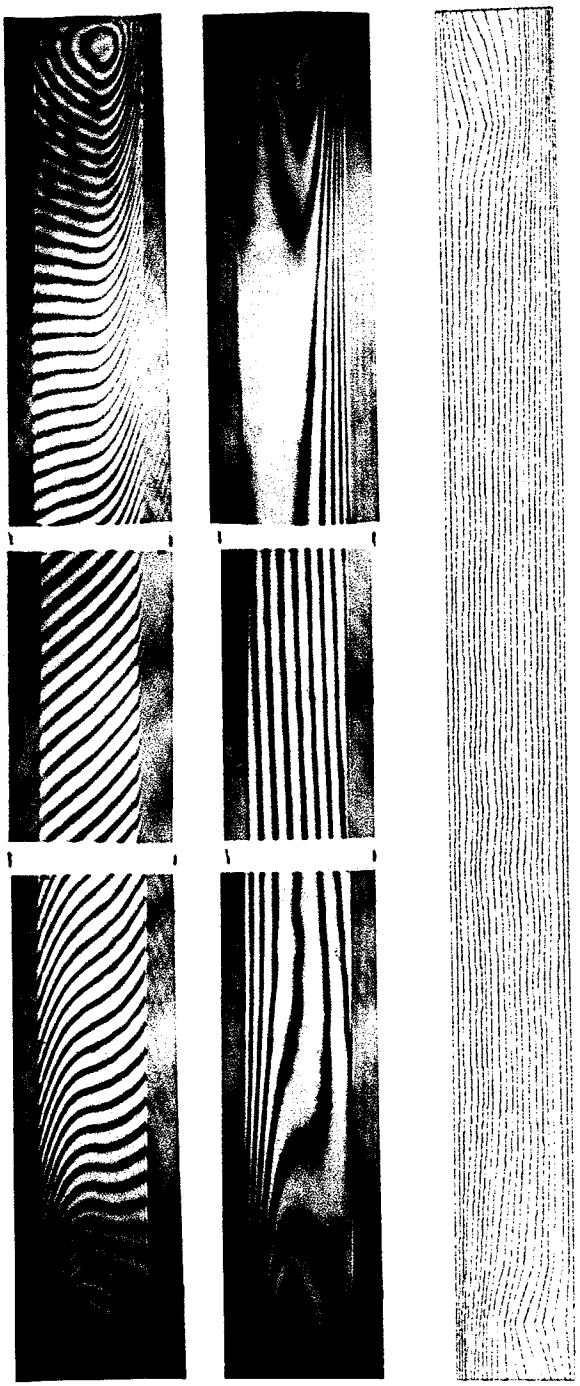

Test Run # 5

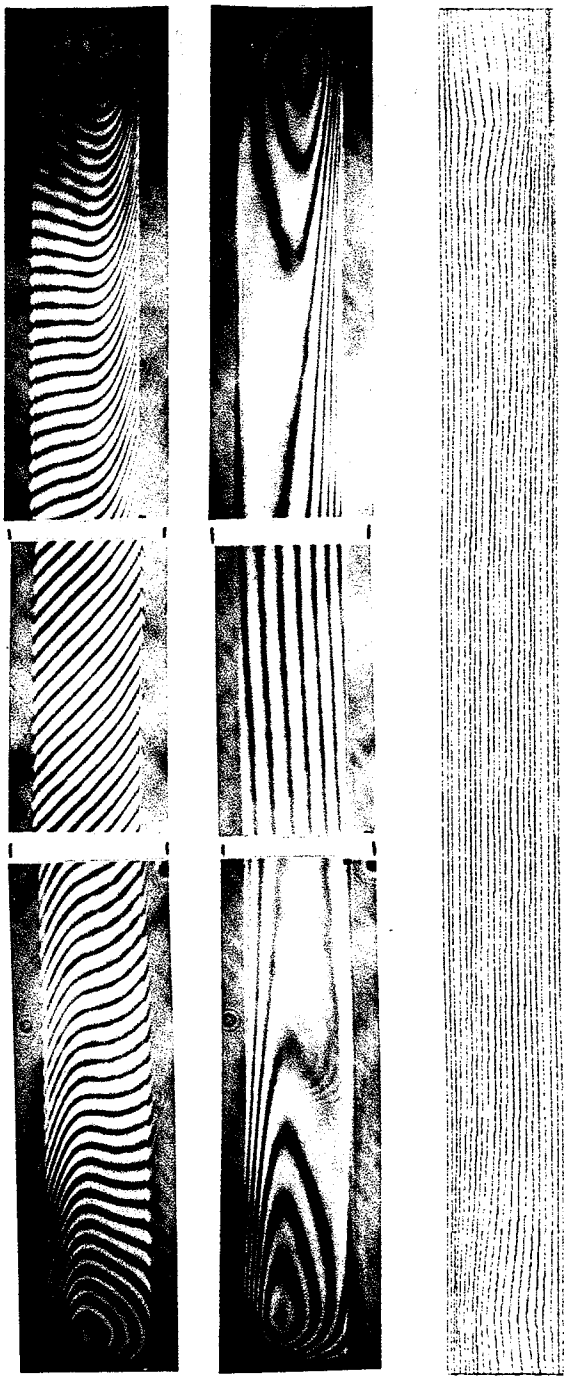

Test Run # 6

Finite and Infinite Interferograms and Calculated Isotherms

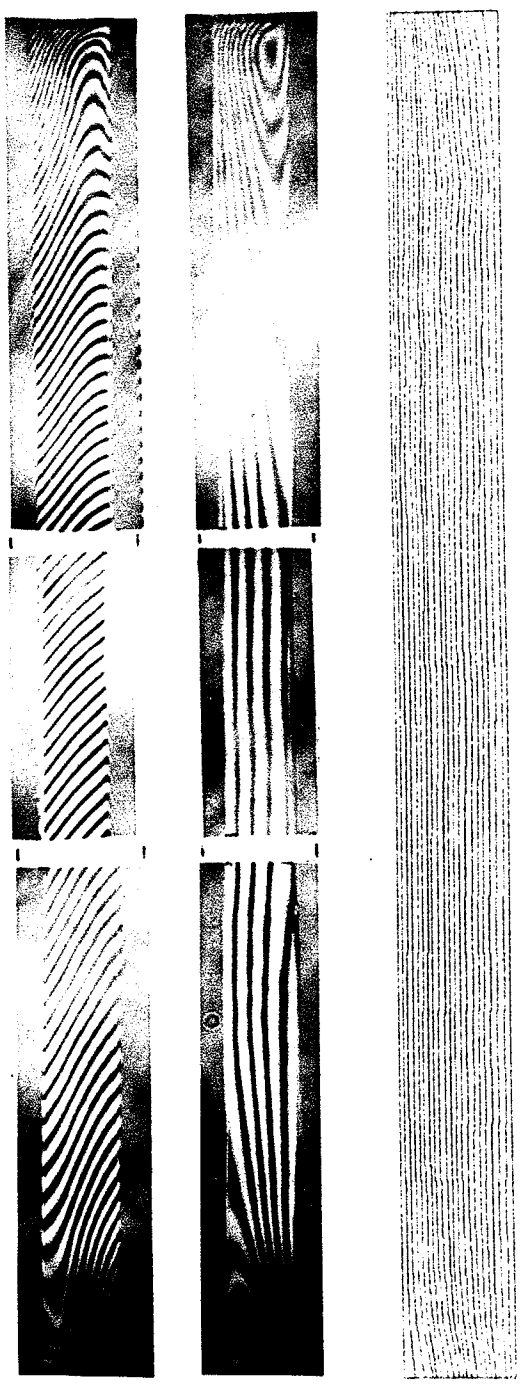

Test Run # 7

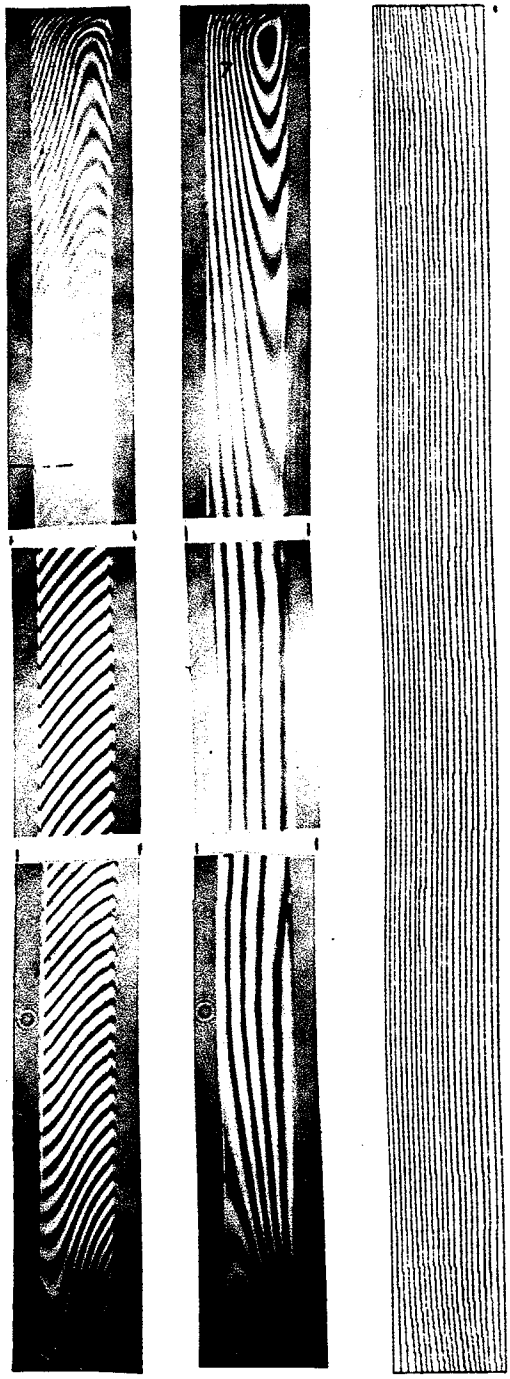

Test Run # 8

Finite and Infinite Interferograms and Calculated Isotherms

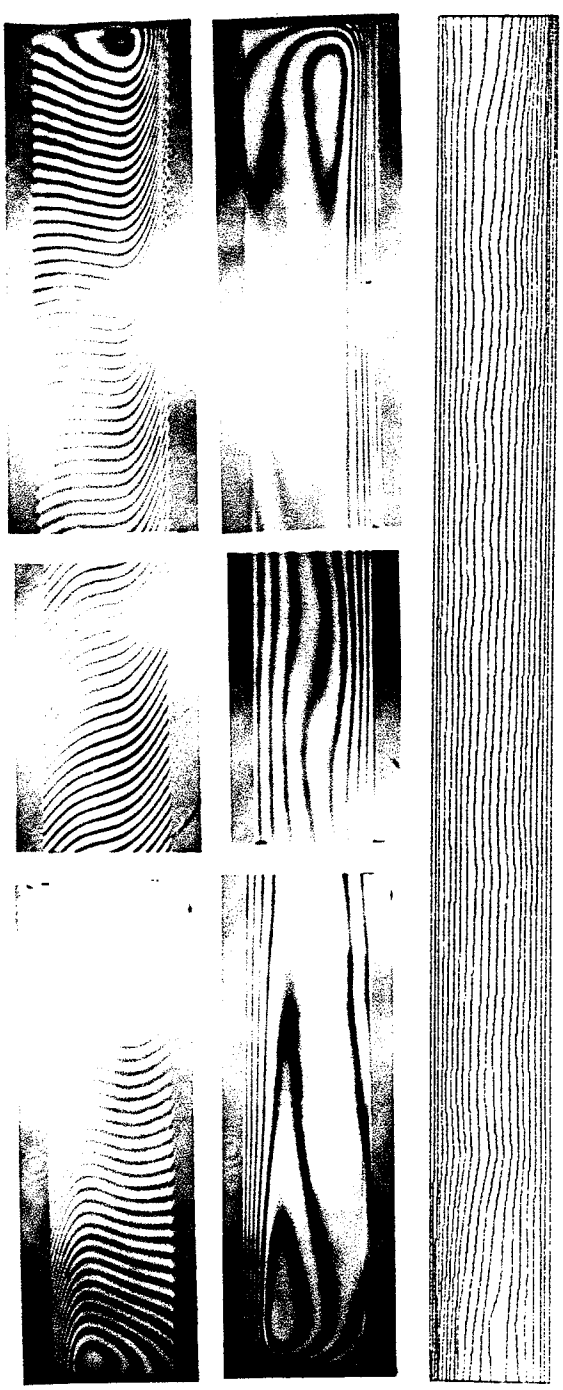

Test Run # 9

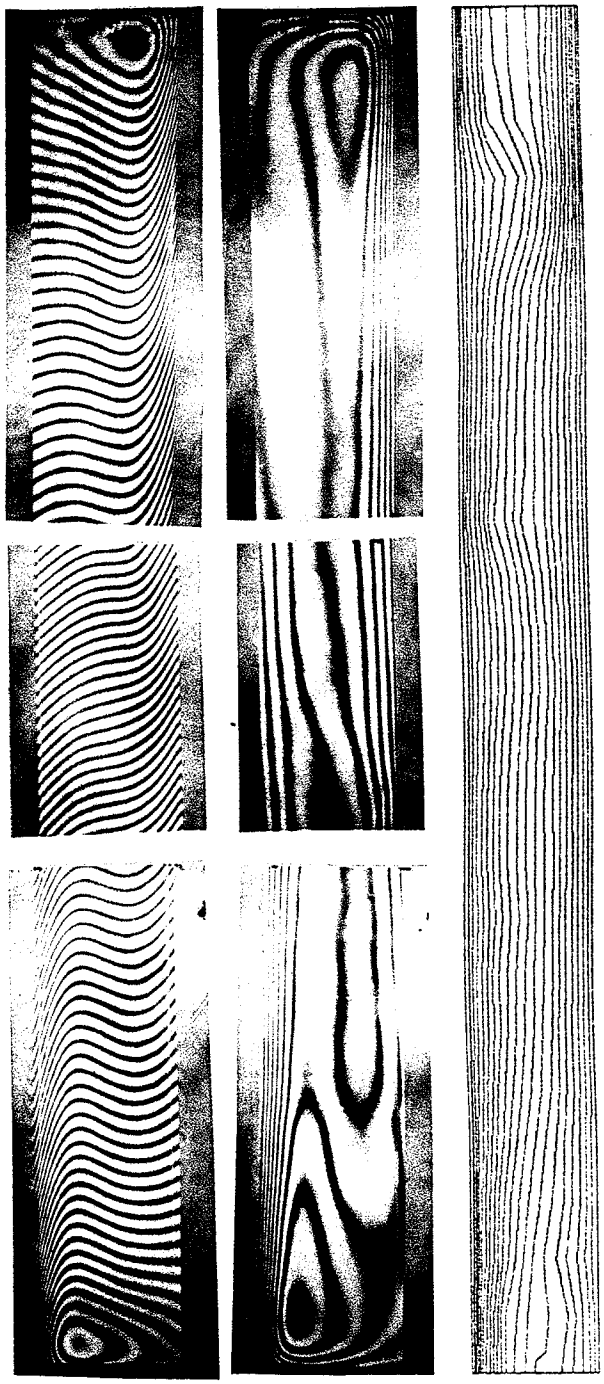

Test Run # 10

Finite and Infinite Interferograms and Calculated Isotherms

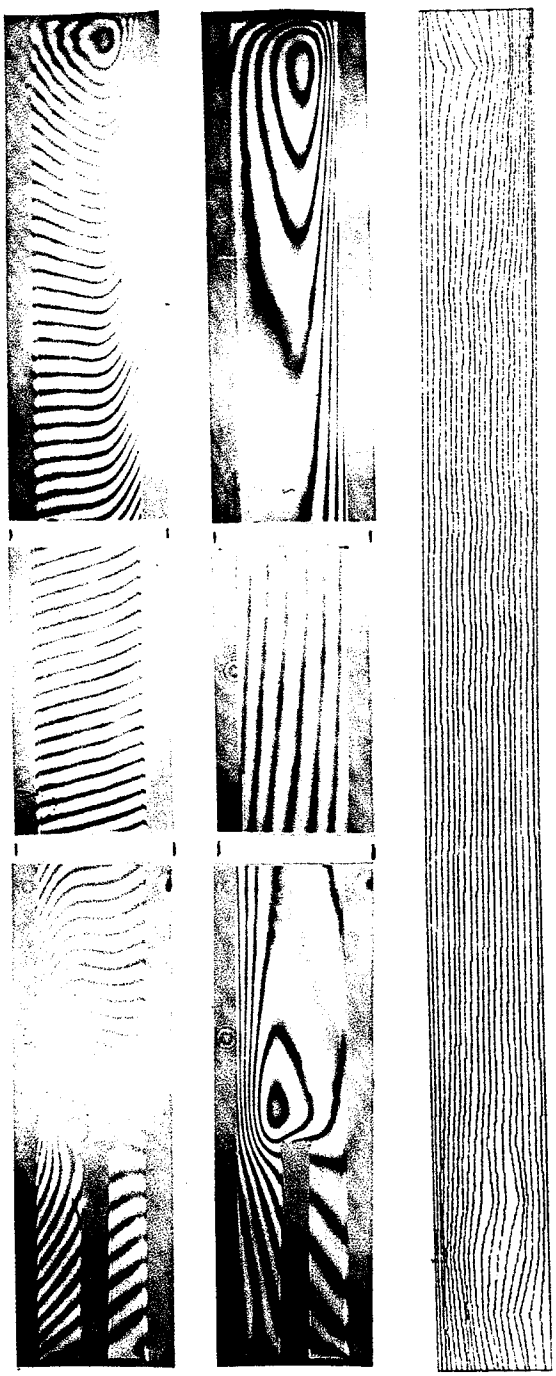

Test Run # 11

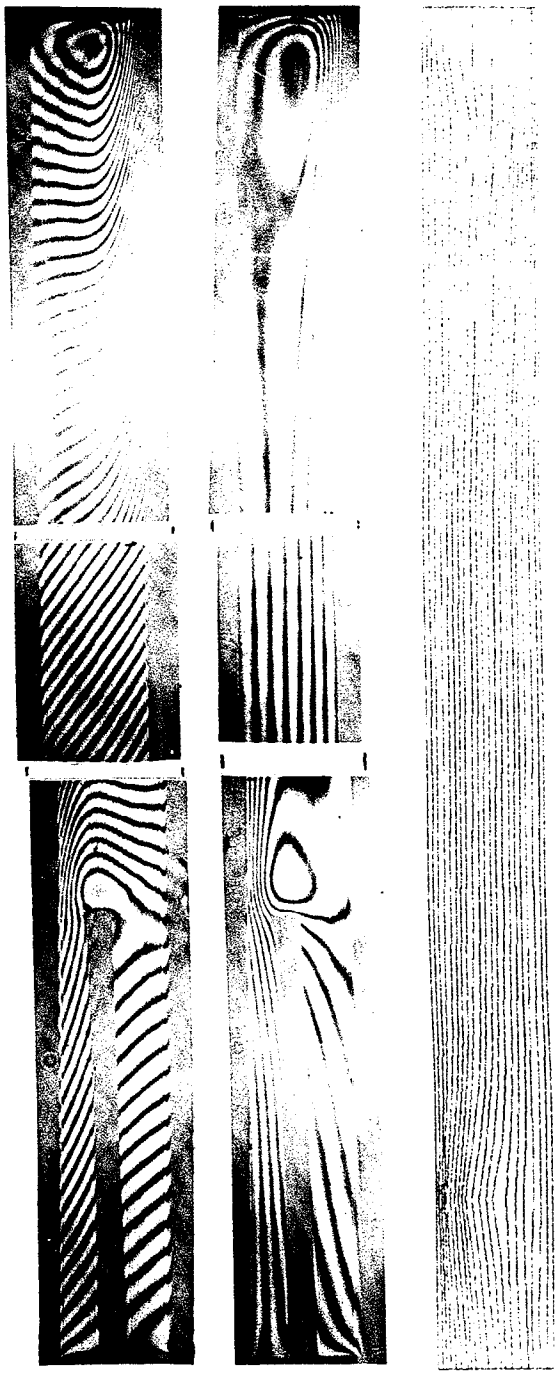

Test Run # 12

Finite and Infinite Interferograms and Calculated Isotherms

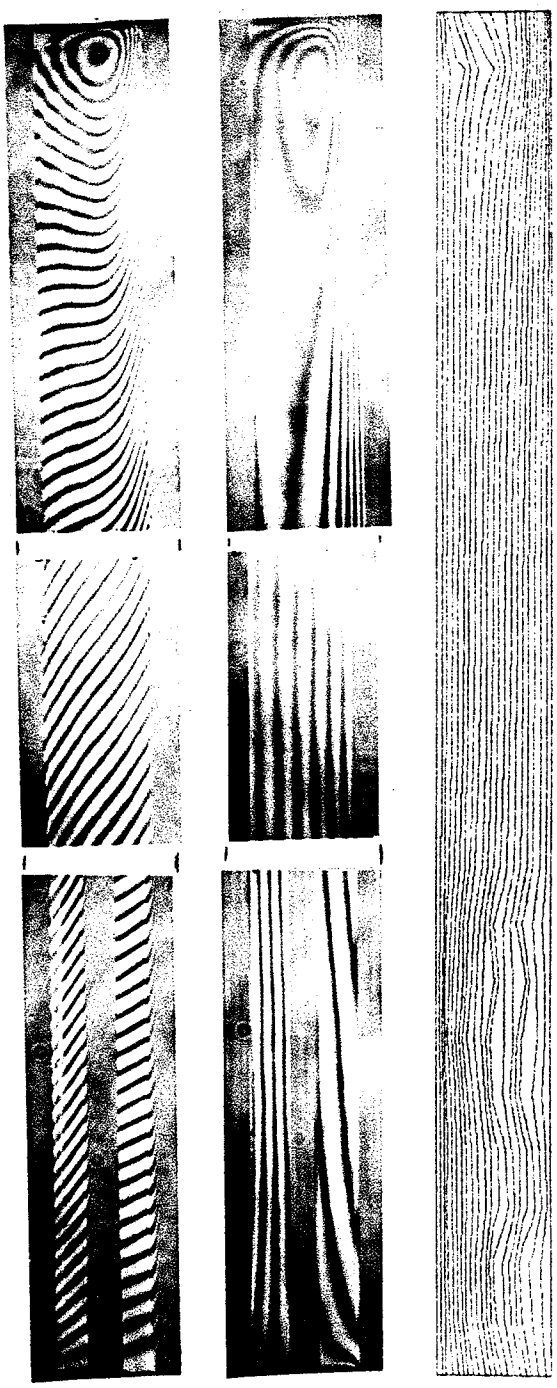

Test Run # 13

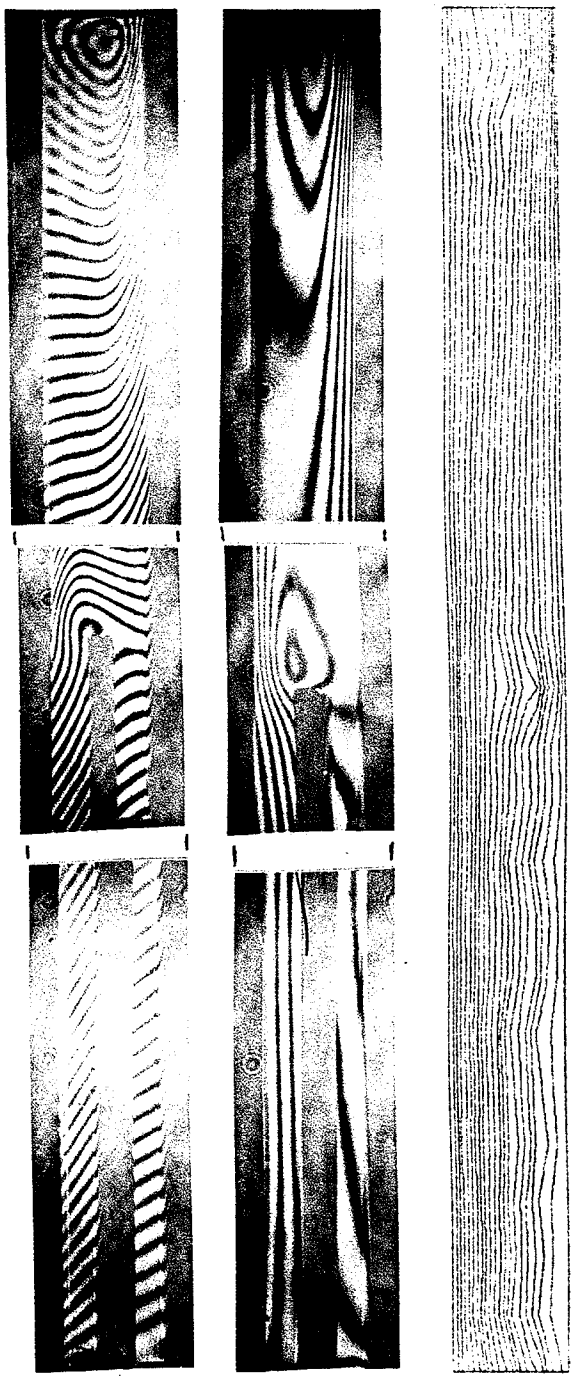

Test Run # 14

Finite and Infinite Interferograms and Calculated Isotherms

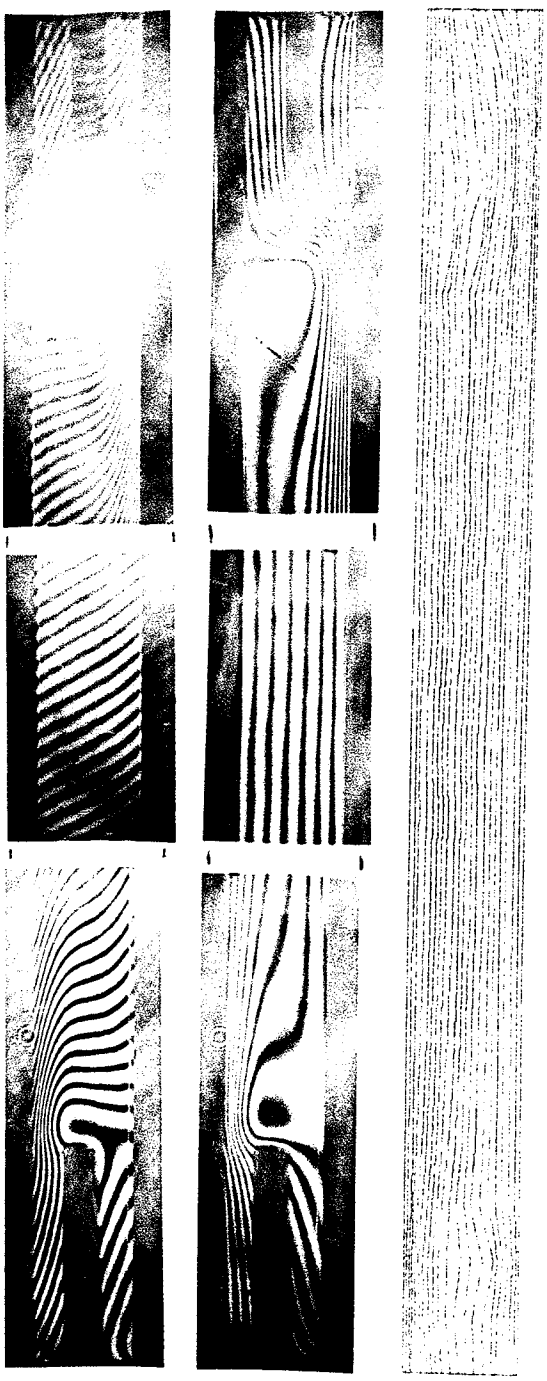

Test Run # 15

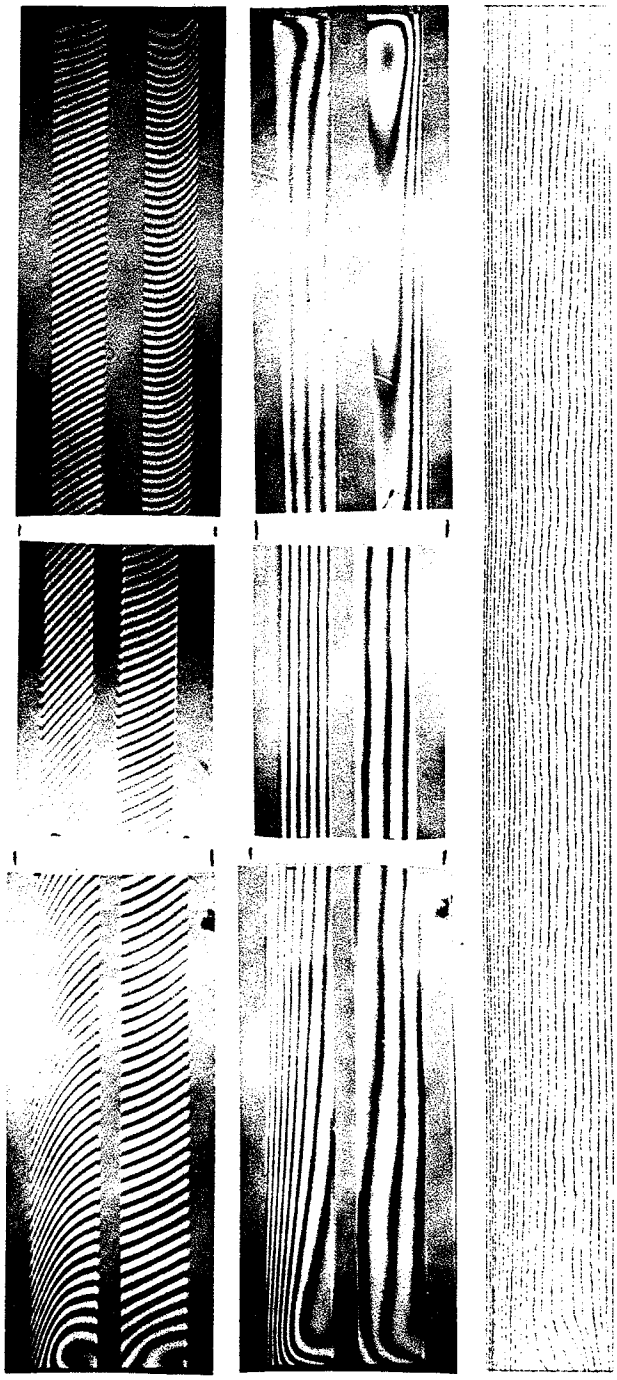

Test Run # 16

Finite and Infinite Interferograms and Calculated Isotherms

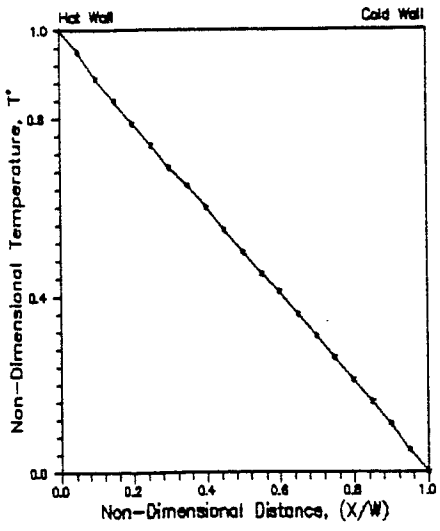

Test Run # 1

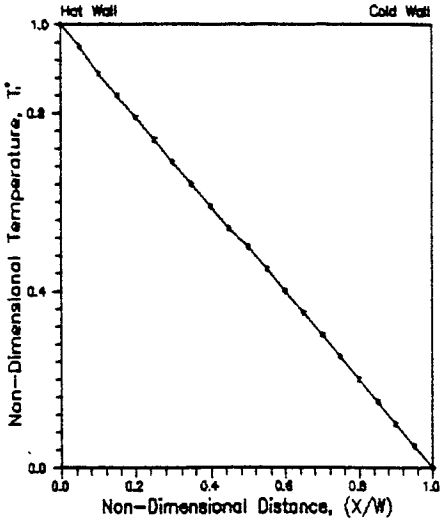

Test Run # 2

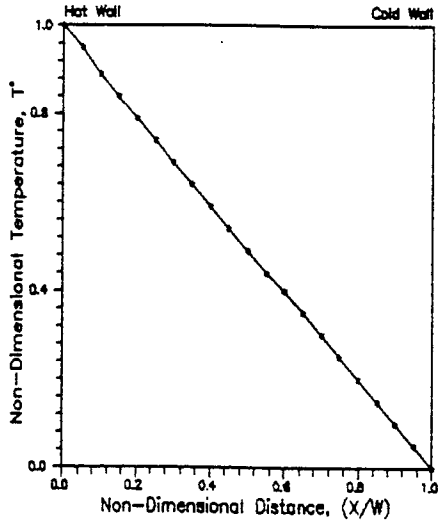

Test Run # 3

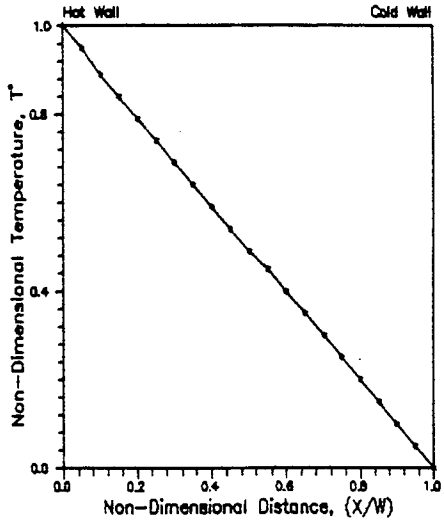

Test Run # 4

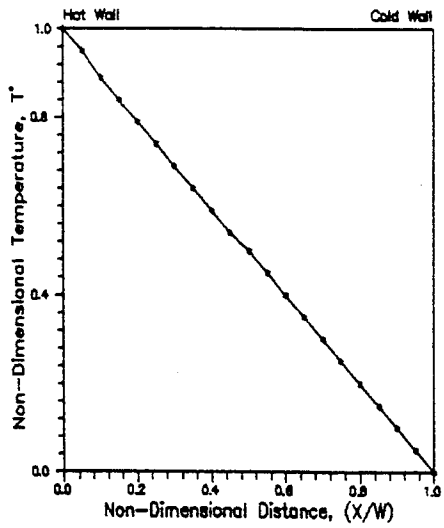

Test Run # 5

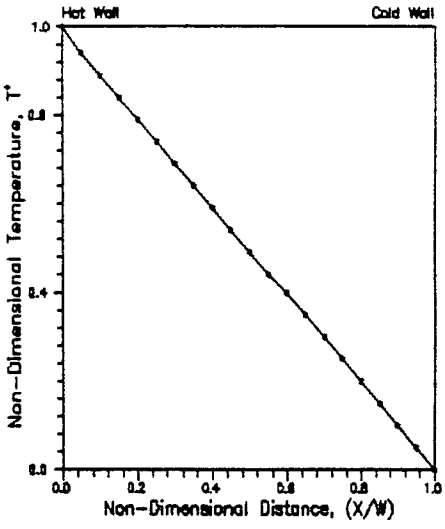

Test Run # 6

Temperature Profile Along The Horizontal Centre Line of The Air Gap

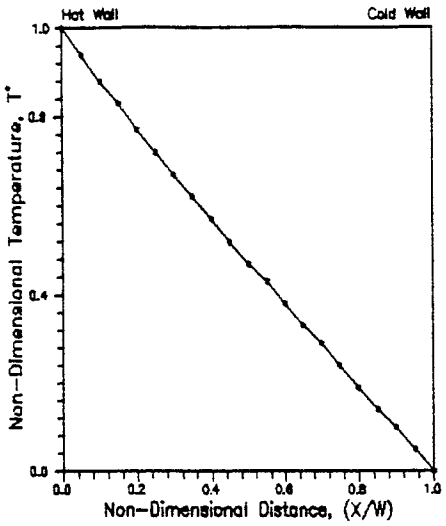

Test Run # 7

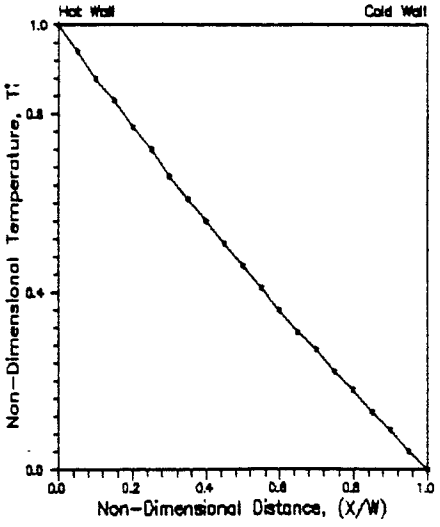

Test Run # 8

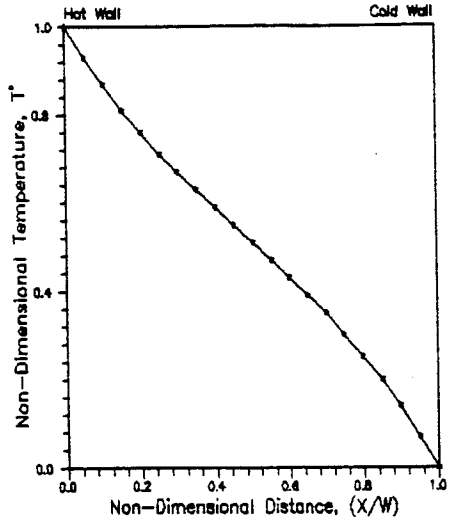

Test Run # 9

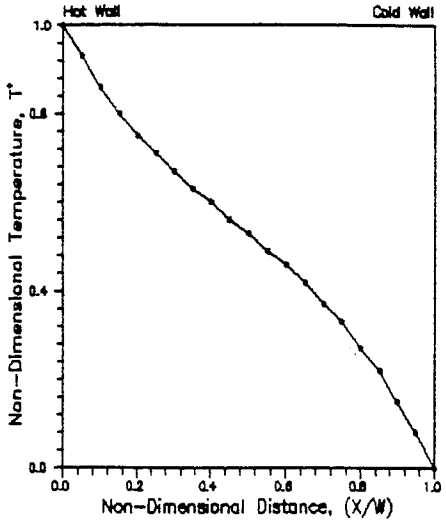

Test Run # 10

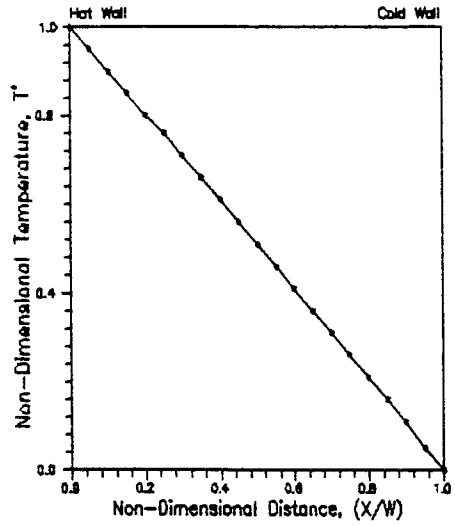

Test Run # 11

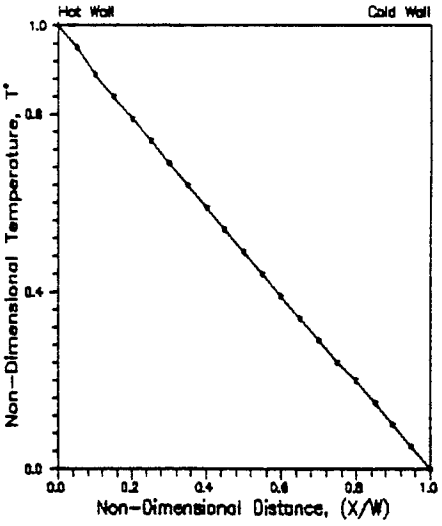

Test Run # 12

Temperature Profile Along The Horizontal Centre Line of The Air Gap

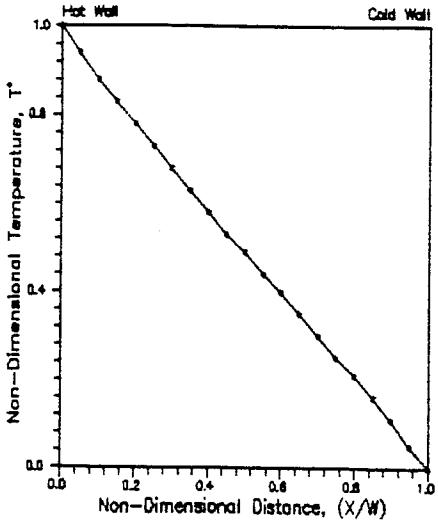

Test Run # 13

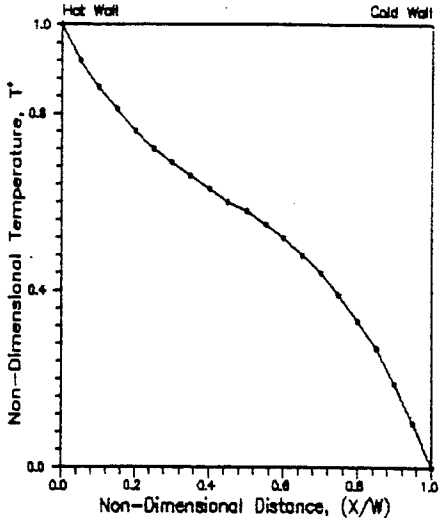

Test Run # 14

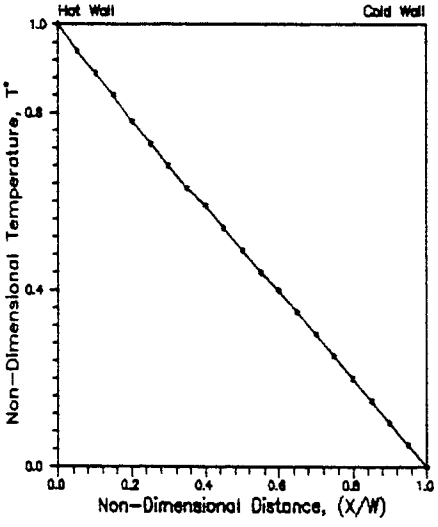

Test Run # 15

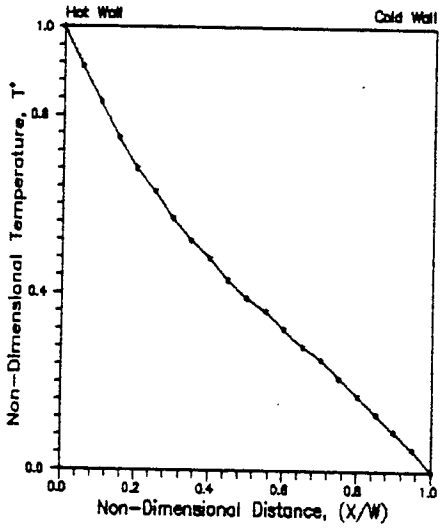

Test Run # 16

Temperature Profile Along The Horizontal Centre Line of The Air Gap

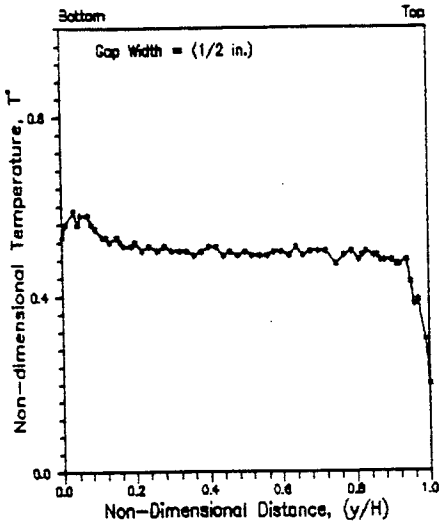

Test Run # 1

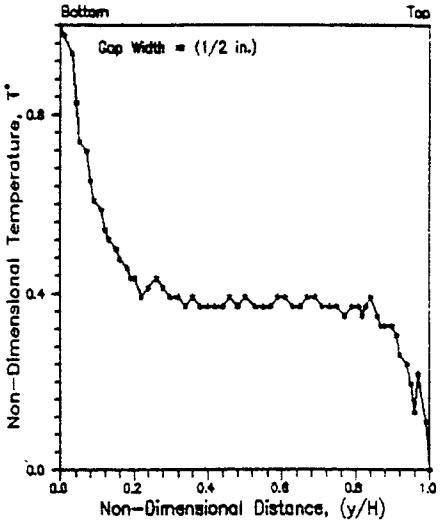

Test Run # 2

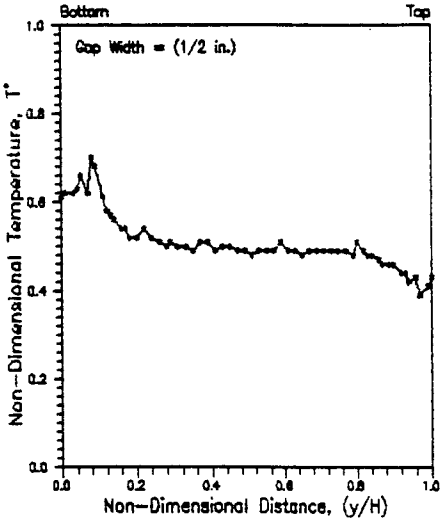

Test Run # 3

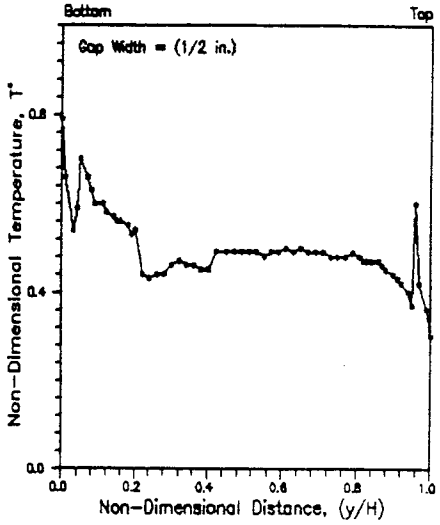

Test Run # 4

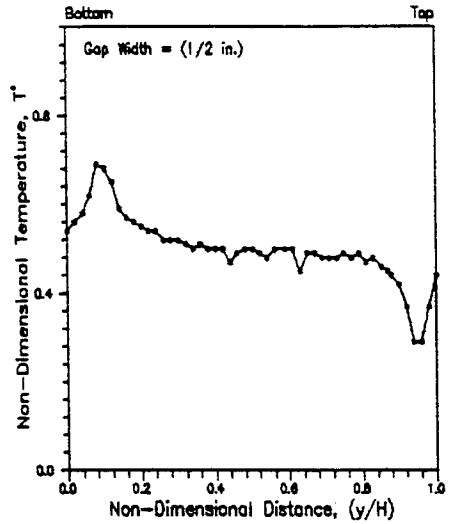

Test Run # 5

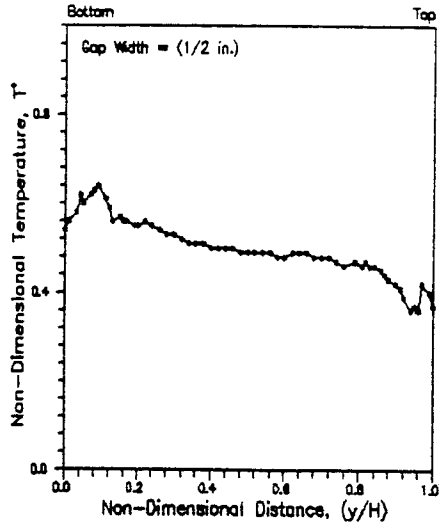

Test Run # 6

Temperature Profile Along the Vertical Centre Line of The Air Gap

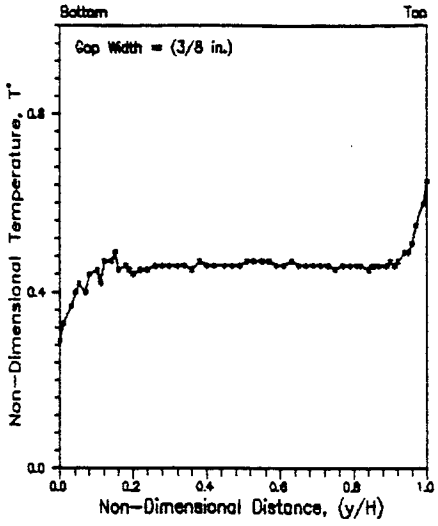

Test Run # 7

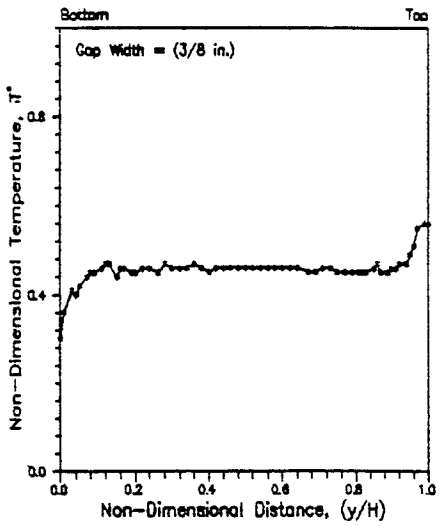

Test Run # 8

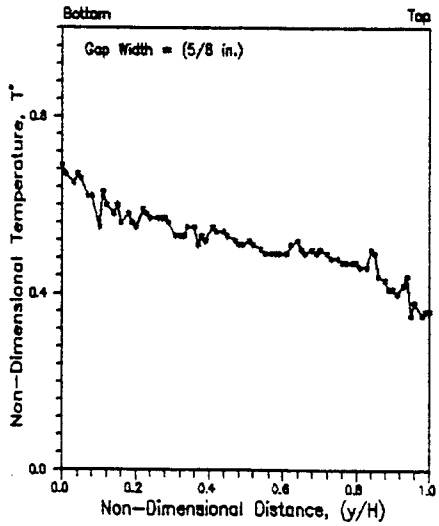

Test Run # 9

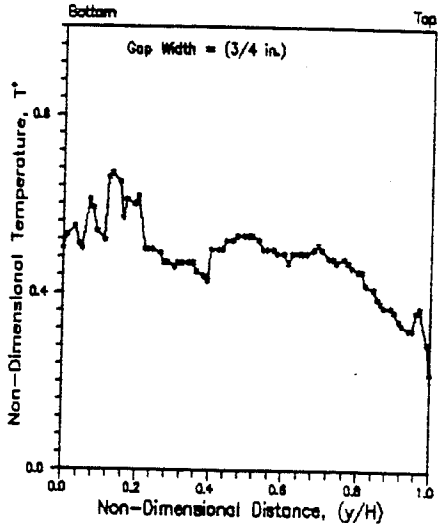

Test Run # 10

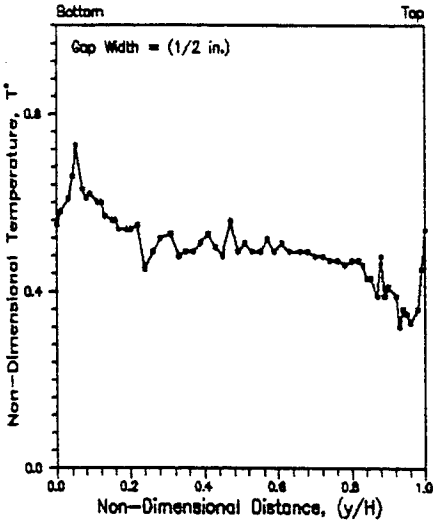

Test Run # 11

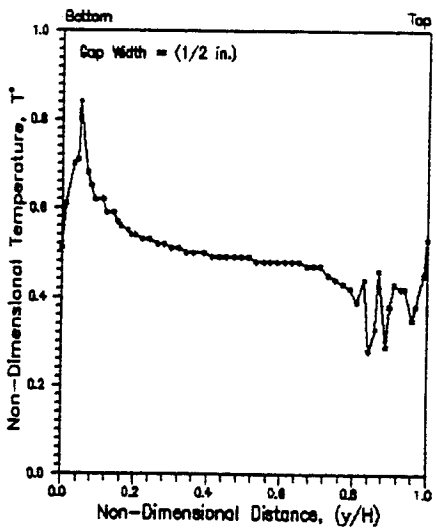

Test Run # 12

Temperature Profile Along the Vertical Centre Line of The Air Gap

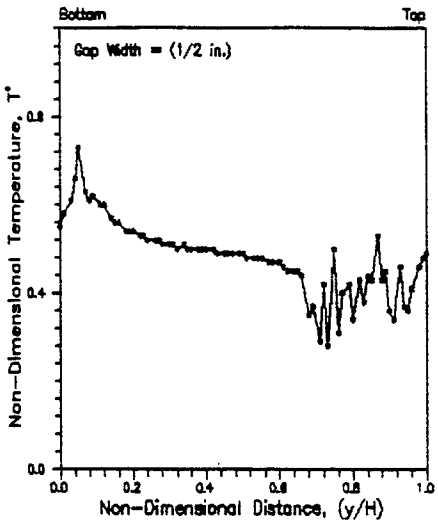

Test Run # 13

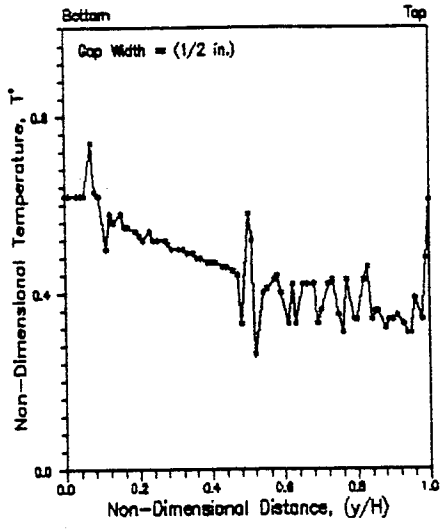

Test Run # 14

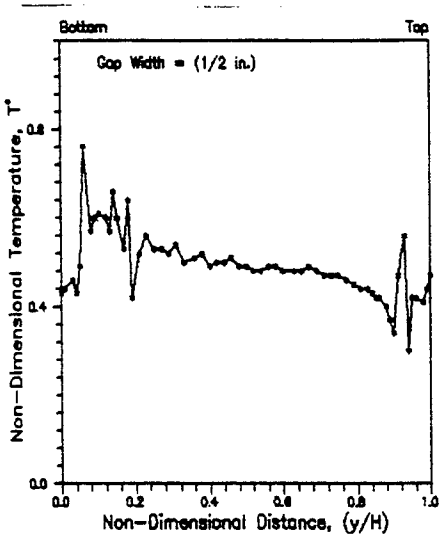

Test Run # 15

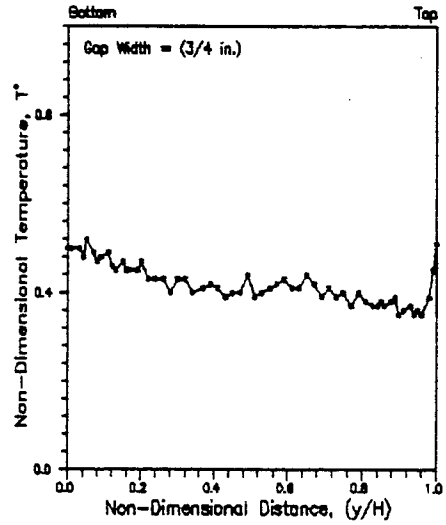

Test Run # 16

Temperature Profile Along the Vertical Centre Line of The Air Gap

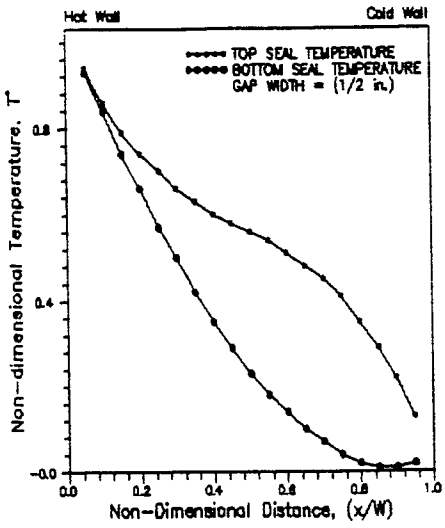

Test Run # 1

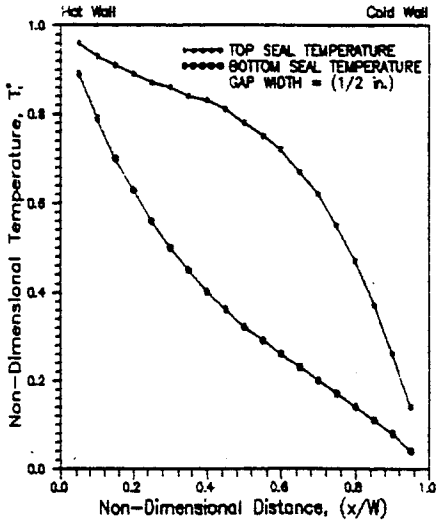

Test Run # 2

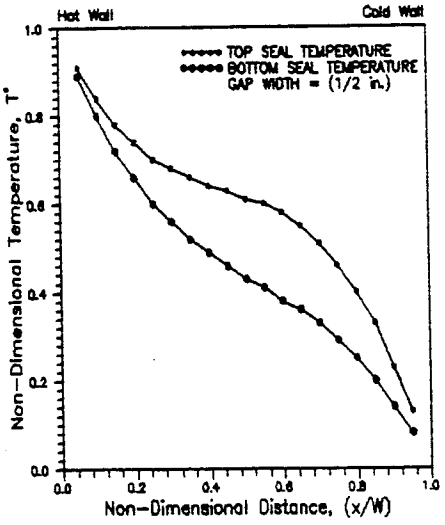

Test Run # 3

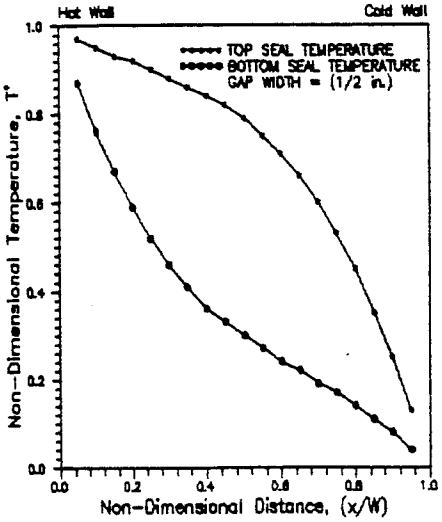

Test Run # 4

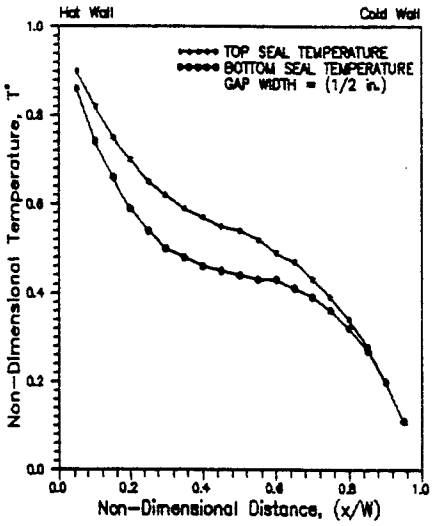

Test Run # 5

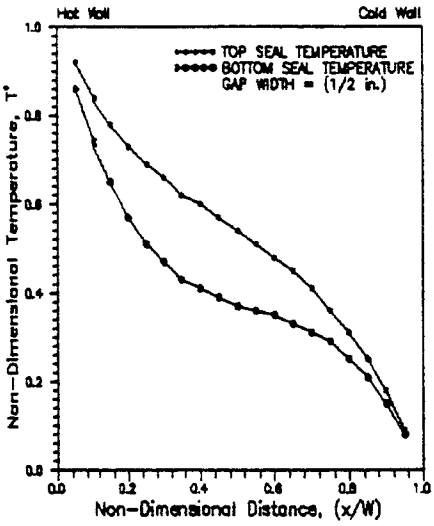

Test Run # 6

Temperature Profiles on Top and Bottom Surfaces of The Air Gap

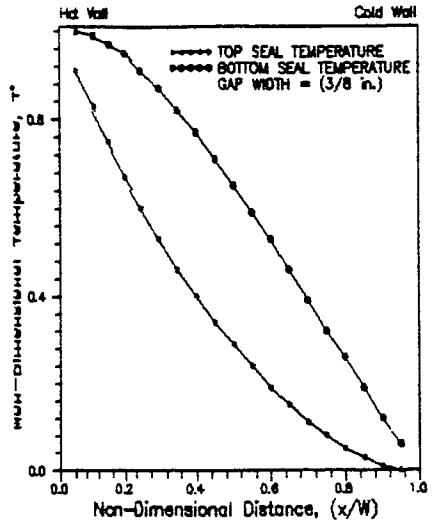

Test Run # 7

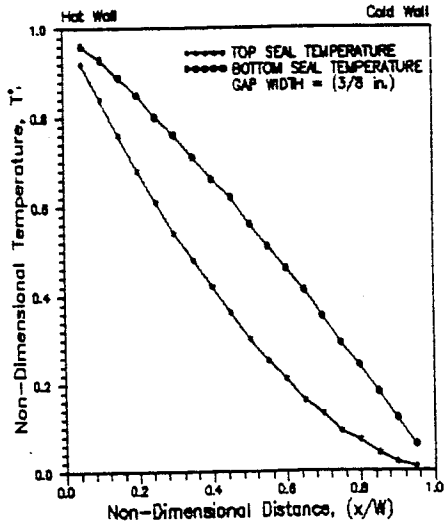

Test Run # 8

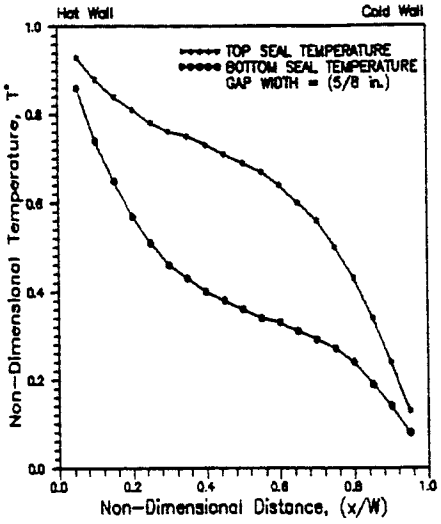

Test Run # 9

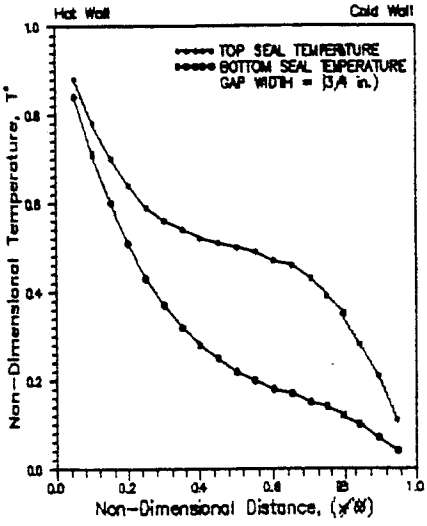

Test Run # 10

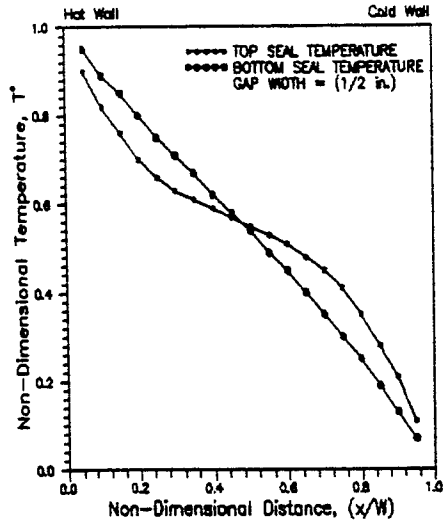

Test Run # 11

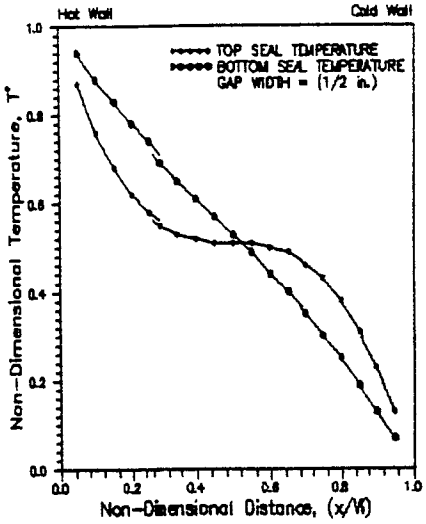

Test Run # 12

Temperature Profiles on Top and Bottom Surfaces of The Air Gap

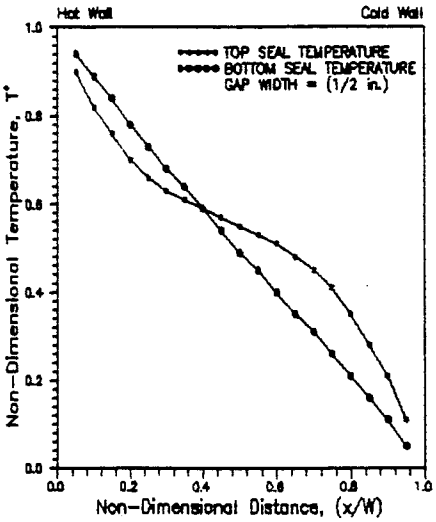

Test Run # 13

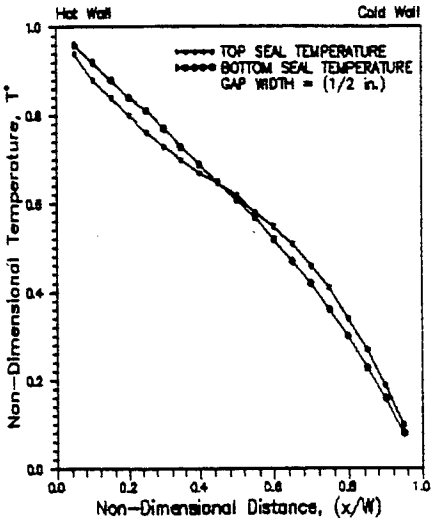

Test Run # 14

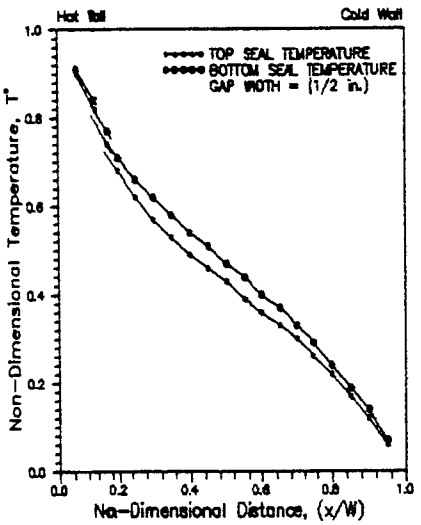

Test Run # 15

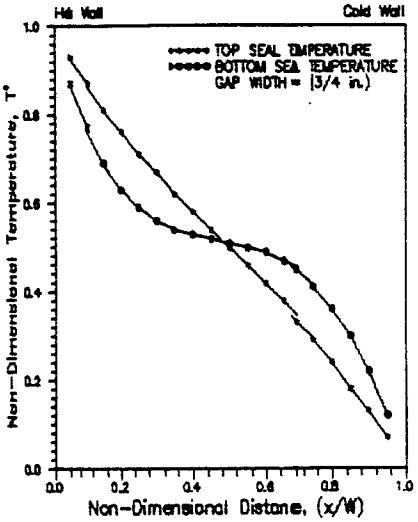

Test Run # 16

Temperature Profiles on Top and Bottom Surfaces of The Air Gap

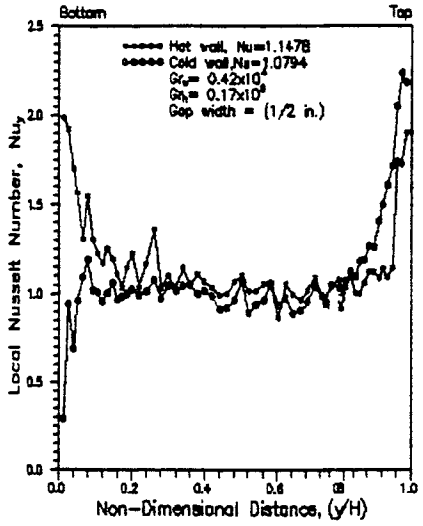

Test Run # 1

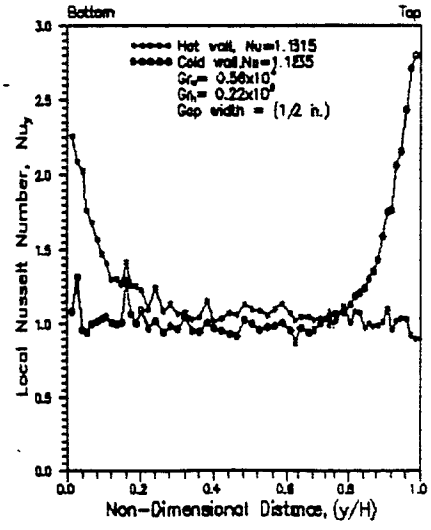

Test Run # 2

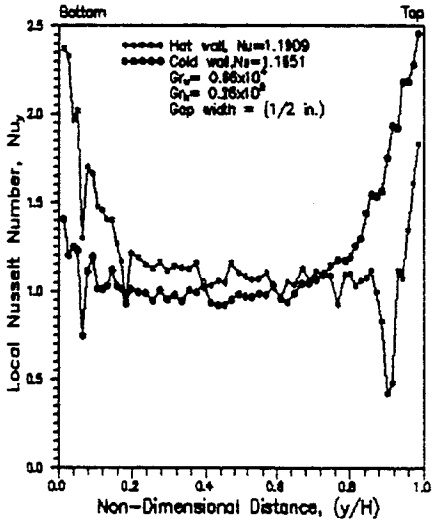

Test Run # 3

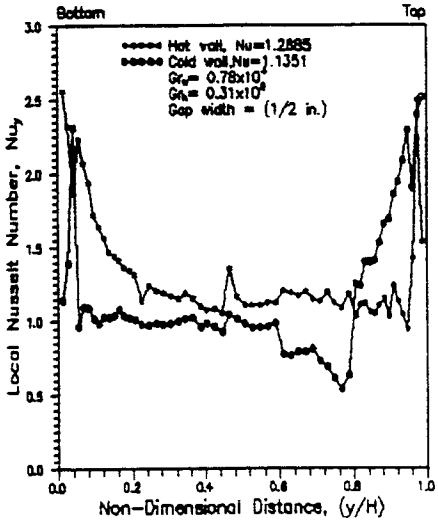

Test Run # 4

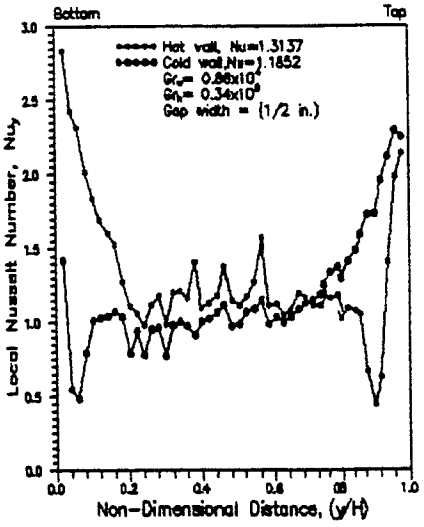

Test Run # 5

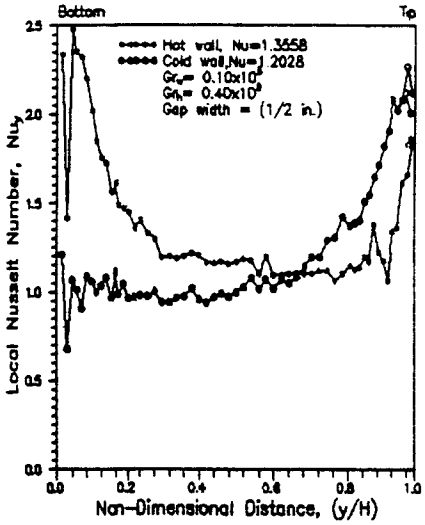

Test Run # 6

Local Heat Transfer on Hot and Cold Glass Surfaces

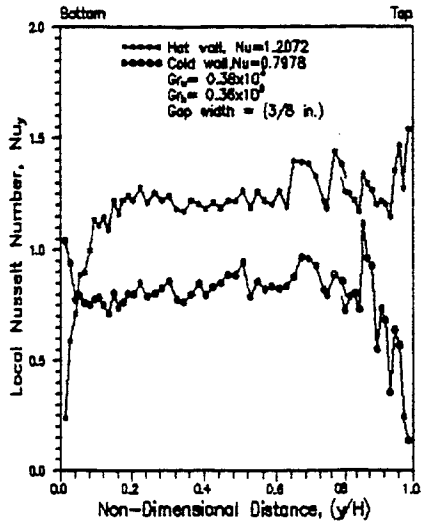

Test Run # 7

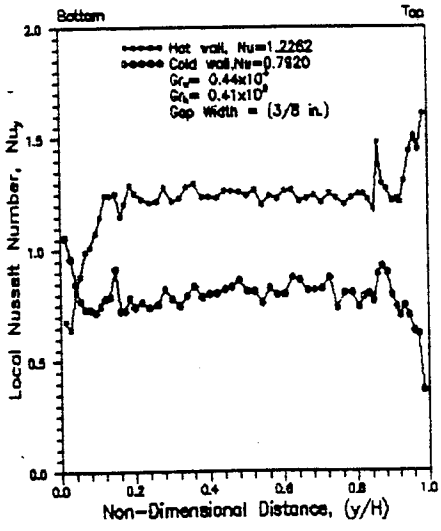

Test Run # 8

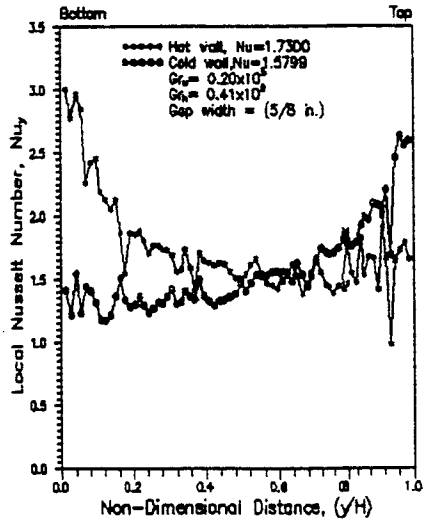

Test Run # 9

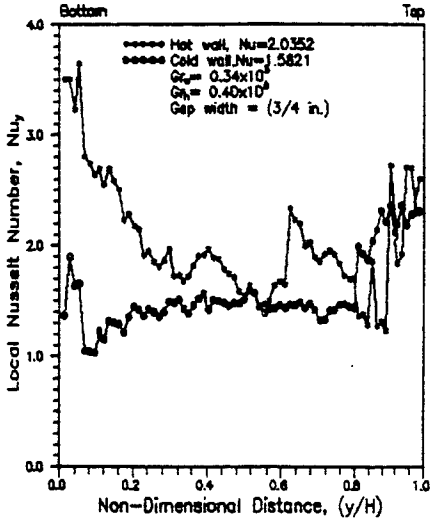

Test Run # 10

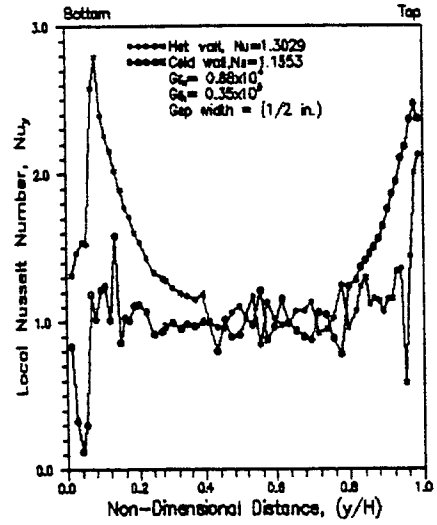

Test Run # 11

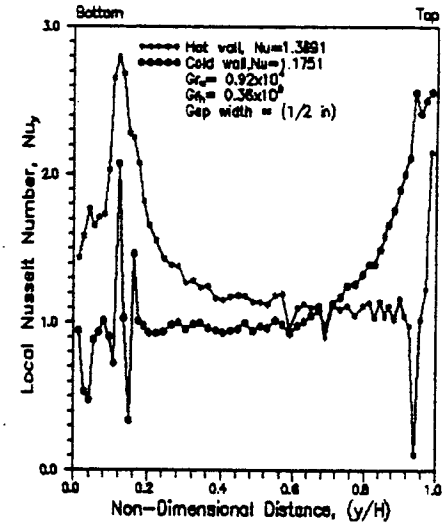

Test Run # 12

Local Heat Transfer on Hot and Cold Glass Surfaces

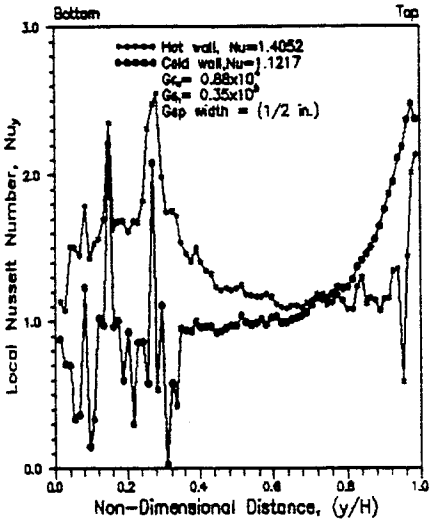

Test Run # 13

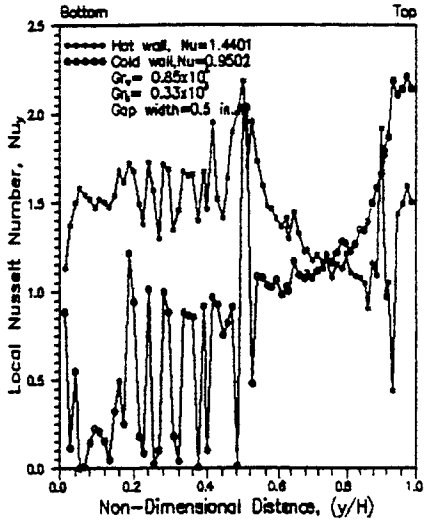

Test Run # 14

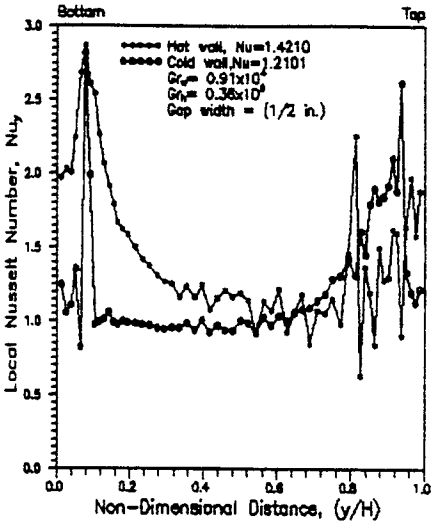

Test Run # 15

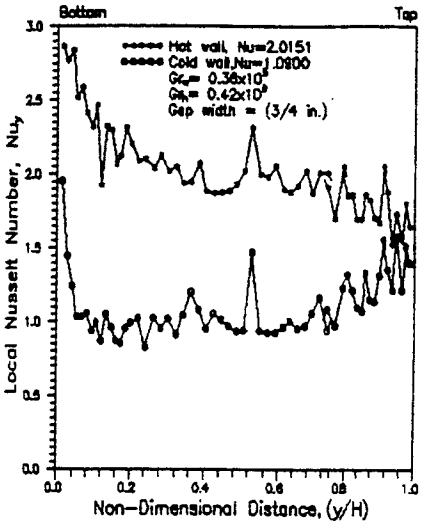

Test Run # 16

Local Heat Transfer on Hot and Cold Glass Surfaces

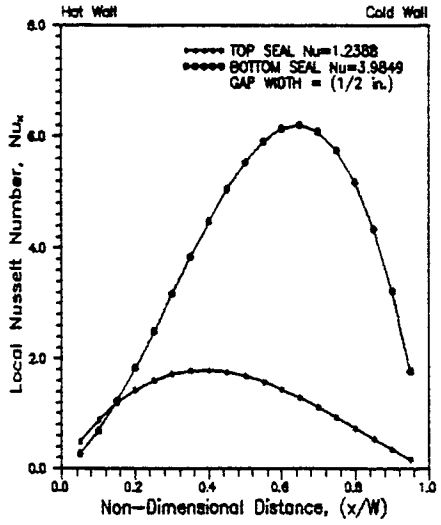

Test Run # 1

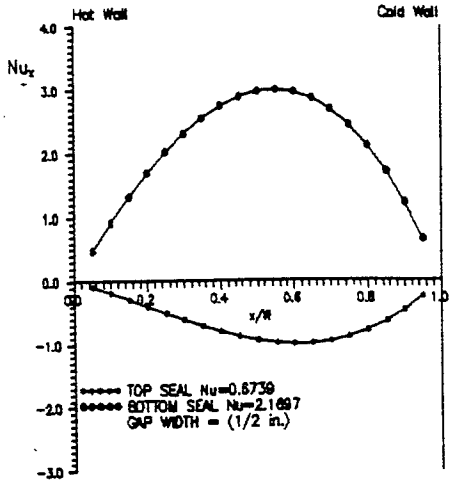

Test Run # 2

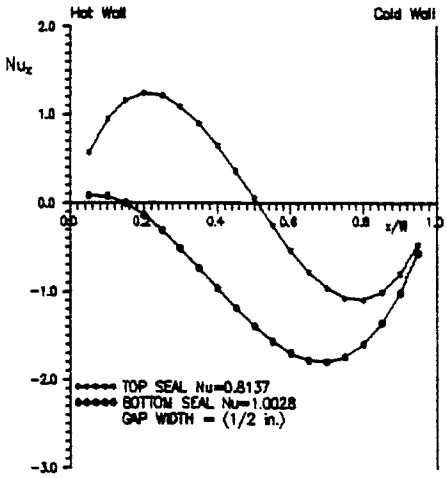

Test Run # 3

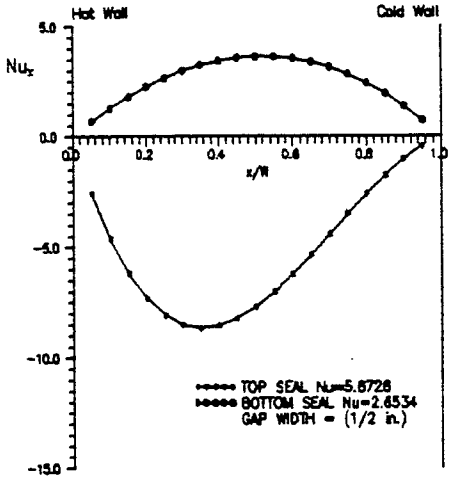

Test Run # 4

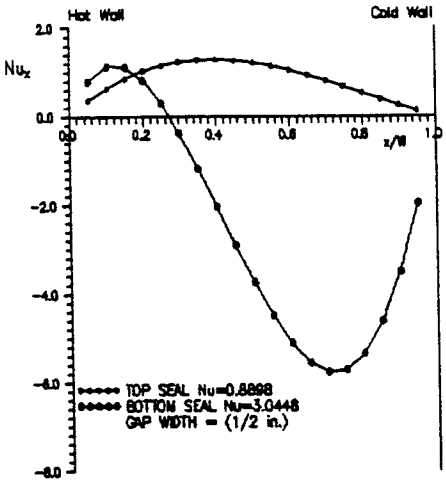

Test Run # 5

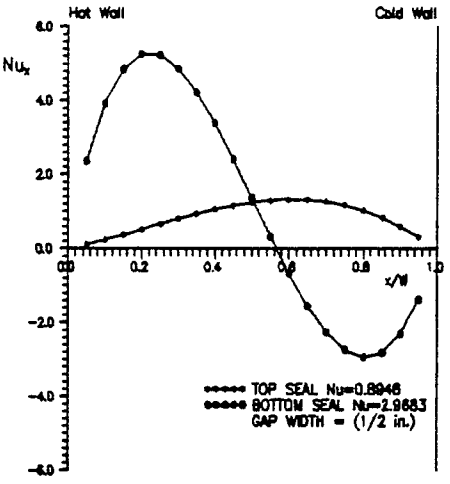

Test Run # 6

Local Heat Transfer on Top and Bottom Surfaces of The Air Gap

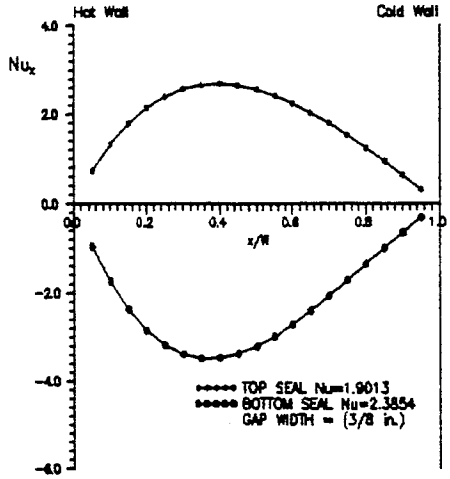

Test Run # 7

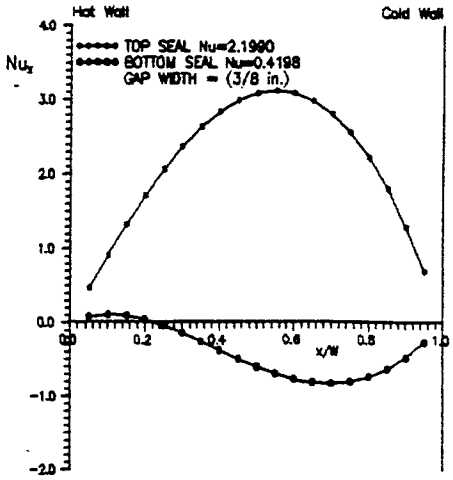

Test Run # 8

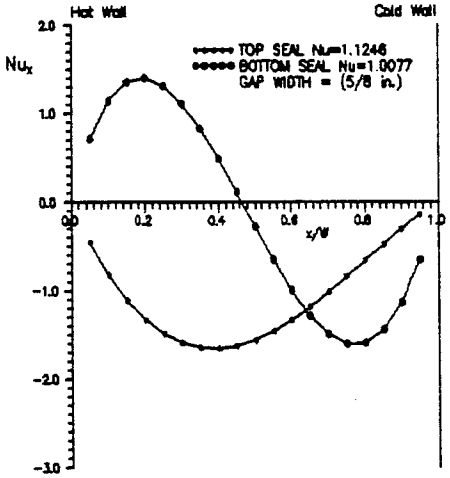

Test Run # 9

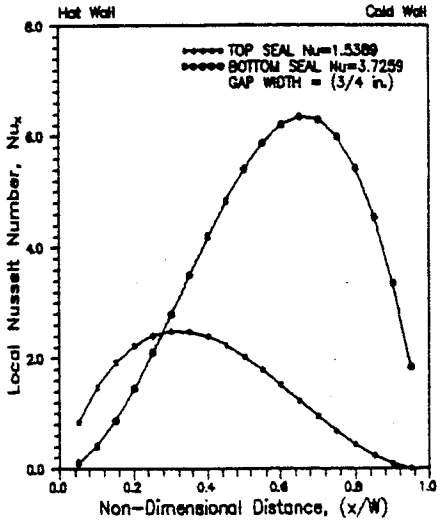

Test Run # 10

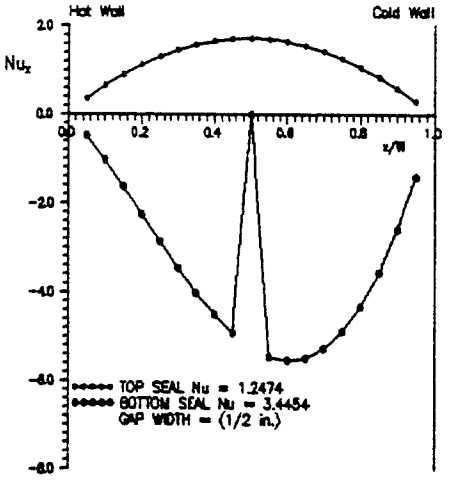

Test Run # 11

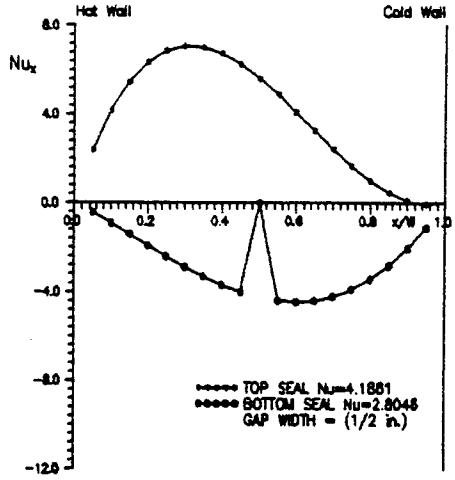

Test Run # 12

Local Heat Transfer on Top and Bottom Surfaces of The Air Gap

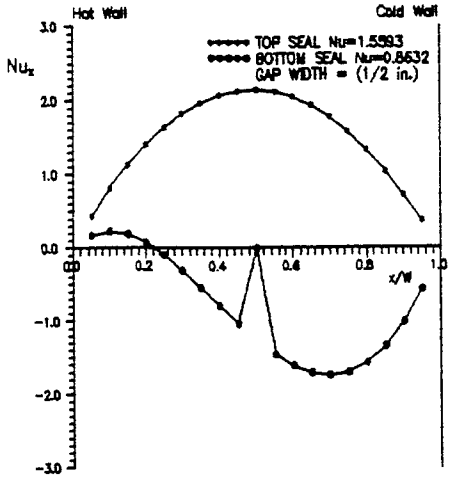

Test Run # 13

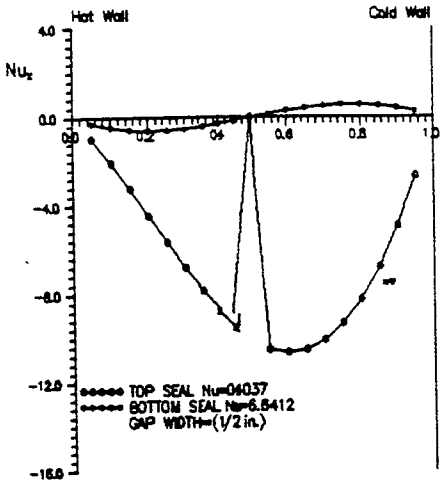

Test Run # 14

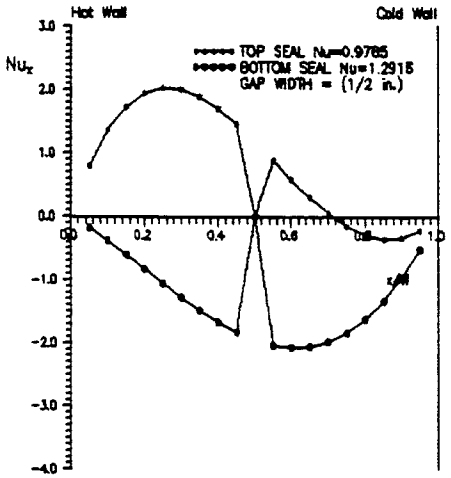

Test Run # 15

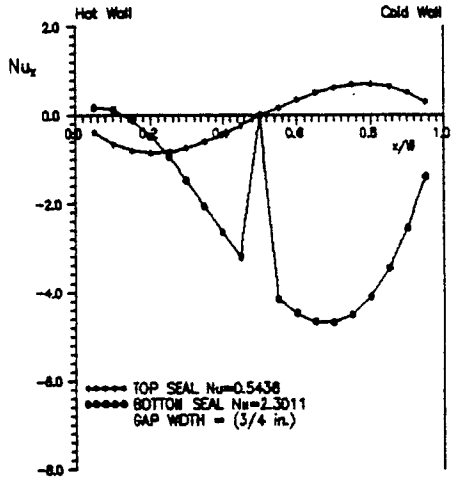

Test Run # 16

Local Heat Transfer on Top and Bottom Surfaces of The Air Gap

APPENDIX C

WINDOW SURFACE CONDENSATION

Surface condensation is a phenomenon by which moisture condenses on surfaces that are at a temperature below the dew point temperature of the surrounding or ambient air. Surface condensation in a double window glazing may occur either on the glass surfaces facing the air gap or on the room side surface of the glazing. The air gap surface condensation occurs when the seal around the double glazing breaks and moist air leaks into the gap. In this study we are concerned with the condensation occurring on the room side surface of a double window glazing. This is governed by three factors: the inside air temperature, the indoor humidity level and the glass surface temperature. The thermodynamic principle dealing with the interaction of these factors is called psychrometry. The interaction between the three factors is illustrated on the psychrometric chart, Figure C.1. More details on the standard psychrometric chart and the relevant technical terms can be found in the ASHRAE book of fundamentals [1989].

Considering the case discussed in section 4.3, the Dry Bulb temperature of the indoor air is 20°C and the Relative Humidity of the room is 60%. The point corresponding to these two conditions is shown in the psychrometric chart, Figure C.1 as point **A**. Other properties of the indoor air at point **A** is shown in Table C.1. The point **B** on the psychrometric chart represents the saturation point of the indoor air. By drawing a vertical line from the point **B** to intersect the Dry Bulb line on the psychrometric chart, the Dry Bulb temperature of the saturated air is found to be 12.3°C. This is the Dew point temperature of the indoor air. Other properties of the air at the Dew point condition is also shown in Table C.1. The recorded temperature of the

Table C.1

Psychrometric Data For Figure C.1

Points on Psychro-metric chart	Dry Bulb (°C)	Wet Bulb (°C)	Relative Humidity %	Enthalpy kJ/kg	Humidity Ratio g/kg	Spec. Vol. m^3/kg
A	20.0	15.20	60.00	42.20	8.75	0.842
B	12.30	12.30	100.00	34.40	8.75	0.820

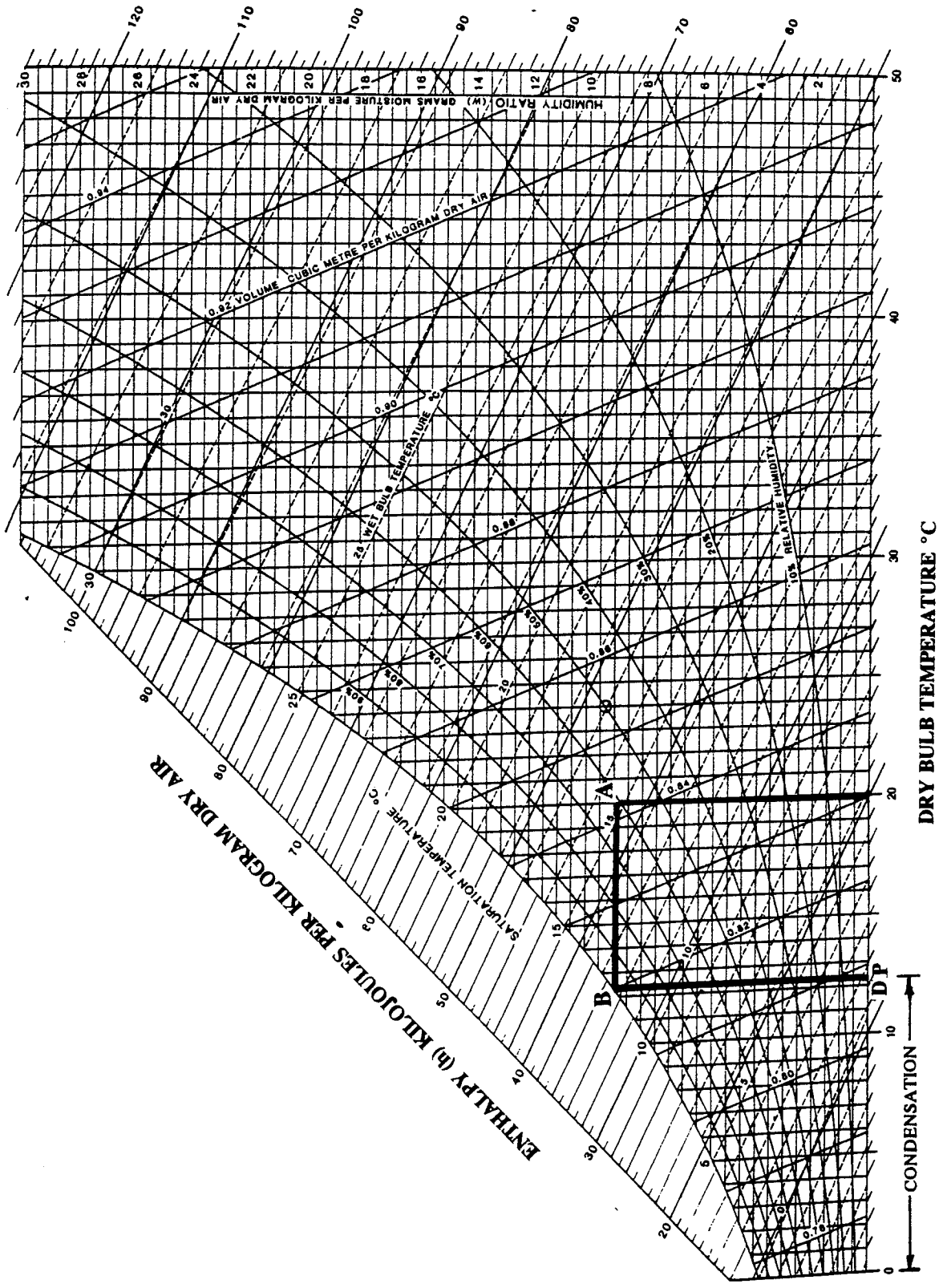

Figure C.1 A Typical Room Air Condition on A Standard Psychometric Chart

bottom section of the window glazing is 8°C. Because this temperature is lower than the Dew point temperature of the indoor air, surface condensation occurs at the bottom section of the glazing.

With the present window glazing technology, there is no technique to keep the temperature of the bottom section of the glass above the Dew point temperature of the indoor air. The traditional solution to the condensation problem is to bring in cold, dry air so that the interior relative humidity levels are diluted and reduced to a level where the glass surface temperature is higher than the Dew point temperature of the indoor air. This solution requires an additional energy consumption to preheat the supply cold air, and the process could be very costly because of the expensive ventilation and heating equipments required to supply the cold dry air. By introducing convection suppressor as described in section 4, the condensation can be eliminated without extra energy requirement and the expensive ventilation and heating equipments.